REPORT DOCUMENTATION PAGE

Form Approved
OMB No. 0704-0188

1. AGENCY USE ONLY *(Leave blank)*	2. REPORT DATE	3. REPORT TYPE AND DATES COVERED
	9 Jan 97	

4. TITLE AND SUBTITLE
On The Causes Of Tropical Cyclone Motion And Propagation

5. FUNDING NUMBERS

6. AUTHOR(S)
Carl Alan McElroy

7. PERFORMING ORGANIZATION NAME(S) AND ADDRESS(ES)
Colorado State University

8. PERFORMING ORGANIZATION REPORT NUMBER
96-135

9. SPONSORING/MONITORING AGENCY NAME(S) AND ADDRESS(ES)
DEPARTMENT OF THE AIR FORCE
AFIT/CIA
2950 P STREET
WPAFB OH 45433-7765

10. SPONSORING/MONITORING AGENCY REPORT NUMBER

11. SUPPLEMENTARY NOTES

12a. DISTRIBUTION AVAILABILITY STATEMENT
Unlimited

12b. DISTRIBUTION CODE

13. ABSTRACT *(Maximum 200 words)*

14. SUBJECT TERMS	15. NUMBER OF PAGES
	124
	16. PRICE CODE

17. SECURITY CLASSIFICATION OF REPORT	18. SECURITY CLASSIFICATION OF THIS PAGE	19. SECURITY CLASSIFICATION OF ABSTRACT	20. LIMITATION OF ABSTRACT

THESIS

ON THE CAUSES OF TROPICAL CYCLONE MOTION AND PROPAGATION

Submitted by

Carl Alan McElroy

Department of Atmospheric Science

In partial fulfillment of the requirements

for the degree of Master of Science

Colorado State University

Fort Collins, Colorado

Summer, 1996

COLORADO STATE UNIVERSITY

June 20, 1996

WE HEREBY RECOMMEND THAT THE THESIS PREPARED UNDER OUR SUPERVISION BY CARL ALAN MCELROY ENTITLED ON THE CAUSES OF TROPICAL CYCLONE MOTION AND PROPAGATION BE ACCEPTED AS FULFILLING IN PART REQUIREMENTS FOR THE DEGREE OF MASTER OF SCIENCE.

Committee on Graduate Work

_____

Committee Member

_____

Committee Member

_____

Committee Member

_____

Adviser

_____

Department Head

ABSTRACT OF THESIS

ON THE CAUSES OF TROPICAL CYCLONE MOTION AND PROPAGATION

The physics of tropical cyclone (TC) motion and propagation are examined using both climatological and composite rawinsonde data. Propagation is defined as TC motion relative to its surrounding steering flow. Tropical cyclones are observed to move 1-2 ms^{-1} faster and usually 10-20° to the left of the surrounding deep layer steering current(850-300mb deep layer flow averaged through a 5-7° radial band). Tropical cyclones move in response to a deep tropospheric current which advects them after they form.

The primary factor causing TCs to propagate faster than their steering flow is their formation and continued residence within a baroclinic environment. This baroclinic environment is evidenced by positive and negative tropospheric wind shears on opposite sides of the storm track. The presence of this wind shear on each side of the storm track causes a deep layer wind profile with the weakest flow away from the storm center. Hence, the TC center is embedded in the strongest tropospheric mean flow. The deep layer parallel wind flow to each side of the TC in the (MOT) frame of reference must, as a consequence of the temperature gradient induced wind shears, be weaker than the deep layer flow over the TC center. Tropical cyclones are situated in the warmest part of the environment with a cooler deep layer current to both right and left sides. These deep layer flow properties are applicable to the vicinity of the TC regardless of latitude or direction of motion.

Most TCs propagate to the left of their steering flow because they move from a relatively warm environment to a relatively cool environment. Westward moving TCs in the Atlantic are the exception. These are a special class of TCs which move from a relatively cool to a relatively warm environment. In this case, rear (cold) to front (warm) relative environmental temperatures cause a right deviation from the steering flow.

The faster movement of the TC relative to its surrounding flow creates tangential wind asymmetries in the 5-7° radial band 850-300 mb deep layer flow measured using the (MOT) system. These asymmetries cause wind-pressure adjustments in the TC vortex which induce TC propagation toward the southeast. This is opposite to Beta drift, which is assumed to be to the northwest.

The north-south pressure gradient asymmetry of the TC is smaller than the TC's north-south asymmetry of the Coriolis parameter. This difference in asymmetries induces an enhanced divergence to the south and west sides of the TC which acts to balance or modify Beta drift. Thus, propagation occurs as a result of the right to left and front to rear baroclinicity in which the TC exists.

Hence, a complete understanding of TC movement and propagation requires an appreciation of the fundamental role of the baroclinicity the TC resides within.

Carl Alan McElroy
Department of Atmospheric Science
Colorado State University
Fort Collins, Colorado 80523
Summer, 1996

ACKNOWLEDGEMENTS

First, I'd like to thank my committee members for taking the time to review my thesis and make constructive comments. My committee members are Dr Herbert H. Frisinger (CSU Department of Mathematics), Dr William M. Gray, and Dr Wayne H. Schubert.

I especially would like to thank Dr Gray, for "Planting the Seed" and suggesting this topic.

I also would like to thank everyone on the Project, especially John Knaff, for acquiring and processing the climatological data. Bill Thorson's provision of data processing support in handling the massive amount of composite sounding data to be analyzed saved a lot of valuable time so I could concentrate on the research at hand. Dr Raymond Zehr supplied GMS IR satellite imagery which visibly confirmed convergence patterns in NW Pacific tropical cyclones that were computed from composite sounding data sets.

Judy Sorbie-Dunn performed extensive graphics support in a short period of time when her schedule was already full to complete most of the illustrations in this thesis.

Barbara Brumit and Amie Hedstrom were the instrumental technical support in converting unorganized thoughts into concise, written text.

The Air Force was a source of key financial support and career direction. This indeed was an excellent career advancement opportunity.

Finally, I would like to thank all my AFIT classmates for their friendship and sharing their knowledge of meteorology with me.

TABLE OF CONTENTS

LIST OF FIGURES

LIST OF TABLES

LIST OF SYMBOLS AND ACRONYMS

AVA : Absolute Vorticity Advection.

Beta : $\partial f/\partial y$, or the meridional gradient of the Coriolis parameter.

CIRA : Cooperative Institute for Research in the Atmosphere.

CPC : Climate Prediction Center.

CSU : Colorado State University.

GMS : Geostationary Meteorological Satellite; a Japanese weather satellite in geosynchronous orbit.

GMT : Greenwich Mean Time; also known as Universal Time(UT), or Zulu Time.

IR : InfraRed.

mb : millibar; a unit of pressure in the mks system equal to 1 HPa.

MOT : MOTion System. A frame of reference with respect to the cyclone center in a geographical coordinate system with cyclone motion subtracted out of all the winds (portrayal of data relative to the moving cyclone center in geographical coordinates).

MOTROT : MOTROT System. A frame of reference with respect to the cyclone center and the direction to which the storm is moving with the cyclone motion subtracted out of all the winds.

NAT : NATural System. A frame of reference with respect to the instantaneously fixed cyclone center in a N-S geographical coordinate system.

NCAR : National Center for Atmospheric Research.

NHDT : Northern Hemisphere Data Tabulation (tapes of rawinsonde data).

NOAA : National Oceanic and Atmospheric Administration.

NVA : Negative Vorticity Advection; is taken to mean Negative absolute Vorticity Advection in this thesis.

PVA : Positive Vorticity Advection; is taken to mean Positive absolute Vorticity Advection in this thesis.

RMW : Radius of Maximum Winds.

ROCI : Radius of Outer Closed Isobar. A measure used to determine the size of TCs.

ROT : ROTated System. A frame of reference with respect to the instantaneously fixed cyclone center and the direction to which the storm is moving.

TC : Tropical Cyclone.

VE : Vorticity Equation. The equation for local absolute vorticity tendency, $\frac{\partial \zeta_a}{\partial t} = -\vec{V} \bullet \vec{\nabla}\zeta_a - (\vec{\nabla} \bullet \vec{V})\zeta_a$

LIST OF SYMBOLS

c : environmental wind speed

C : Centigrade

f : Coriolis parameter

F : frictional dissipation

g : acceleration due to gravity

h : moist static energy

$\hat{k}$: unit vector in the local vertical

K : Kelvins

p : pressure

$\bar{P}$: mean pressure between two pressure levels

q : specific humidity

r : radius

$\bar{r}_m$: average radius of maximum wind

R : gas constant for dry air

RH : relative humidity

S : dry static energy

t : time

T : temperature(C or K)

T_v : virtual temperature

U : zonal wind

U_t : total wind speed

$\bar{v}$: mean tangential wind

V : meridional wind

$\vec{V}$: wind velocity

$\bar{v}_m$: average maximum wind between the left and right sides of the TC

V_r : radial wind

V_θ : tangential wind

x : eastward ordinate

y : northward ordinate

$\mathbf{z}$: the local vertical direction in Cartesian coordinates in meters

β : meridional variation of the Coriolis parameter($\partial f/\partial y$)

ζ_r : vertical component of relative vorticity

ζ_a : vertical component of absolute vorticity ($\zeta_r + f$)

θ : potential temperature; or, azimuthal direction in cylindrical coordinates

θ_E : equivalent potential temperature

θ_{ES} : saturated equivalent potential temperature

θ_v : virtual potential temperature

ω : vertical motion in pressure coordinates(dp/dt)

$)_p$: on a constant pressure surface

Chapter 1

INTRODUCTION

Tropical cyclone motion has always been a key forecasting problem. It could even be considered the most important storm prediction problem. Knowing the precise intensity of a typhoon will be of little value if the forecaster remains uncertain as to its future path. Forecasting a major storm such as a typhoon entails a serious responsibility to those potentially affected. Frequently, the precise fate of large numbers of people and billions of dollars worth of property hinges on the track a typhoon or hurricane ultimately takes. Timely and accurate warnings are valuable in that they enable people to protect themselves and their property with a minimum of wasted effort. Therefore, the professional forecaster owes it to himself, as well as to those he serves, to become as proficient at predicting the motion of TCs as possible. An important goal of this thesis will be to provide a better understanding of the physics of TC motion. Hopefully, this will ultimately lead to better hurricane and typhoon forecasting skill through a more complete understanding of just how the most destructive storm on this planet moves.

1.1 Tropical Cyclone Motion and Propagation Concepts

Many conceptual and numerical models have been developed to obtain a better understanding in this arena. Many of these are currently used as forecasting aids. The basic concept that a TC moves as a point vortex in a non-interacting flow still remains valid. The deep layer tropospheric flow surrounding a TC definitely acts as a steering flow. Furthermore, the deep layer flow surrounding a TC is the primary cause of TC motion. Chan and Gray (1982) as well as Gray et al. (1988) have determined that the 5-7° 850-300 mb mass-weighted deep layer flow represents the TC's steering environment quite well.

Tropical cyclones also exhibit tendencies to move in a direction different than the direction of their outer radius deep layer steering current just discussed. This behavior is called propagation. Many recent studies have looked into Beta as the primary factor in explaining TC propagation. Basically, all tropical cyclones are situated in a Beta environment. This environment promotes positive absolute vorticity advection (PVA) in the tropical cyclone's northwest quadrant. Positive vorticity advection in turn should create a positive local vorticity tendency where it occurs. Thus, propagation in a northwesterly direction should follow. Beta definitely remains a key player when considering TC propagation, because PVA certainly occurs to the northwest of a TC's center. However, when all TC propagation influences and behaviors are considered, Beta falls short of explaining everything.

Rawinsonde compositing studies of stalled and slowly moving ($< 3ms^{-1}$) TCs in the NW Pacific and Atlantic basins show no obvious northwest propagation of the TC center relative to the ambient surrounding 850-300 mb mean wind flow. Numerous barotropic model runs over the years on a Beta plane with zero mean flow have predicted northwesterly drift. Also, no evidence has been found that the inner radii winds of eastward moving TCs move slower than outer radii winds as Beta-drift theory implies. In contrast, eastward moving storms and their inner radius deep layer flows are observed to track as fast or faster than their surrounding outer radius flows. Observations do not support large differences in the relative orientations of the gradients of relative vorticity for eastward versus westward moving cyclones.

In fact, the TC evolves through its life cycle in a baroclinic atmosphere. Other factors besides Beta influence the propagation of the TC. A more complete explanation of what influences TC motion and propagation should examine the influence an atmosphere with a certain baroclinic structure has on a TC. Other factors besides Beta which combine with it to determine the absolute vorticity tendency at a given point within the TC should be considered. It is the goal of this thesis to provide a more comprehensive explanation of the causes of TC motion and propagation.

1.2 Approach and Goals of this Study

The approach of this study is observational and analytical. Answers will come via the route of seeking information about TCs from the atmosphere itself. Climatological, composite rawinsonde, and composite satellite data will be collected and analyzed to clarify the physics of TC motion and propagation. These different data types should corroborate each other in providing answers to motion and propagation questions.

This study has two main goals. The first one is to show that the TC's motion is profoundly affected by the baroclinic environment it is embedded in. This baroclinic environment will be shown to remain remarkably similar in both the genesis phase as well as the motion after formation stage of a TC. Furthermore, the baroclinic environment containing the TC has a particular structure. The strongest deep layer tropospheric winds and highest 850-200mb thicknesses will be found to lie right over the storm track. Temperature gradients along the storm track determine whether or not the TC propagates to the left or right of its steering flow.

The second main goal is to provide a more comprehensive picture of TC propagation. It is the local vorticity tendency, and not just Beta alone, which plays the major role in TC propagation which is not caused by baroclinicity along the storm track. The TC has a convergence profile which is correlated with the local vorticity tendency. This convergence profile, in turn, will be shown to be affected by wind asymmetries in the TC's surrounding deep layer flow as well as pressure-wind adjustments to Beta. A tendency for asymmetric convergence on the south sides of TCs will be shown to exist. Ageostrophy, due to a TC's symmetric height field relative to Beta, will be shown to be the cause.

In short, to more completely understand TC motion and propagation, the structure of the TC's baroclinic environment needs to be understood, as well as all the influences on the local absolute vorticity tendency at a given location in a storm's deep layer flow (850-300 mb) vortex.

Chapter 2

DATA TYPES AND ANALYSIS PROCEDURES

Often the best way to learn about something is to observe its natural behavior, then analyze the data collected through observations. Much remains to be learned about TCs. Following an approach of collecting and analyzing data from the TC environment should provide a lot of insight about the physics of TC propagation. Hopefully, the three data types collected for this study will agree with each other. Composite rawinsonde sounding data sets stratified by motion, size and intensity constitute most of the data employed. Gridded climate data over a 10-year period, as well as GMS IR composite satellite imagery, are the other two data types used. Additionally, each of these three data types should complement each other by providing information about TCs which is unavailable from the other two data sources.

2.1 Composite Sounding Data

Tropical cyclones and similar weaker systems spend most of their lifetimes over tropical oceans. Traditional data sources are very sparse in such regions, and daily tropical weather analyses are notoriously unreliable. The strong winds found in TCs further reduce the availability of such data. It is not possible to obtain enough rawinsonde data or surface observations around an individual storm in one time period to permit a reliable quantitative analysis.

Aircraft data have provided the best information concerning the activities in the intense central core regions of TCs. However, logistical considerations have limited the ability of aircraft to provide information concerning the outer convective regions of the storm and its broader-scale environment. Aircraft data also have been limited to a few

flight levels per storm time period. This is due to the usually low number of available aircraft, maximum aircraft ceilings of 200 mb or lower, and the danger of low-level flight conditions.

None of the above data sources can produce an accurate vertical profile of the radial wind pattern around a system. Without such a profile, it is impossible to compute meaningful budgets of energy, water vapor, momentum, vorticity, etc. Given these observing limitations it is desirable to composite very large amounts of data from many similar weather systems at many time periods to obtain meaningful quantitative measurements.

Although the extreme variabilities and individual asymmetries of TCs and cloud clusters are well known, the nature of the basic dynamic and energetic processes which govern these systems is likely to be largely invariant. Rawinsonde compositing allows quantitative analyses of these features. Any compositing technique smoothes out many of the individual characteristics of single systems, but a great deal of information concerning asymmetrical or 'eddy' quantities can be deduced by the use of proper data-handling techniques.

Rawinsonde compositing has been performed on a 15° latitude radius cylindrical grid extending from sea level to 50 mb about many hundreds of tropical cloud clusters and cyclones. The system circulation center of the lowest level was located at each time period and positioned with the grid center. Whenever rawinsonde information became available within this grid at a given time period for a given storm, these soundings were positioned relative to the storm center in a cylindrical coordinate system. Figure 2.1 shows the grid and the number of soundings per grid space for a typical class of cloud cluster or TC stratification. All the parameters to be composited, whether directly measured or computed from the directly measured parameters, were determined at the observation station locations at 21 pressure levels. All parameters were assigned to a point at the center of the grid box in which the sounding fell. All soundings which fell in that grid space for the particular composite were averaged.

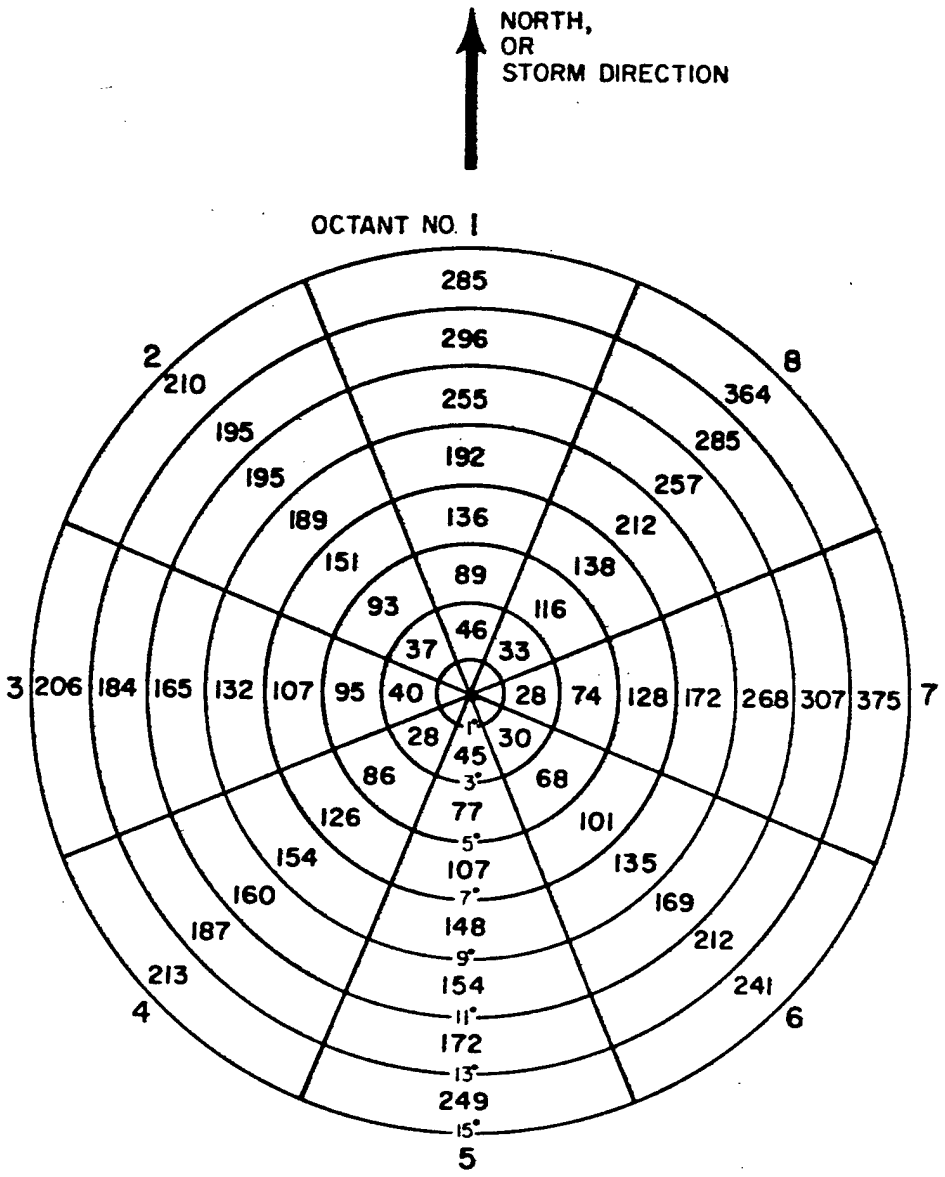

Figure 2.1: Compositing grid (15° latitude radius) with the number of rawinsonde reports in each octant and each 2° radial band for a typical stratification. Azimuthal octant numbers are outside the circle, 3 to the left, 7 to the right, etc.

The analyses to follow involve the use of 21 years (1957-77) of western Atlantic and Northwest Pacific rawinsonde data to provide high density coverage around all cyclones occurring in those regions. Many thousands of soundings from 54 stations in the Northwest Pacific (30 of those stations are shown in Fig. 2.2) have been processed. A similarly sized data sample for 105 west Atlantic stations (Fig. 2.3) has also been utilized.

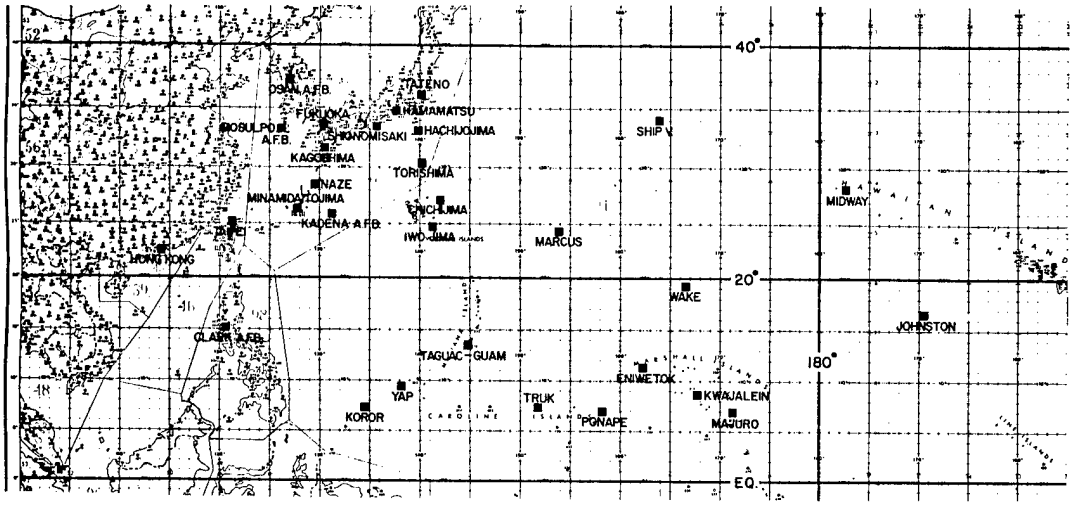

Figure 2.2: Northwest Pacific rawinsonde data network.

Due to the extremely large quantity of data it is possible to form subsets stratified according to a variety of characteristics. By compositing sets of storms with different characteristics, it is possible to systematically examine the subtle structural and dynamic differences which are related to such changes.

The following parameters are measured or computed at each level for each sounding:

Wind Parameters	Thermodynamic Parameters
zonal wind (u)	Height (H)
meridional wind (v)	Temperature (T)
Radial wind (V_r)	Virtual temperature (T_v)
Tangential wind (V_θ)	Potential temperature (θ)
Total wind speed (V)	Virtual potential temperature (θ_v)
	Equivalent potential temperature (θ_E)
	Saturated equivalent potential temperature (θ_{ES})
	Relative humidity (RH)
	Specific humidity (q)
	Dry static energy (S)
	Moist static energy (h)

The above parameters are composited at each of the 64-grid spaces at each level. The composite wind values are used to compute the divergence, vorticity and other wind

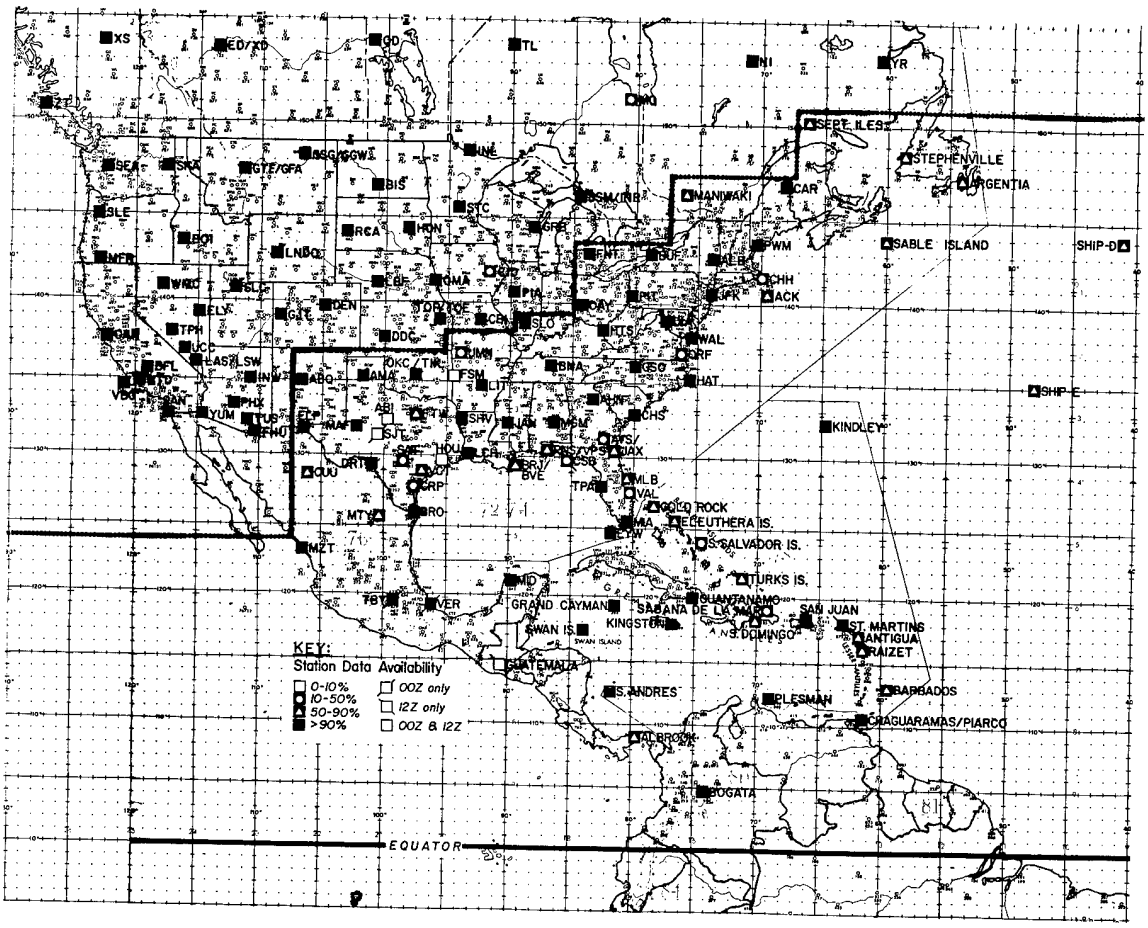

Figure 2.3: North Atlantic rawinsonde data network.

related parameters for each grid space. Similar composites are made for thermodynamic variables.

When performing composite studies, the most critical observed parameter is the radial wind (V_r). In general, the closer the observed vertical profiles of V_r come to achieving mass balance (defined as vertically integrated net radial mass flux between the surface and 100 mb), the better the data may be considered. Also, these mass balance corrections are quite small, especially when one considers the typical large standard deviation of individual V_r radial band data of about 7-8 ms^{-1}. It appears that the only way that these mean V_r corrections can be so small is that the usual meteorological sub-grid scale turbulence fluctuations and instrument errors largely cancel themselves out in the large sample.

Our rawinsonde compositing procedures involved the use of four separate reference frames:

1. With respect to the instantaneously fixed cyclone center in a N-S geographical coordinate system — Natural or NAT system.

2. With respect to the cyclone center in a geographical coordinate system with cyclone motion subtracted out of all the winds (portrayal of data relative to the moving cyclone center in geographical coordinates)— Motion or MOT system.

3. With respect to the instantaneously fixed cyclone center and the direction to which the storm is moving — rotated or ROT system.

4. With respect to the cyclone center and the direction to which the storm is moving with the cyclone motion subtracted out of all the winds — MOTROT system.

The relative position of the system center and the balloon changes due to their respective motions during the balloon's ascent are noted. These motions were estimated from the data, and the position of each was corrected at every pressure level. It is also possible to remove obviously atypical systems or time periods from a data group to improve the quality of the data set.

All the rawinsonde data used in these TC studies are taken from daily Northern Hemisphere Data Tabulation (NHDT) tapes from the US National Climatic Center Asheville Records Center, National Center for Atmospheric Research (NCAR), and from Japanese and East Asian upper air soundings. The latter soundings were card punched by the US Navy Environmental Prediction Research Facility, Monterey, CA for William M. Gray's Colorado State University (CSU) TC research project.

See the papers of Williams and Gray (1973), George and Gray (1976), Frank (1977), and Núñez (1981) for more detailed information on our rawinsonde compositing techniques and philosophy. Also, most of this composite sounding data section is excerpted from Gray (1981).

Rawinsonde composite analysis is an especially powerful tool for distinguishing physical differences between two data sets. As shown in Fig. 2.4, any systematic rawinsonde errors should be observed in both data sets and largely eliminated through the subtracting of one data set from the other. It is possible to composite different periods of the life cycle of storms to study the systematic changes that occur with time. The potential number of subsets is limited only by the minimum number of data points needed to provide meaningful composites. The stratification criteria which have been employed in this study are: size, central pressure, movement and character.

Forty-two basic TC data sets have been assembled for this study. Listings of these basic data sets for TC motion, intensity and size are given in Table 2.1. Tables 2.2 and 2.3 provide identifications of size of each data set.

2.2 Climate Prediction Center (CPC) Data

Data for the Climatology of TC Motion chapter come from the CPC 10-Year Climate Diagnostics Data Base. The data base consists of 32 megabytes of gridded climate data from 1979 to 1988. Data are organized into a global 144 × 73, 2.5° × 2.5° grid. Long term statistics are maintained for 8 atmospheric levels. These are 1000 mb, 850 mb, 700 mb, 500 mb, 300 mb, 250 mb, 200 mb, and 100 mb. Variables available for use in computations include z, T, U, and V. Respective units are m, K, ms^{-1}, and ms^{-1}. The source of this

Table 2.1: A listing of the types of TC stratifications used in this study.

ATLANTIC MOTION COMPOSITES

Label	Description	Stratification Criterion: Azimuthal Range (360=000=North)	Stratification Criterion: Speed Range (ms^{-1})	Stratification Criterion: Lat Range (°N)
WI070	Slow West	240-315	4-7	≤ 30
WI071	Fast West	240-315	> 11	≤ 30
WI072	Slow North	315-045	4-7	≤ 35
WI073	Fast North	315-045	> 11	≤ 35
WI074	No Motion	——	≤ 3	—
WI075	All West	240-315	≥ 4	≤ 30
WI076	All North	315-045	≥ 4	≤ 35
WI077	Intermediate West	240-315	8-11	≤ 30
WI078	Intermediate North	315-045	8-11	≤ 35
WI079	All Northeast	020-090	≥ 4	—
WI080	Fast Northeast	020-090	> 17	—
WI081	Slow Northeast	020-090	4-12	—
WI082	All Southwest	210-260	≥ 4	≤ 40

ATLANTIC INTENSITY COMPOSITES

Label	Description & Azimuthal Range	Stratification Criterion: Speed Range (ms^{-1})	Stratification Criterion: SFC Press Range (mb)	Stratification Criterion: Lat Range (°N)
WI090	Weak West, 240-330	> 4	990-1005	≤ 35
WI091	Interm. West, 240-330	> 4	965-990	≤ 35
WI092	Intense West, 240-330	> 4	< 965	≤ 35
WI093	Weak West, 240-330	> 4	980-1005	≤ 35
WI094	Strong West, 240-330	> 4	< 980	≤ 35
WI095	Weak N thru NE, 340-090	> 4	980-1005	≤ 40
WI096	Strong N-NE, 340-090	> 4	< 980	≤ 40

PACIFIC MOTION COMPOSITES

Label	Description	Stratification Criterion: Azimuthal Range (360=000=North)	Stratification Criterion: Speed Range (ms^{-1})	Stratification Criterion: Lat Range °N)
WP180	Slow West	240-315	4-7	—
WP181	Fast West	240-315	> 11	—
WP182	Slow North	315-045	4-7	—
WP183	Fast North	315-045	> 11	—
WP184	No Motion	—	< 3	—
WP185	All West	240-315	—	—
WP186	All North	315-045	—	—
WP187	Intermediate West	240-315	8-11	—
WP188	Intermediate North	315-045	8-11	—
WP189	All Northeast	020-090	—	—
WP190	Fast Northeast	020-090	> 17	—
WP191	Slow Northeast	020-090	< 12	—
WP192	All Southwest	210-260	—	—

Table 2.1: Continued

PACIFIC INTENSITY COMPOSITES

Label	Description & Azimuthal Range	Stratification Criterion Speed Range (ms^{-1})	SFC Press Range (mb)	Lat Range (°N)
WP200	Weak West, 240-330	> 4	980-1000	≤ 35
WP201	Interm. West, 240-330	> 4	955-980	≤ 35
WP202	Intense West, 240-330	> 4	< 955	≤ 35
WP203	Weak West, 240-330	> 4	970-1000	≤ 35
WP204	Strong West, 240-330	>4	<970	≤ 35
WP205	Weak N thru NE, 340-090	> 4	970-1000	≤ 40
WP206	Strong N - NE, 340-090	> 4	< 970	≤ 40

PACIFIC SIZE COMPOSITES

Label	Description	Stratification Criterion
WP303	Small ROCI*	ROCI ≤ 3° latitude
WP304	Large ROCI	ROCI 3-15° latitude
	* denotes Radius of Outer Closed Isobar	

data is the Climate Prediction Center, W/NP52, NOAA Science Center, Room 605, 5200 Auth Road, Camp Springs, MD 20746 . The CPC point of contact is Dr. Muthuvel Chelliah, TEL: (301)-763-8227, FAX: (301) 763-8395.

2.3 Satellite Data

Geostationary Meteorological Satellite (GMS) 10 km resolution infrared (IR) imagery was used for composite IR images of individual as well as composite storms. The typhoon eye was located at the center of each image so that averaging is with respect to the IR cloud distribution relative to the center. The source of the images is the satellite image archive of CIRA (Cooperative Institute for Research in the Atmosphere), courtesy of Dr. Raymond Zehr of CIRA. CIRA is affiliated with both Colorado State University and the National Oceanic and Atmospheric Administration(NOAA).

Composite 3-hourly GMS IR imagery was used to create a 64-image average for Supertyphoon Vanessa. 64 images covering a time span from 0000 GMT, 22 Oct 84 to 2100 GMT, 29 Oct 84 were averaged for this single storm image.

Table 2.2: Number of storms and number of rawinsonde observations for each composited Atlantic TC data set.

ATLANTIC TC MOTION, INTENSITY, AND SIZE DATA SET

MOTION COMPOSITES

Case Number	Description	Number Of Storms	Number of Observations Within 11° Radius
WI070	Slow West	67	3,642
WI071	Fast West	77	3,425
WI072	Slow North	103	6,621
WI073	Fast North	89	4,016
WI074	No Motion	71	4,358
WI075	All West	112	11,417
WI076	All North	158	15,978
WI077	Intermediate West	82	4,350
WI078	Intermediate North	103	5,341
WI079	All Northeast	146	13,636
WI080	Fast Northeast	87	3,030
WI081	Slow Northeast	101	6,662
WI082	All Southwest	48	2,680
	INTENSITY COMPOSITES		
WI090	Weak West	67	1,899
WI091	Intermediate West	39	1,778
WI092	Intense West	26	1,867
WI093	Weak West	73	2,759
WI094	Strong West	35	2,785
WI095	Weak North through NE	88	4,352
WI096	Strong North through NE	43	2,320

Table 2.3: Number of storms and number of rawinsonde observations for each composited TC data set for the Northwest Pacific.

NORTHWEST PACIFIC TC MOTION, INTENSITY, AND SIZE DATA SET

Case Number	Description	Number Of Storms	Number of Observations Within 11° Radius
	MOTION COMPOSITES		
WP180	Slow West	291	8,182
WP181	Fast West	336	13,721
WP182	Slow North	285	9,656
WP183	Fast North	311	10.330
WP184	No Motion	158	4,015
WP185	All West	499	35,773
WP186	All North	472	32,050
WP187	Intermediate West	393	12,616
WP188	Intermediate North	335	10,508
WP189	All Northeast	341	16,758
WP190	Fast Northeast	202	4,652
WP191	Slow Northeast	237	8,405
WP192	All Southwest	189	4,674
	INTENSITY COMPOSITES		
WP200	Weak West	444	17,054
WP201	Intermediate West	265	9,653
WP202	Intense West	152	7,381
WP203	Weak West	462	22,370
WP204	Strong West	209	11,718
WP205	Weak North through NE	294	11,023
WP206	Strong North through NE	190	7,365
	SIZE COMPOSITES		
WP303	Small ROCI	352	14,948
WP304	Large ROCI	360	29,251

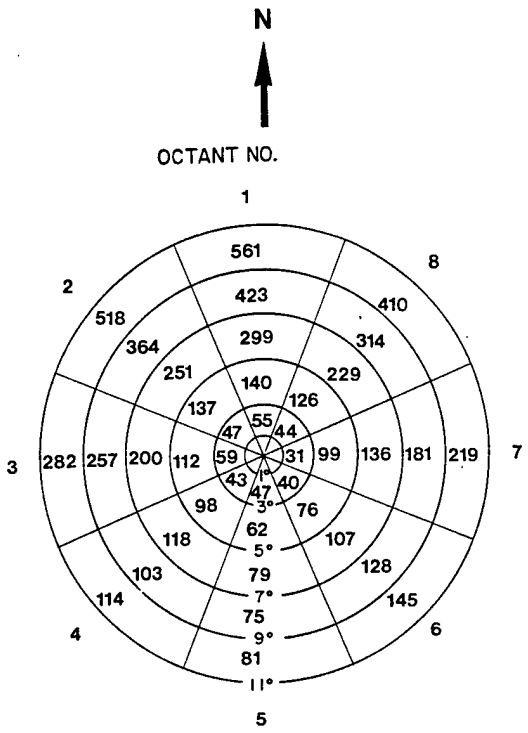

Figure 2.4: Typical illustration of one Northwest Pacific typhoon data set – the Fast West moving typhoon at 900 mb. Each figure represents the number of rawinsonde reports per grid space.

Composite 3-hourly GMS IR imagery for 10 different Northwest Pacific typhoons was also used to create average images. A separate average IR image was created for each of five different life cycle stages as determined by Weatherford (1989). Typhoons Wayne, Abby, Forrest, Marge, and Orchid from 1983 were used, as well as Typhoons Vanessa, Agnes, Bill, Clara, and Doyle from 1984. The following is a breakdown by life cycle stage for number of images used in the average from the above 10 typhoons: Stage 1: 117 images, Stage 2: 134 images, Stage 3: 52 images, Stage 4: 96 images, and Stage 5: 102 images. Stages 1 and 5 were not used because mature typhoon imagery was easier to work with.

The same enhancement scheme was used to create all the IR images displayed in this thesis. Table 2.4 below provides the particulars on the IR enhancement scheme used.

Table 2.4: Infrared enhancement color table for GMS averaged images. (Used for composites by storm life cycle stage).

IR T (°C)	COLOR RANGE
> 20	Black
20 to 1	Dark blue to white
0 to -19	Black to yellow
-20 to -29	Dark blue to light blue
-30 to -39	Dark green to light green
-40 to -49	Dark red to light red
-50 to -59	White to dark blue
-60 to -69	White to dark green
-70 to -79	White to dark red
-80 to -89	White to yellow
< -90	Black

Chapter 3

CLIMATOLOGY OF TROPICAL CYCLONE MOTION

For quite some time it has been known that TCs in both the Atlantic and Northwest Pacific Oceans, as well as in other ocean basins, form and move within certain preferred areas. Once formed, TCs will initially tend to move along preferred paths. These can be easily resolved in monthly climatological atlases for both the Atlantic and Northwest Pacific Ocean Basins. Within any given month, the initial tropical cyclone paths tend to coincide with the preferred genesis areas. A climatologically preferred area for tropical cyclone formation and subsequent movement comprises a storm track. Along a storm track, the tropospheric deep layer flow magnitude displays a characteristic profile. This profile can be found either in the Atlantic or NW Pacific. In both the NW Pacific (see Fig. 3.1) and the Atlantic (see Fig. 3.2), the tropospheric deep layer flow is strongest over the storm tracks with weaker deep layer flow to either side. Why the tropospheric deep layer flow behaves in this way in the vicinity of tropical cyclone tracks will be discussed in section 3.2.

Gray (1968) and McBride (1979) have already shown that strong values of low-level relative vorticity as well as small values of tropospheric vertical wind shear where a sign change in 200-900 mb U wind shear (200-850 mb U wind shear is examined here) occurs are conducive to TC formation. Zonal wind shear is positive if the U component of the wind increases (or becomes less negative) with height. Zonal wind shear would be negative in the U component of the wind decreased (or became less positive) with height. Specifically, negative 200-850 mb zonal wind shear occurs to the equatorward side of where TCs form and move, and positive 200-850 mb zonal wind shear can be found to the poleward side of the storm track (see Fig. 3.3). This chapter will attempt to also show that these same

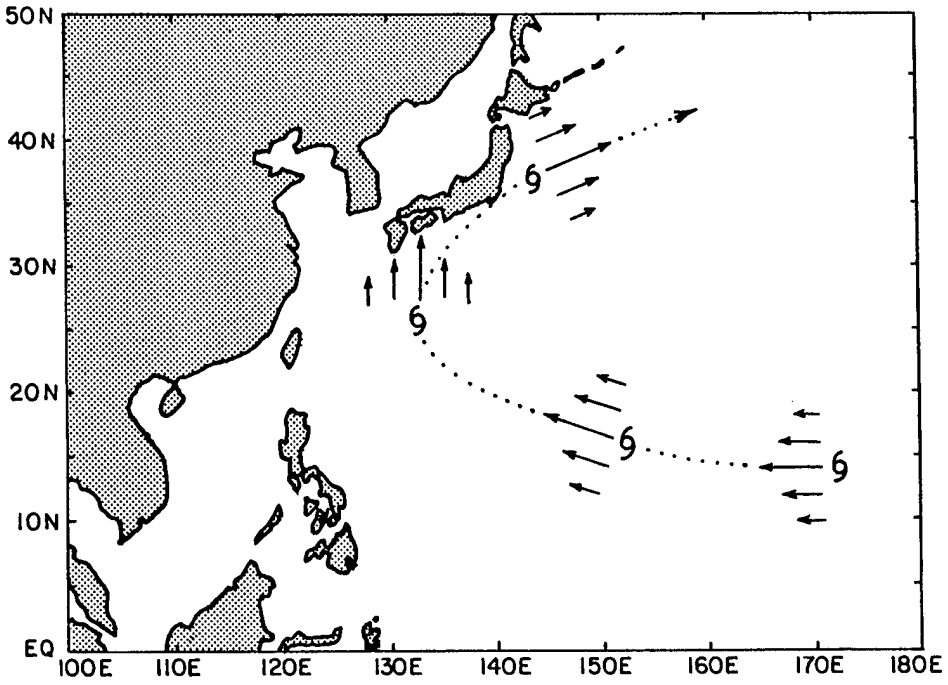

Figure 3.1: Tropical cyclone track idealized from 1946-1969 climatology, with associated magnitude of deep layer flow for the Northwest Pacific in August.

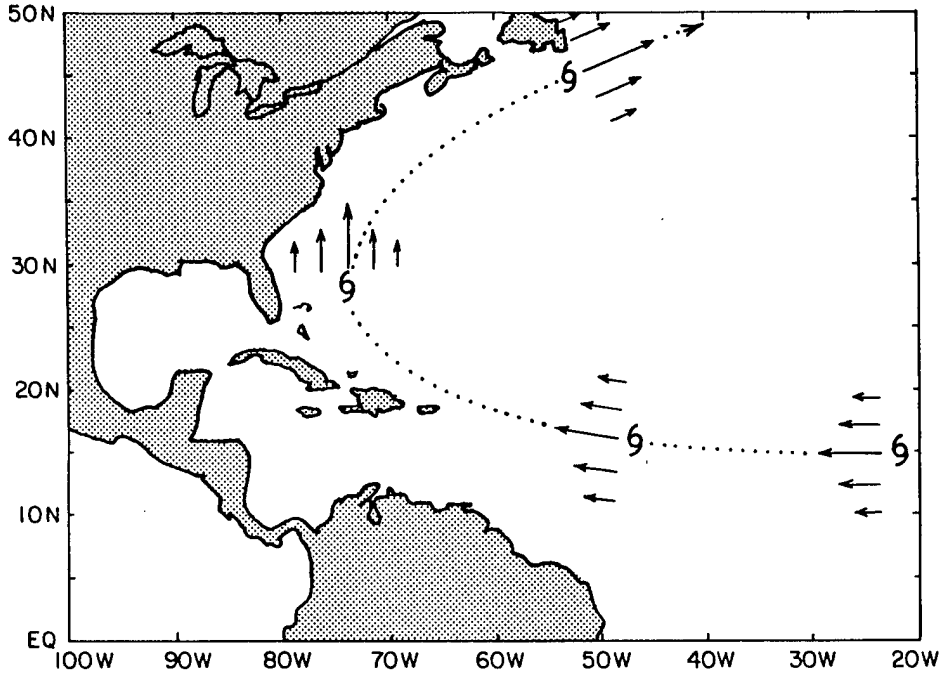

Figure 3.2: Tropical cyclone track idealized from 1886-1986 climatology, with associated magnitude of deep layer flow for the Atlantic in August.

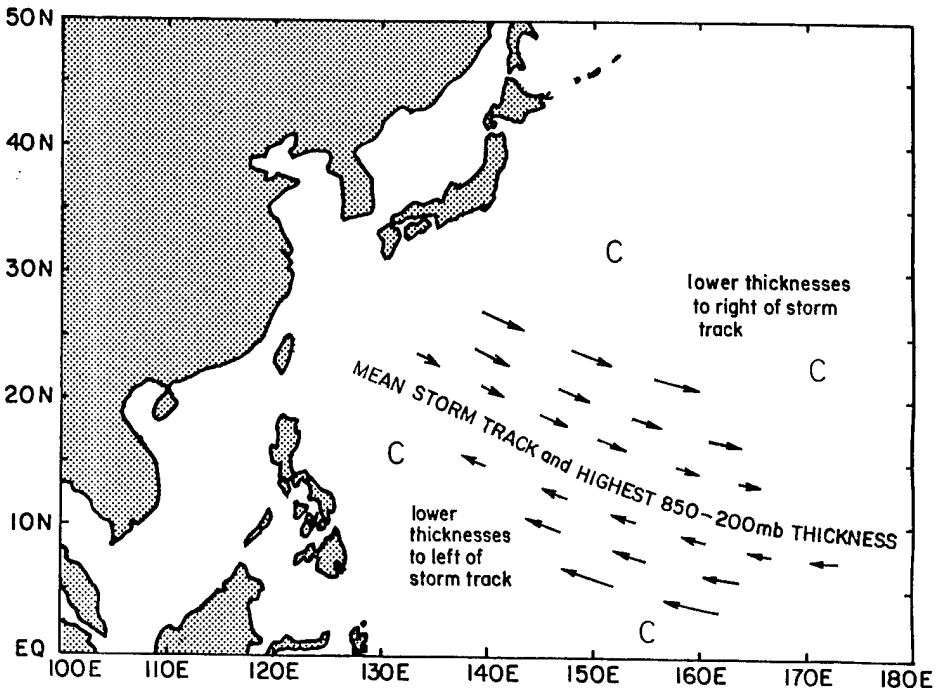

Figure 3.3: Idealized 200-850 mb wind shear vectors in the NW Pacific for August. Increasing easterly shear is found to the equatorward side and increasing westerly shear to the poleward side of the area of warmest mean tropospheric temperature. Cyclones usually track westward along this warm air axis.

preferred genesis and movement areas for TCs exhibit prevailing climatological maxima for tropospheric deep layer flows. Furthermore, in the Northwest Pacific Ocean, where a deep layer flow is strongest in the troposphere, the thickness of that same layer will be the greatest. In the Atlantic Ocean, a thickness maximum is not evident in the climatological data discussed below.

3.1 Climatologically Prevalent Deep Layer Flow Characteristics Near Storms

The 10 year climatology extracted from the Climate Analysis Center's 10 Year Climate Diagnostics Data Base can be used to examine deep layer flows for both the Atlantic and Northwest Pacific. Such an examination will reveal additional characteristics about deep-layer flows in the vicinity of TCs.

First, TCs form and move in areas where the deep layer wind flow is the strongest. Local maxima in the August deep layer flow (see Fig. 3.4) can be seen to coincide with the prevailing monthly storm tracks in Fig. 3.5. Furthermore, individual monthly plots

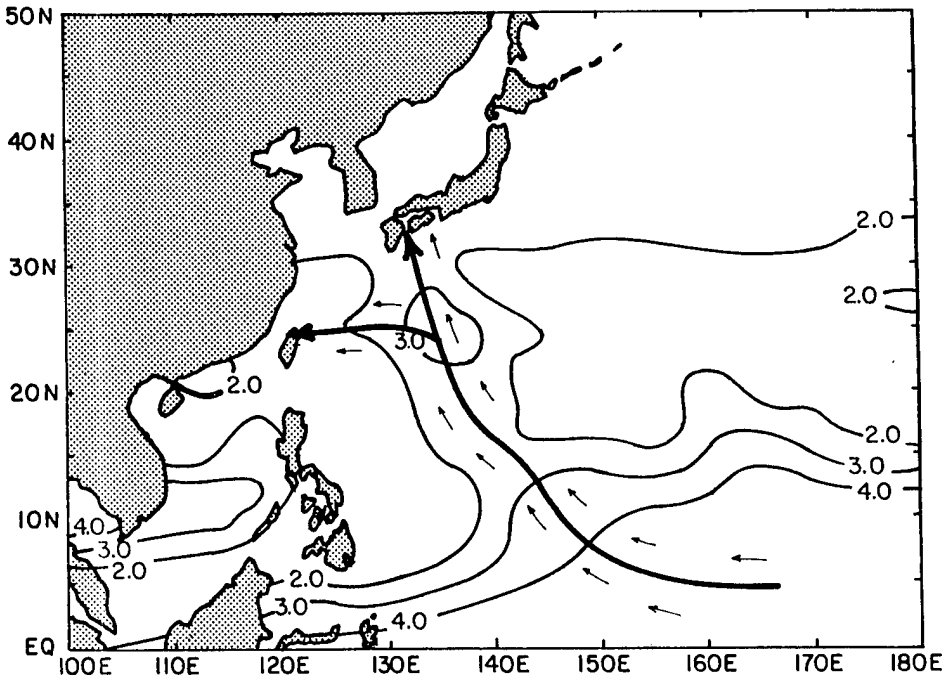

Figure 3.4: a. Deep layer 850-300 mb mass weighted wind flow magnitude in ms^{-1} for the month of August in the Northwest Pacific (small arrows show flow direction). Data come from the Climate Prediction Center (CPC) 10-year climate diagnostics data base for 1979-1988. Note higher values in the flow field prevail in the vicinity of the idealized storm track centroid (long bold arrows) based upon 1886-1986 storm track climatology.

of the deep layer U flow for both the Northwest Pacific (Figs. 3.6a,b) between 110-150°E longitude and the Caribbean (Figs. 3.6c,d) between 70-90°W longitude show distinct maxima in the deep layer U flow in the vicinity of each respective monthly prevailing storm track. Also note that the deep layer U graphs for both surface-100 mb and 850-300 mb are surprisingly similar(virtually identical).

Additionally, thermal wind arguments using the thermal wind equation $\frac{\Delta U}{\Delta p} = -\frac{R}{f\bar{p}}\frac{\Delta T}{\Delta y}$ indicate that a warm pocket in the 850-300 mb thickness field also exists in the Northwest Pacific Ocean where this deep layer flow is the strongest. In the thermal wind equation $\frac{\Delta U}{\Delta p}$ refers to the wind shear in a given pressure layer, R is the gas constant for dry air, f is the Coriolis parameter, $\bar{p}$ is the mean pressure of the layer referred to by Δp, and $\frac{\Delta T}{\Delta y}$ is the temperature gradient (perpendicular to U).

A glance at Fig. 3.7 will show this in the August climatology for the Northwest Pacific 850 to 300 mb and surface to 1000 mb deep layer flows. In the Atlantic Ocean, in contrast, no clear thickness maximum corresponds with these two deep layer flow peaks

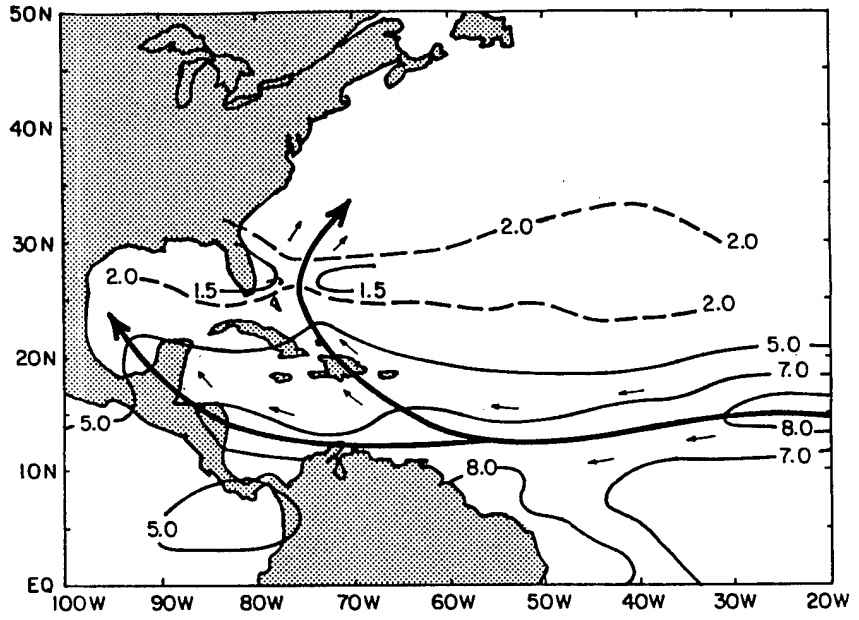

Figure 3.4: b. Deep layer 850-300 mb mass weighted wind flow magnitude in ms^{-1} for the month of August in the Atlantic (small arrows show flow direction). Data come from the Climate Prediction Center (CPC) 10-year climate diagnostics data base for 1979-1988. Note higher values in the flow field prevail in the vicinity of the idealized storm track centroid (long bold arrows) based upon 1946-1969 storm track climatology.

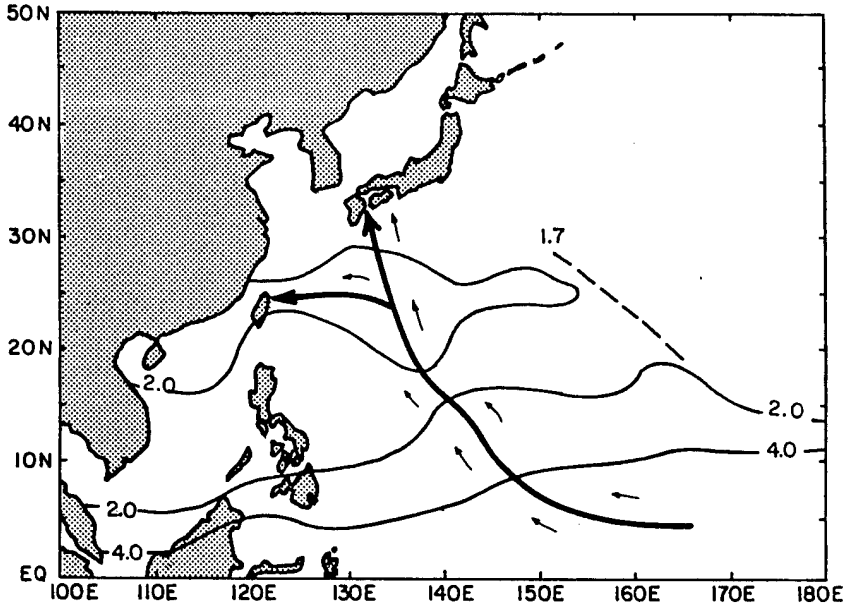

Figure 3.4: c. Surface to 100 mb deep layer mass weighted wind flow magnitude in ms^{-1} for the month of August in the Northwest Pacific (small arrows show flow direction). Data come from the Climate Prediction Center (CPC) 10-year climate diagnostics data base for 1979-1988. Note the local maximum in the flow field coincident with the prevailing TC track (long bold arrows) for August.

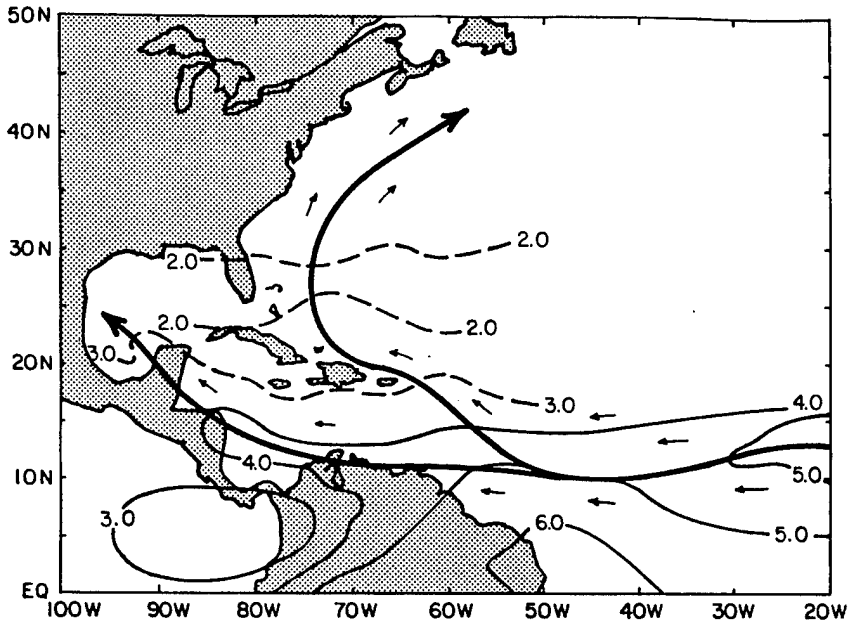

Figure 3.4: d. Surface to 100 mb deep layer mass weighted wind flow magnitude in ms^{-1} for the month of August in the Northwest Pacific (small arrows show flow direction). Data come from the Climate Prediction Center (CPC) 10-year climate diagnostics data base for 1979-1988. Note the local maximum in the flow field coincident with the prevailing TC track (long bold arrows) for August.

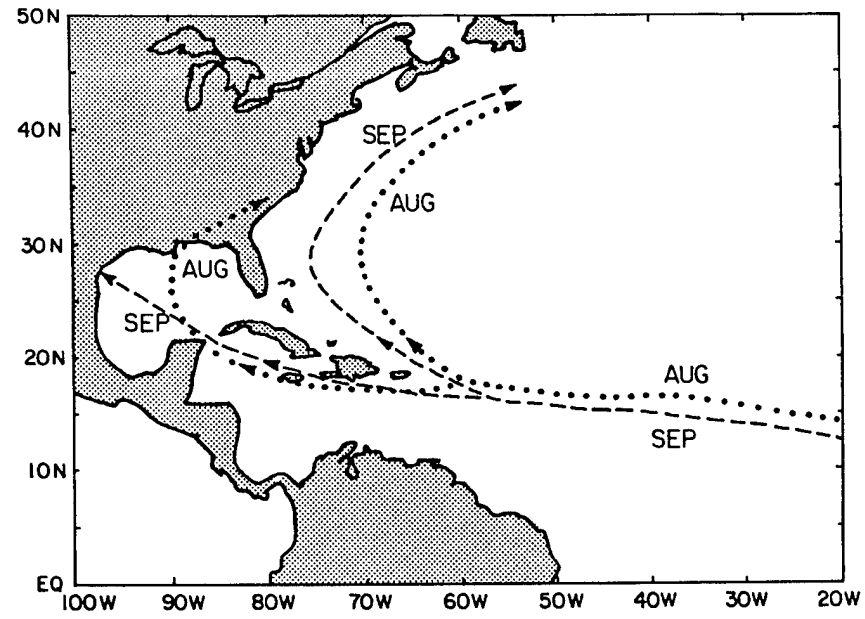

Figure 3.5: a. Monthly TC track centroids for the Atlantic from 1886-1986 climatology. Dotted and dashed lines denote mean TC tracks for the months of August and September, respectively.

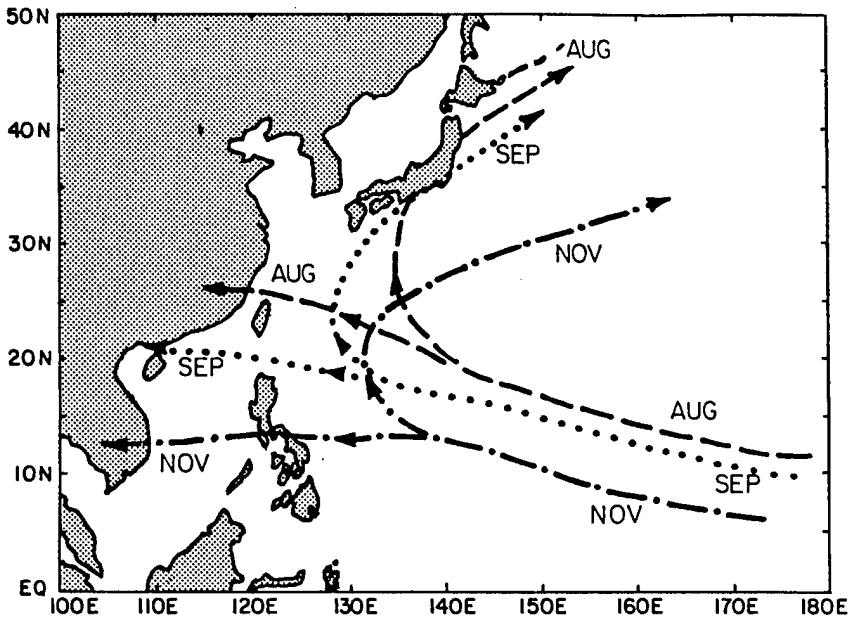

Figure 3.5: b. Monthly TC track centroids for the Northwest Pacific from 1946-1969 climatology. Dashed, dotted and dot/dashed lines denote mean TC tracks for the months of August, September and November, respectively.

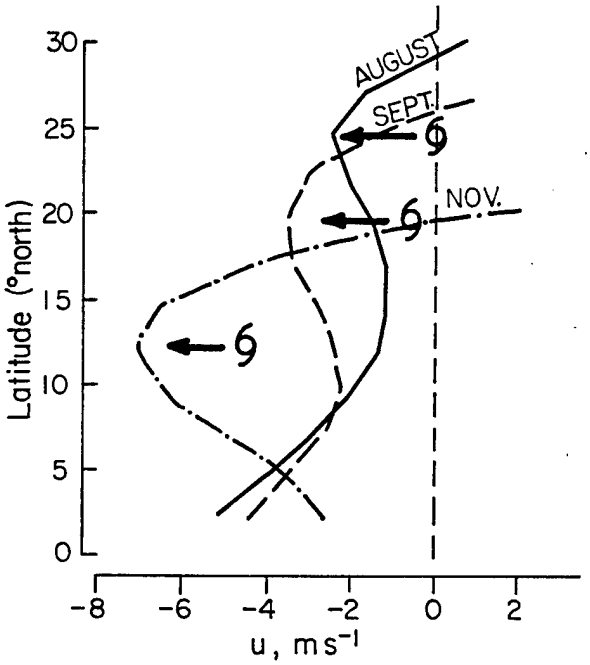

Figure 3.6: a. Mass weighted monthly deep layer U flows in m s^{-1} between the surface and 100 mb for the Northwest Pacific, with the mean monthly storm track position superimposed. Deep layer flow values were measured every 2.5° of longitude and averaged between 110°E and 150°E. Note the correlation between the latitude of the strongest deep layer flow and the storm track. Also, note how similar these flow patterns are to the ones for the 850 mb to 300 mb layer.

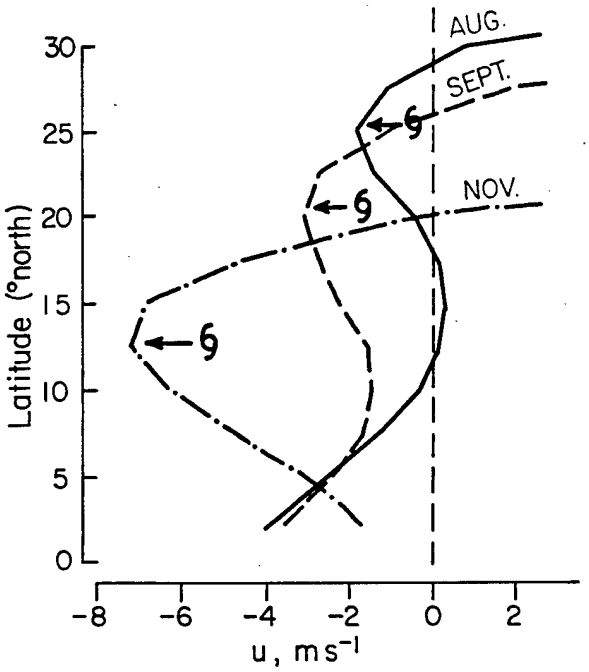

Figure 3.6: b. Mass weighted monthly deep layer U flows in m s^{-1} between 850 mb and 300 mb for the Northwest Pacific. Deep layer flow values were measured every 2.5° of longitude and averaged between 110°E and 150°E.

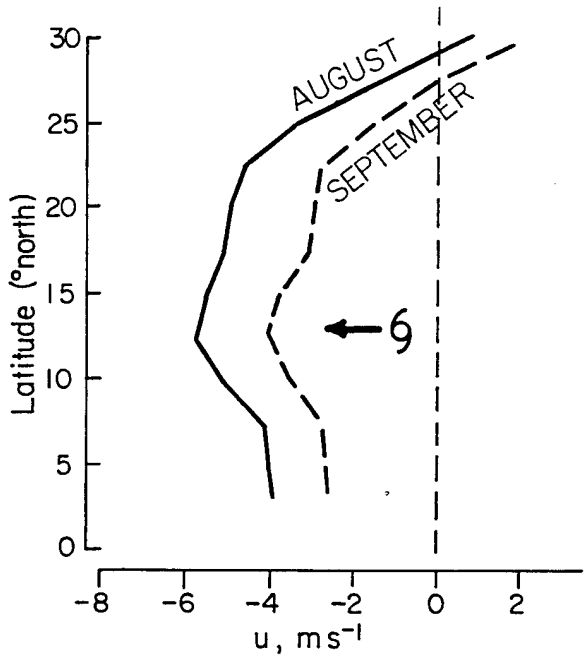

Figure 3.6: c. Mass weighted monthly deep layer U flows in m s^{-1} between the surface and 100 mb for the Atlantic, with the mean monthly storm track position superimposed. Deep layer flow values were measured every 2.5° of longitude and averaged between 70°W and 90°W. Note the correlation between the latitude of the strongest deep layer flow and the storm track.

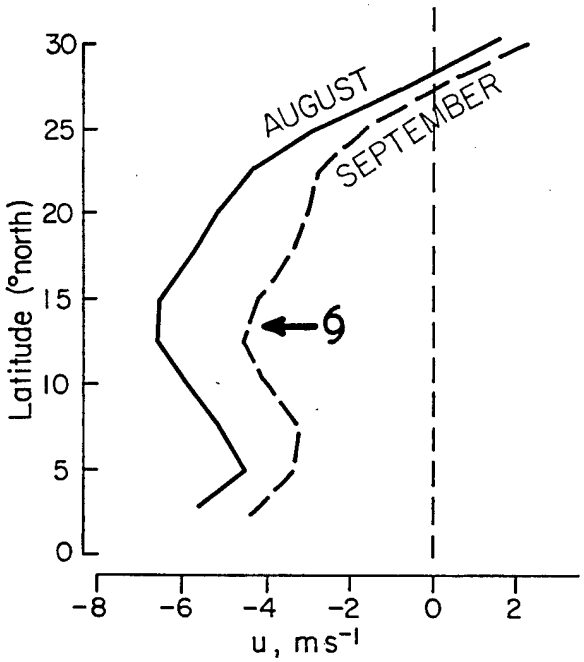

Figure 3.6: d. Mass weighted monthly deep layer U flows in m s^{-1} between 850 mb and 300 mb for the Atlantic, with the mean monthly storm track position superimposed. Deep layer flow values were measured every 2.5° of longitude and averaged between 70°W and 90°W. Note the correlation between the latitude of the strongest deep layer flow and the storm track. Also, observe how similar these flow patterns are to the ones for the surface to 100 mb layer.

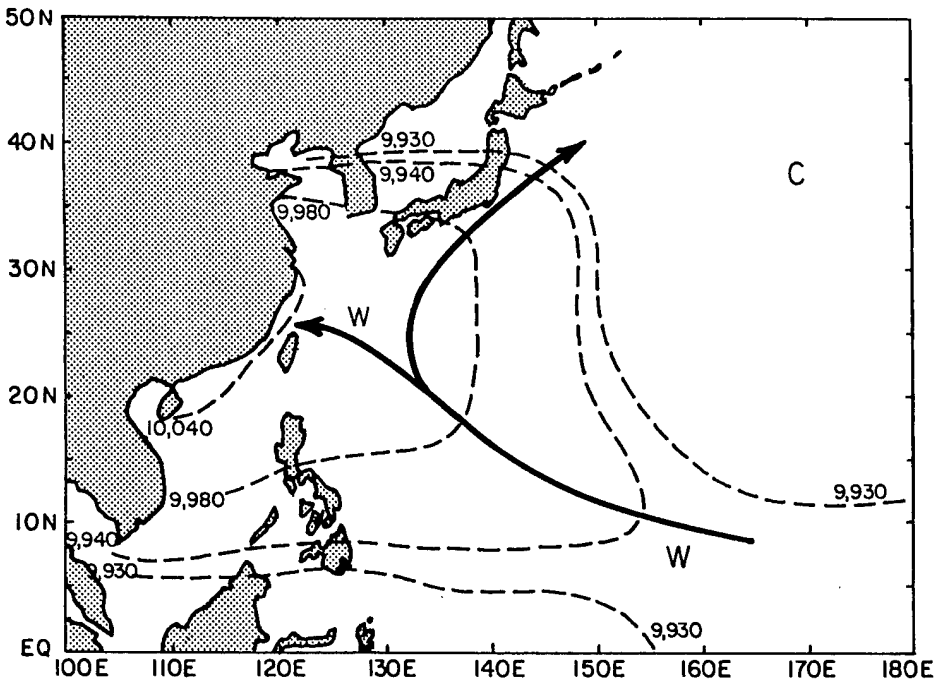

Figure 3.7: Climatology (1979-1988) for August 200-850 mb thickness in the Northwest Pacific with an idealized mean monthly TC track from 1946-1969 climatology superimposed. Note the relative deep layer warmth along the storm track.

in the vicinity of the climatologically greatest storm track density. This could be due to a "masking effect" created by solar heating of the South American landmass. The absence of a thickness maximum along the initial mean storm track in the Atlantic may also be symptomatic of movement in a trade wind environment versus movement within a monsoon trough in the Northwest Pacific Ocean. The NW Pacific Ocean does exhibit a thickness maximum in the vicinity of the strongest deep layer flow, right where the storm formation loci and motion tracks lie. Seasonal trade wind fluctuations can mask this local maximum in the deep layer flow in both the Atlantic and Northwest Pacific Oceans, especially with the onset of Autumn in both ocean basins. Also, during the Atlantic Ocean hurricane season, strong southeasterly trades, especially along the northern Brazilian coast generate a strong deep layer (850-300 mb) easterly wind maximum just south of the equator which serves to mask the deep layer flow maximum for the 10-year climatology data field in the vicinity of the prevailing storm tracks.

The deep layer 200-850 mb U shear profile in the Northwest Pacific shows a well defined zero line along the axis of prevailing initial storm movement (see Fig. 3.3). A correspondingly well defined zero deep layer 200-850 mb U flow does not exist for the Atlantic Ocean. Again, this would be indicative of storm formation and initial movement within a monsoon trough in the Northwest Pacific, versus formation and initial movement as an easterly wave within the trades of the Atlantic.

A recap of the deep layer flow for the Northwest Pacific has 3 characteristics in the vicinity of the initial storm tracks. These are 1) a local maximum in the deep layer flow; 2) a local maximum in the thickness measured for that same deep layer in question; and 3) a zero deep layer U shear line. The deep layer flow for the Western Atlantic only clearly exhibits characteristic 1) above.

In Chapter 4, a comparison will be made between the deep layer flow and thickness profiles observed in the 10 year climatology to those analyzed from composite sounding data.

3.2 Using Deep-Layer Flow Climatology to Explain Slow Motion and Looping in Storms

A case can be made that there is a correlation between minimums in the 10 year climatology deep layer flow data and climatologically preferred areas for storm slow motion and looping. A comparison of Figs. 3.8a-b from Environmental Circulations Associated with TCs Experiencing Fast, Slow, and Looping Motion (Xu and Gray, 1982) with areas of deep layer flow less than 2 ms^{-1} (see Fig. 3.4) will show several things. First, areas of slow motion and looping from Xu and Gray appear to take place in the same general areas. Second, deep layer flow strength minima (both surface-100 mb and 850-300 mb) primarily lie along the axis of the subtropical ridge. Third, deep layer flow minima occur in a pattern very similar to that shown by the aforementioned areas of slow motion and looping.

Monthly intersection points of zero U and zero V deep layer flow also correlate well with preferred areas for slow motion and looping.

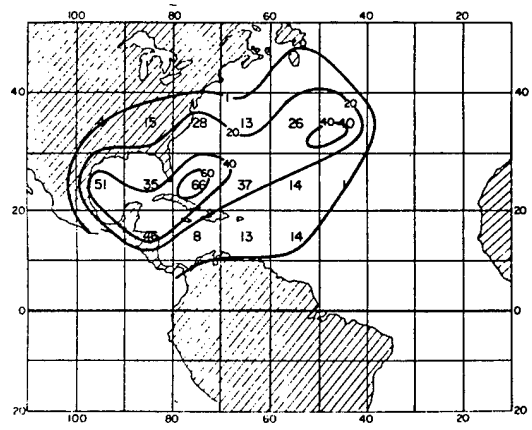

a) Distribution of Atlantic slow moving tropical storms per 10° Marsden square per 21 years.

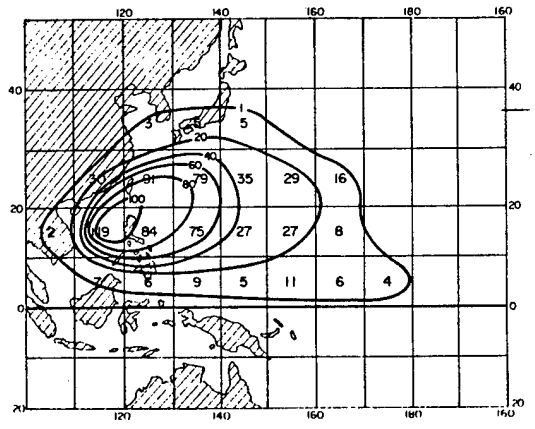

b) Distribution of western Pacific slow moving storms per 10° Marsden square per 21 years.

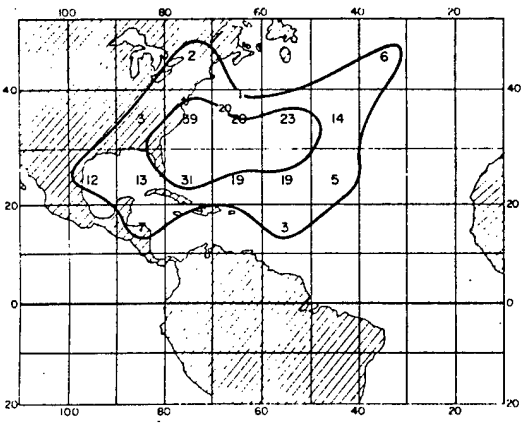

c) Distribution of Atlantic looping storms per 10° Marsden square per 21 years.

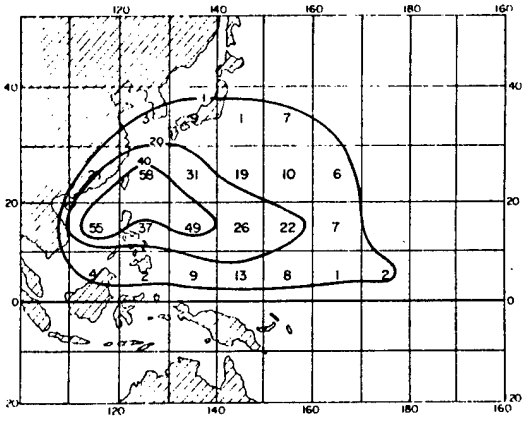

) Distribution of western Pacific looping storms per 10° Marsden square per 21 years.

Figure 3.8: Climatology of both Atlantic and Northwest Pacific TCs exhibiting slow motion (a-b) and looping (c-d) behavior. Note the tendency for slow motion and looping to occur in the same areas, as well as coincide with points of intersecting zero U and zero V deep layer surface to 100 mb deep layer flow (from Xu and Gray, 1982).

There were only single points of zero U and zero V deep layer flow during the months of August and September in the Northwest Pacific west of 140°E (see Fig. 3.9). There was very good agreement between these two intersection points and the climatological maxima for slow motion and looping for the same region depicted in Fig. 3.8. Other points of zero U and zero V deep layer flow intersection exist farther east in the Northwest Pacific, but they are not illustrated and have less significance in indicating climatologically preferred areas for TC slow motion and/or looping. In the Atlantic, the westernmost intersection points for zero U and zero V deep layer flow correlate the best with the most favored slow motion and looping areas (see Figs. 3.8 and 3.10). Overall, there is good agreement between areas which tend to have both zero U and zero V deep layer flow and areas where motion and looping occur most frequently.

3.3 Deep Layer Flow Climatology Used to Explain Storm Recurvature

A short study was performed to see if the centroids of recurvature for TCs in both the Atlantic and Northwest Pacific Ocean Basins coincided with any points of intersection of zero U and zero V deep layer surface-100 mb flows. Visual approximation of TC recurvature centroids was done in the Atlantic using tracks compiled by the U.S. Dept of Commerce from 1886-1986. Pacific tracks from 1946-1969 were obtained for visual approximation from a Navy technical paper (Gray 1970). The points of intersection from Fig. 3.9 were close to visually approximated centroids of recurvature (see Fig. 3.4a). Recall that only the westernmost points of intersection are illustrated in Fig. 3.9.

The pattern of recurvature centroid agreement with zero U and zero V deep layer flow intersection points is similar in the Atlantic (see Figs. 3.5a and 3.10). Again, easternmost zero U and zero V deep layer flow intersection sites were farthest from the visually determined centroids of recurvature. August had six points of zero U and zero V deep layer flow intersection, with the second from the west lying closest to the centroid of track recurvature. September had 4 points of zero U and zero V deep layer flow intersection, with one point of near intersection signified by a square lying at about 27.5°N, 72.5°W.

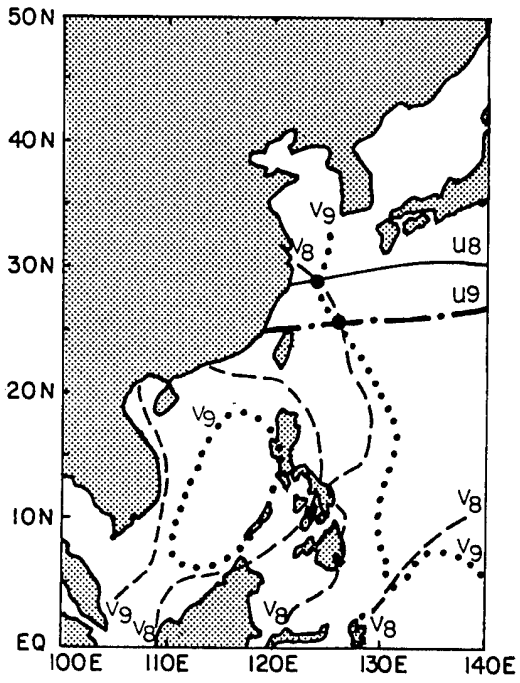

Figure 3.9: Climatology of 1979-1988 for the position of both zero U and zero V deep layer surface to 100 mb flows in the Northwest Pacific for the months of August and September. The solid, dot/dashed, dashed, and dotted lines denote where zero surface to 100 mb deep layer flows exist for August U, September U, August V and September V, respectively.

By coincidence, this point of near intersection lies closest to the track recurvature centroid for September.

In general, then, fairly good agreement occurs between visually determined centroids of track recurvature and intersection points for zero U and V deep layer surface to 100 mb flow. However, westernmost points of zero U and zero zero V deep layer flow intersection seem to be more significant indicators of visually estimated centroids of storm track recurvature.

3.4 Summary

Examining a ten-year climatological data set reveals fundamental characteristics about the TC formation and motion environments. The TC formation and motion environments are remarkably similar - both are baroclinic. This baroclinicity is evidenced by a tropospheric deep layer wind flow maximum over the TC center. The TC resides in a "warm pocket", i.e., the greatest 850-200 mb thickness is directly over the TC center,

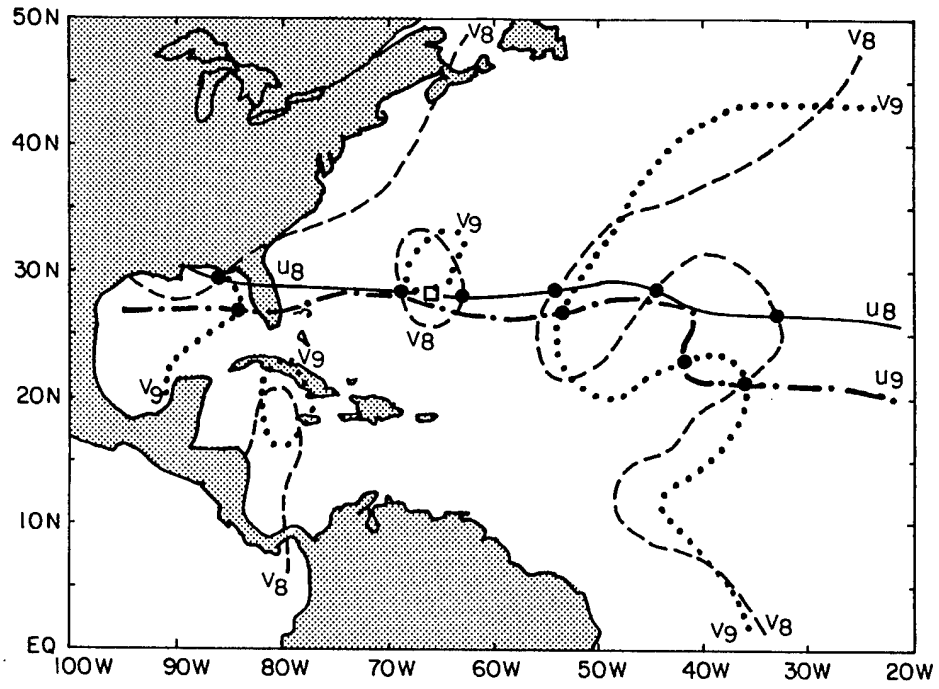

Figure 3.10: Climatology of 1979-1988 for the position of both zero U and zero V deep layer surface to 100 mb flows in the Atlantic for the months of August and September. The solid, dot/dashed, dashed, and dotted lines denote where zero surface to 100 mb deep layer flows exist for August U, September U, August V and September V, respectively.

with lower thicknesses to either side of the TC track. The tropospheric deep layer U zero shear line occurs over the TC center, with shears of opposite signs to each side of the TC track.

The deep layer wind flow maximum follows seasonal shifts in the TC track. The "warm pocket" and zero U shear lines are more evident in the ten-year climatological data set over TCs in the NW Pacific than they are in the Atlantic.

Slow motion and looping of TCs are correlated with each other. They both occur where climatologically weak deep layer flows exist in the troposphere (usually in the vicinity of the subtropical ridge axis). Tropical cyclone recurvature tends to take place near points of intersecting zero U and zero V sfc-100 mb deep layer flows.

Chapter 4

TROPICAL CYCLONE DEEP LAYER STEERING FLOW CHARACTERISTICS

Tropical cyclones move primarily in response to the deep layer flow they are embedded in. Furthermore, TCs can form only under specific environmental conditions. These environmental conditions required for TC genesis don't change very much initially after the TC has formed. Rather, they persist and continue to influence the evolution and motion of the TC as it follows a track which is prescribed by the surrounding winds.

A signature for these environmental flow characteristics exists in both climatological data as well as composite sounding data. The relationship between these two data sets will be provided in the details of this chapter.

Another primary goal of this chapter will be to show that the same environment the TC forms in continues to influence it after formation. Specifically, TC motion will be tied to persistent large scale environmental flow characteristics. There is a connection between the TC motion environment and the TC genesis environment.

4.1 Deep Layer Flow Characteristics

George and Gray (1976) showed that environmental flow was statistically significant in acting to steer TCs. Analyzing the characteristics of this "steering flow" further should cast more light on why TCs move as they do. One way to do this is to determine how the environmental flow varies laterally along a TC track. A couple of these analyses will be performed in this section.

When the environmental flow profile at right angles to the TC track was analyzed using composite sounding data for 16 TC stratifications in both the Atlantic and Northwest

Pacific, a clear trend emerged for the strongest winds following the TC to be situated near the TC's center. When environmental winds following the TC were computed at both 850 mb and 300 mb, then averaged together for all 16 Atlantic and Northwest Pacific TCs, bow shaped profiles were generated. These profiles support the premise of a wind maximum following the TC to be located near the TC center (see Figs. 4.1 and 4.2). Also note in this same figure that the No Motion cases had fairly flat wind profiles and that the fast motion TC cases had relatively peaked wind profiles. This just indicates that a TC center's forward speed is merely a function of the strength of the environmental flow it resides in.

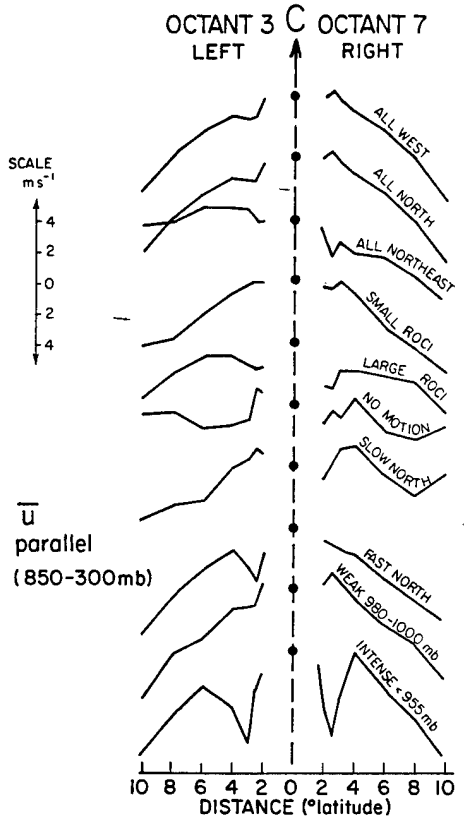

Figure 4.1: Environmental winds following Northwest Pacific TCs were computed at two levels, then averaged in this figure. The two levels averaged were 850 mb and 300 mb. Vortex winds (all octant averaged tangential winds in the (MOT) frame of reference were subtracted from tangential winds in the (MOTROT) frame of reference) to obtain environmental winds following the TC. Note the prevalence for strong following environmental winds near the center, and also the relatively flat environmental wind profile for the no motion case. The arrow and C at the top of the figure indicates the direction of TC motion.

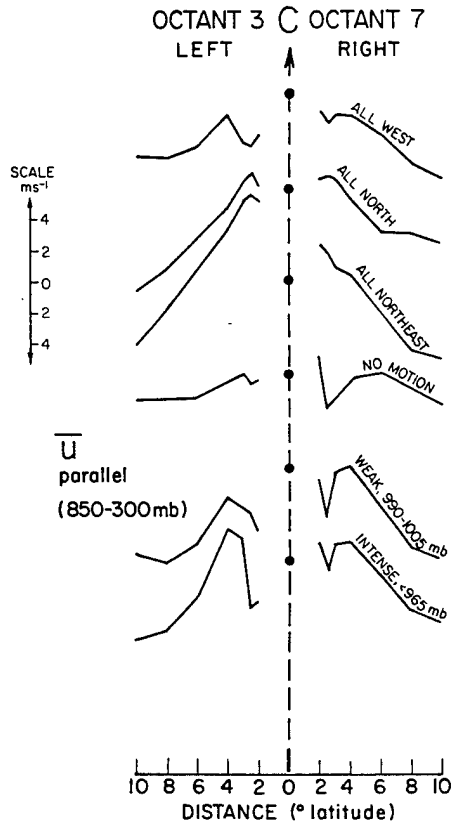

Figure 4.2: Same as for Fig. 4.1 , except Atlantic TC cases are illustrated here.

The environmental wind profile can also be plotted from deep layer flows computed from composite sounding data. When this is done for the mass-weighted deep layer flow between the surface and 100 mb following the TC for six TC cases, profiles with peaks near the TC's center are graphed again. When these profiles are compared with similar deep layer flows plotted from the 10 year climatological data set discussed in Chapter 3, the pattern for strongest following winds to be near the center continues to hold (see Fig. 4.3a-f).

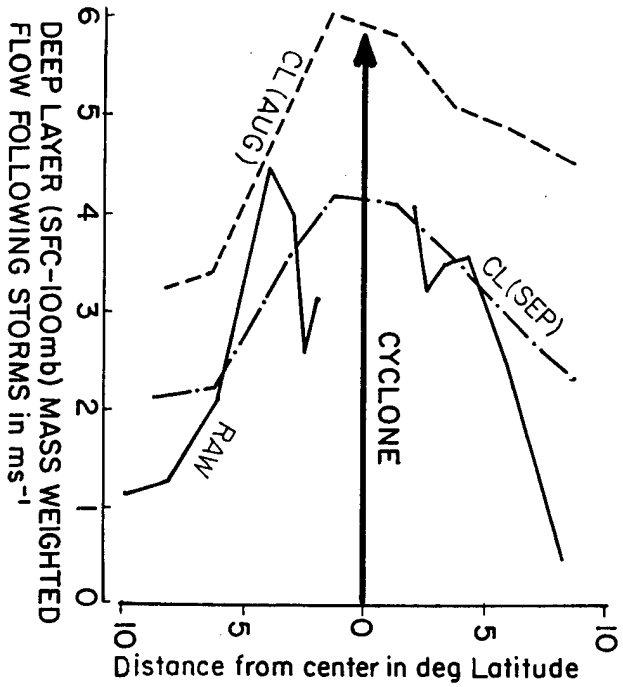

Figure 4.3: a. Comparative environmental winds blowing behind the Atlantic All West moving TCs. The solid line denotes the environmental wind from composite rawinsonde sounding data. Specifically, to compute the environmental wind from rawinsonde data, all octant averaged tangential winds (MOT) are added to/subtracted from parallel winds (ROT) on the left/right sides, respectively. The dashed lines indicate north/south cross-sections centered 13.75°N, 80°W on climatological maps depicting 1979-1988 average monthly surface to 100 mb deep layer flows.

The monthly wind profiles from the climatological data set generally had weaker following wind maxima than the wind profiles from the composite data set. Apparently, climatological variations in TC tracks are acting to smooth out the wind profiles in the climatology data set.

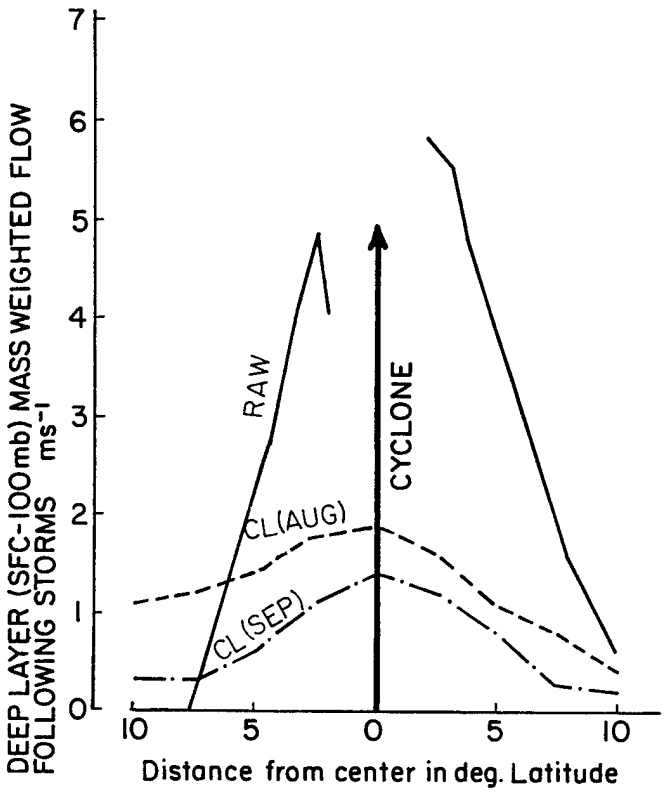

Figure 4.3: b. Same as Fig. 4.3a, but for the Atlantic All North movers. Dashed lines show east/west cross-sections centered at 27.5°N, 75°W.

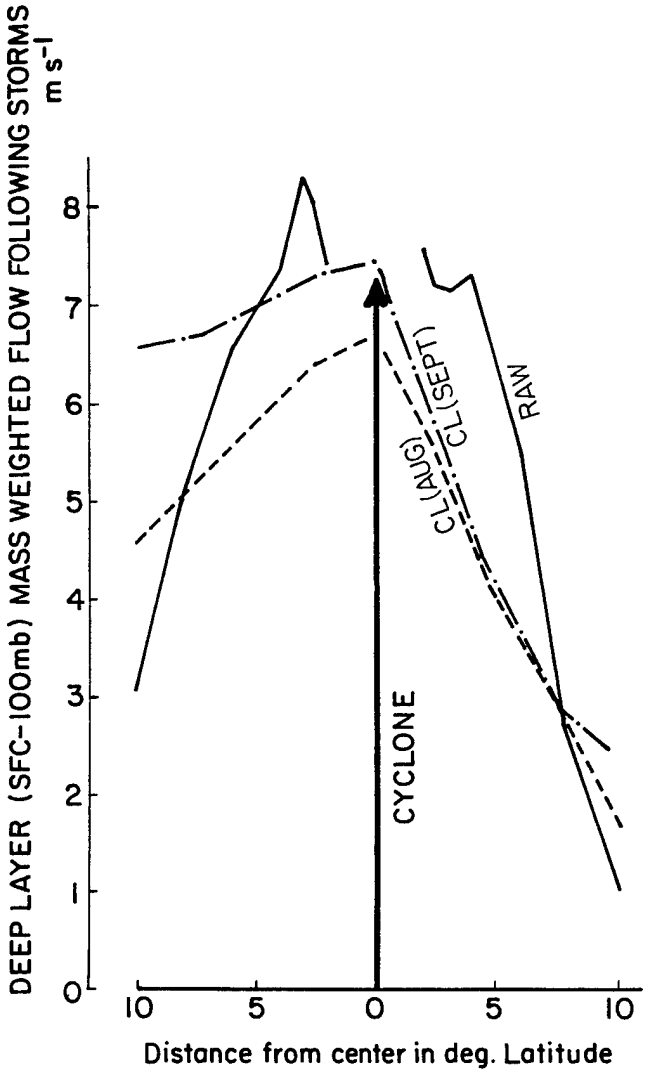

Figure 4.3: c. Same as Fig. 4.3a, but for the Atlantic All Northeast movers. All dashed lines reflect cross sections centered at 35°N, 75°W. On the left side facing the direction the TCs move, the cross section is directly west to 35°N, 85°W. To the right of the TC track facing the direction the TCs move, the cross section is toward the southeast to 30.5°N, 61°W.

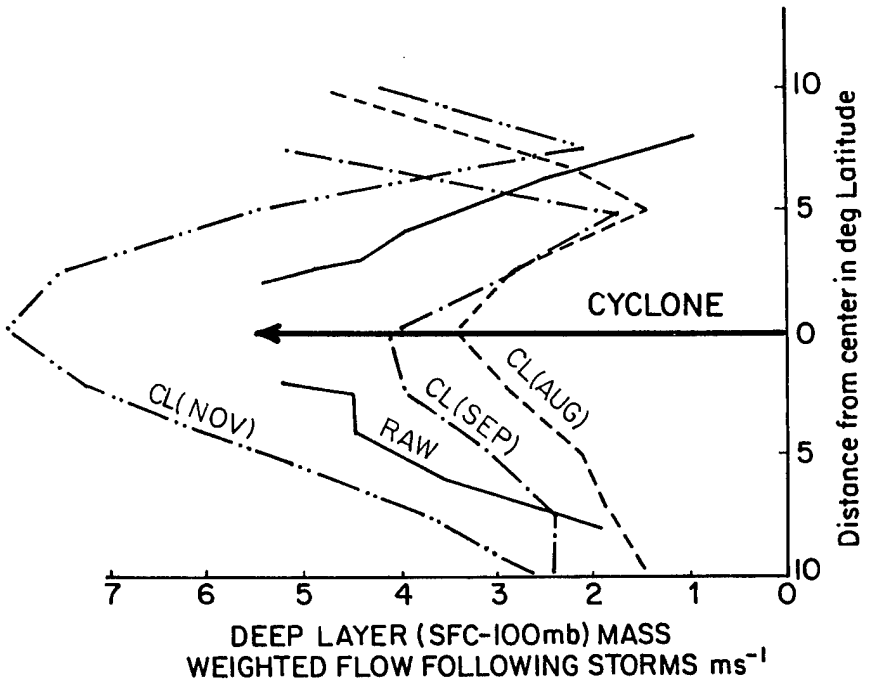

Figure 4.3: d. Same as Fig. 4.3a, but for the Northwest Pacific All West movers. Dashed lines show north/south cross sections along the 137.5°E longitude line. Latitudes used for August, September, and November which intersected 137.5°E are 25°N, 22.5°N and 12.5°N, respectively.

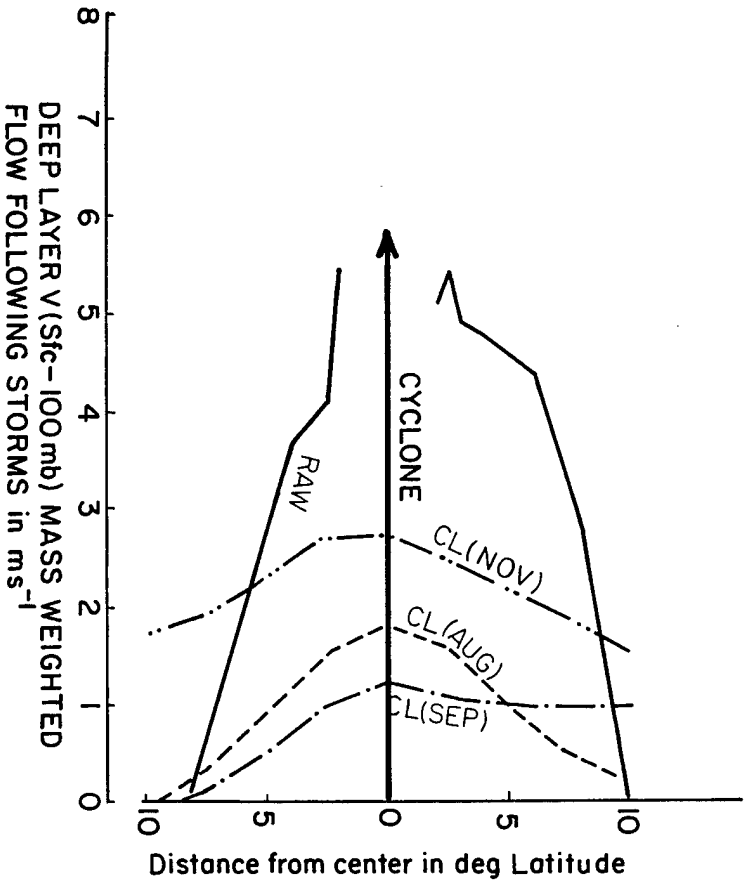

Figure 4.3: e. Same as Fig. 4.3a, but for the Northwest Pacific All North movers. Dashed lines indicate east/west cross sections centered at 25°N, 135°E. Deep layer V flow is used here and in the last figure to more clearly resolve the environmental wind component following the TC.

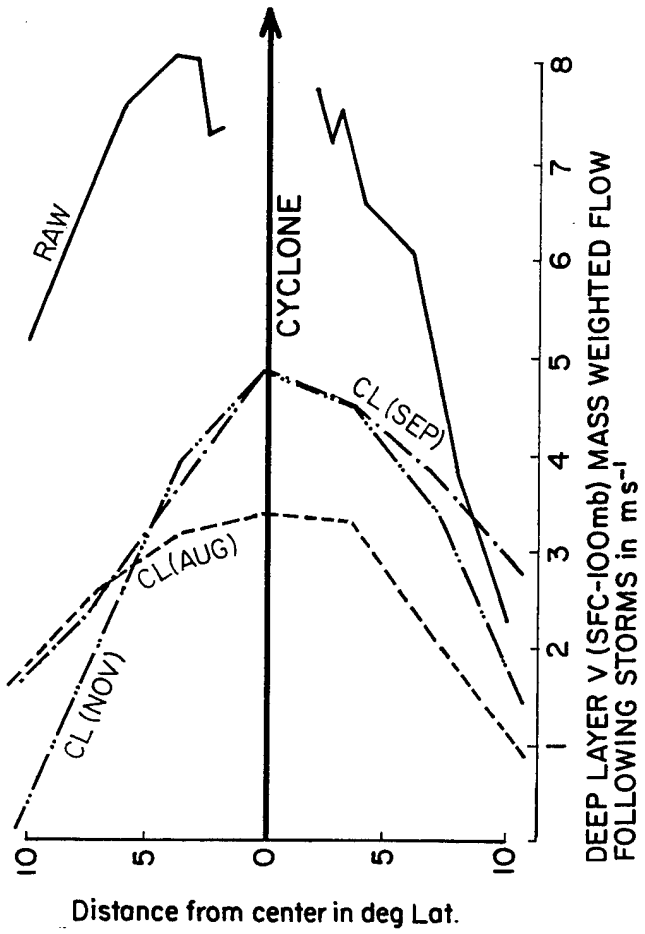

Figure 4.3: f. Same as Fig. 4.3e, but for the Northwest Pacific All Northeast movers. Dashed lines indicate NW/SE cross sections centered at 40°N, 130°E; 40°N, 140°E; and 35°N, 142.5°E for August, September, and November, respectively.

4.2 Forward Propagation Discussed

The peak evident in the environmental flows following TCs in both the Atlantic and Pacific also provides a clue to answering a question regarding forward propagation. George and Gray (1976) observed that TCs in the Northwest Pacific had forward speeds which were greater than the mean surrounding 700 mb winds for the 1-7° radial band. Specifically, the average ratio of TC speed to the surrounding flow just discussed for 13 different TC stratifications was 1.16.

A comparison of average TC speeds for 11 TC stratifications to the all octant averaged deep layer parallel winds in the (ROT) frame of reference within a 5 to 7° radial band results in no surprises. In all 11 cases, the TC speed exceeded the mass weighted winds in both the 1000-100 mb and 850-300 mb deep layers (see Table 4.1).

Table 4.1: Comparison of deep layer flows following the TC to TC speed for Atlantic and Northwest Pacific TCs. Deep layer flows in the first two columns are calculated using an all octant averaged parallel wind in the ROT frame of reference in a 5-7° radial band surrounding the TC. Tropical cyclone speed in the last column is self-explanatory. Note how the TC speeds are uniformly higher than the deep layer flows following the TC.

TC Stratification	1000-100 mb Deep Layer Flow Following TC (ms^{-1})	850-300 mb Deep Layer Flow Following TC (ms^{-1})	TC Speed (ms^{-1})
Atlantic All West	2.90	3.32	5.75
Atlantic All North	3.01	3.10	4.87
Atlantic All Northeast	6.49	6.20	7.24
Northwest Pacific Slow North	1.88	2.69	2.92
Northwest Pacific Fast North	6.60	7.01	9.78
Northwest Pacific All West	3.84	3.67	5.40
Northwest Pacific All Northeast	6.98	7.48	8.50
Northwest Pacific Small ROCI	4.41	4.49	5.67
Northwest Pacific Large ROCI	3.77	4.22	5.66
Atlantic No Motion	0.56	0.75	1.13
Northwest Pacific	0.72	0.78	1.22
Averages	3.74	3.97	5.29

A peak in the environmental wind field near the TC center would provide an explanation for why TC centers always outrun their surrounding mean deep layer flows. Environmental wind profiles just depicted are just as consistent in showing the strongest

environmental winds following the TC near the center as are past studies in showing TCs moving forward faster than their mean surrounding flows.

4.3 Environmental Shear Profile

Another environmental characteristic observed along TC tracks is a reversal of environmental shear between two pressure levels from one side of the TC track to the other. In this study, the pressure levels chosen for examination were 850 and 300 mb. The sign of the 300-850 mb shear did indeed reverse as expected for all 10 TC stratifications examined from the left side of the TC track to the right side. Furthermore, this change was consistent in sign for all 10 cases. On the left side of all the TC tracks, the shear indicated an increase in the component of the wind following the TCs with height. On the right side of all the TC tracks, the shear present showed an increase of the component of the wind in opposition to the TCs' forward motion with height (Fig. 4.4a-d). In other words, the TC track was located on the zero shear line between regions of positive and negative shear.

Furthermore, not only did the sign of the shear change, but the values of shear on both sides of the TC track were significant. 300 - 850 mb shear varied from about $+10 ms^{-1}$ 10 degrees to the left of the TC track to about $-10\ ms^{-1}$ 10 degrees to the right of the TC track.

An attempt was made to remove the TC's influence from the environmental shear profile to obtain an environmental shear profile representative of what would be present in the absence of the TCs. An extra step in the shear computation procedure discussed above was added. At both 850 and 300 mb, tangential winds in the (ROTMOT) frame of reference were subtracted from the parallel winds in the (ROT) frame before the shear computation for 300-850 mb. Unfortunately, no clear pattern other than very weak shear values emerged.

The emergence of the weak shear pattern appears to be a result of an inability to separate baroclinicity attributable to the TC from that of the background environment. Tangential winds circulating around the center of a TC "feel" both the baroclinicity due

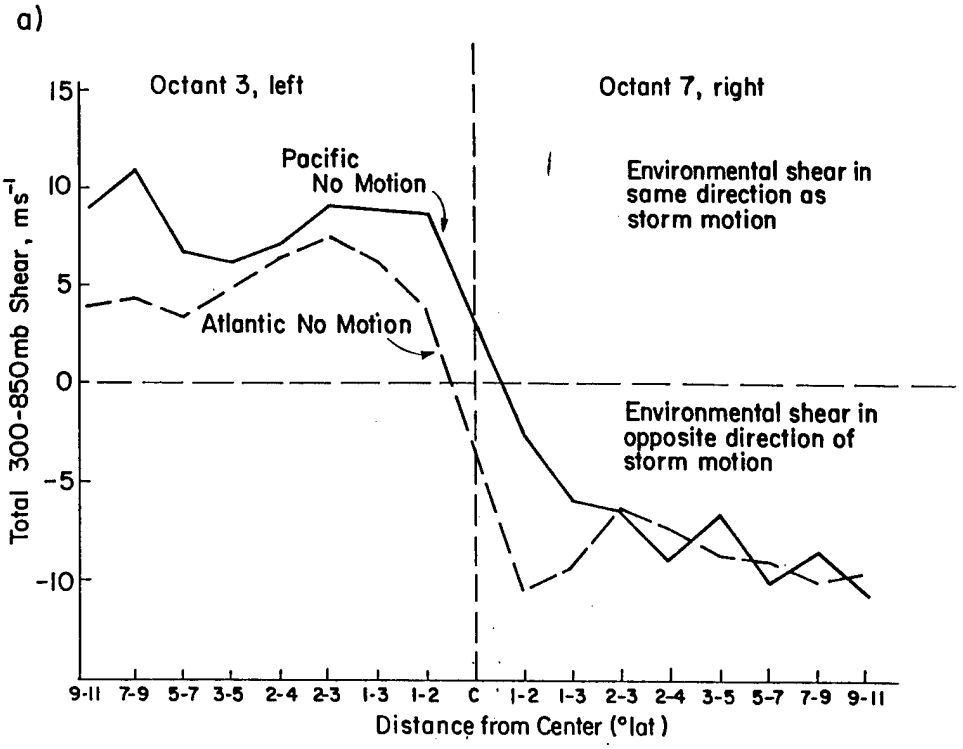

Figure 4.4: (a-d) a. Environmental 850-300 mb shear profiles for Atlantic and Northwest Pacific TCs. Profiles are from left to right across the TC tracks, and parallel winds in the (ROT) system are used in the computations. Positive numbers indicate winds increasing with height (or becoming less negative) in the same direction the TC is moving. Observe that the shear changes sign on opposite sides of the TC track.

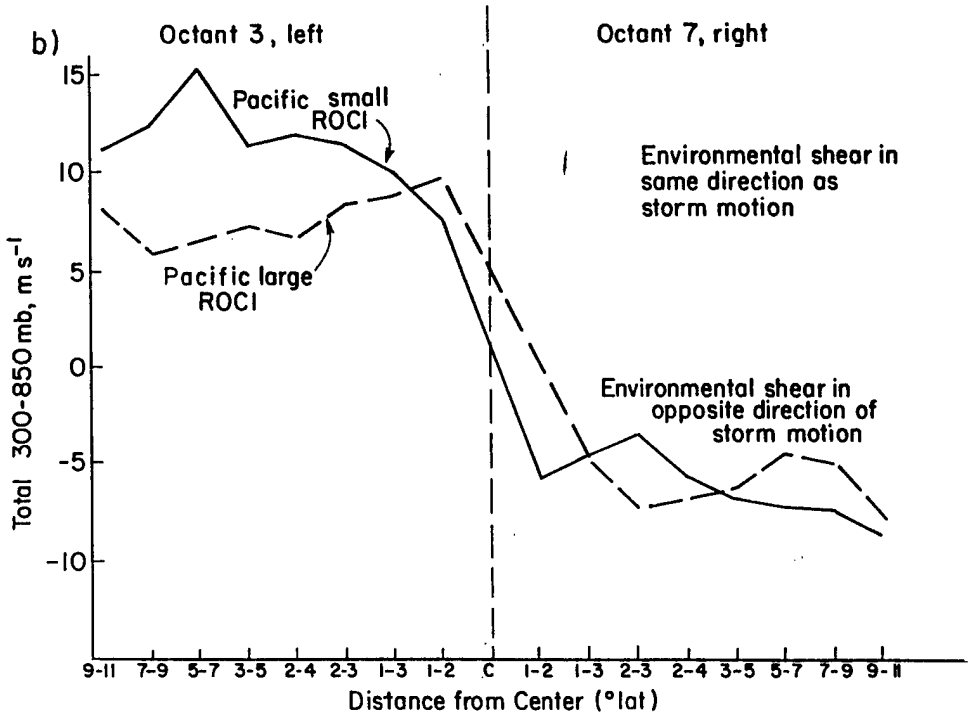

Figure 4.4: b.

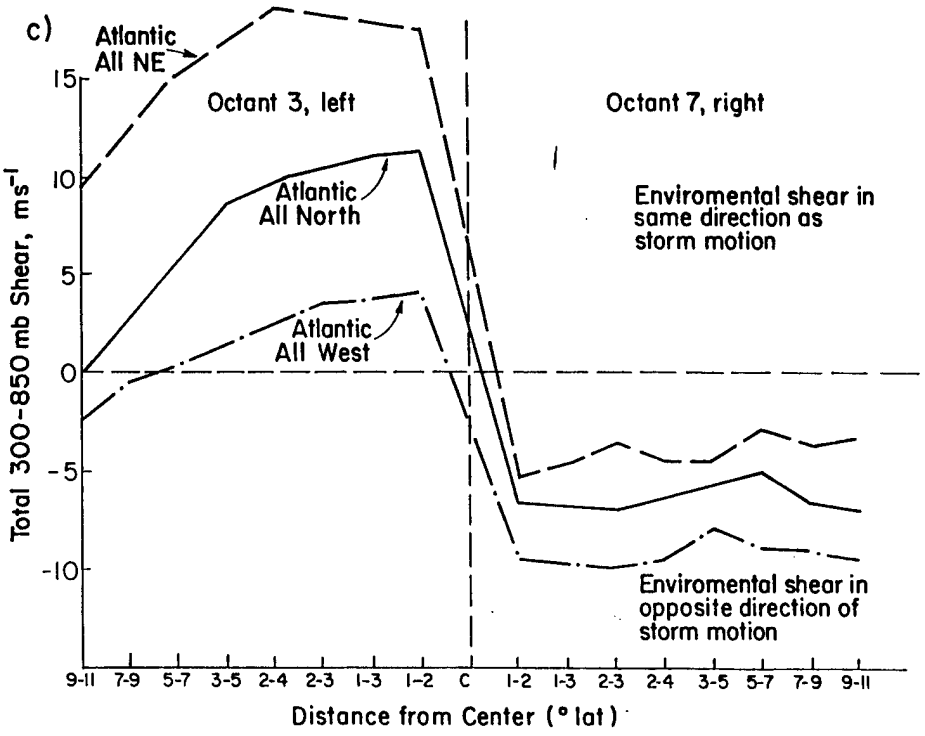

Figure 4.4: c.

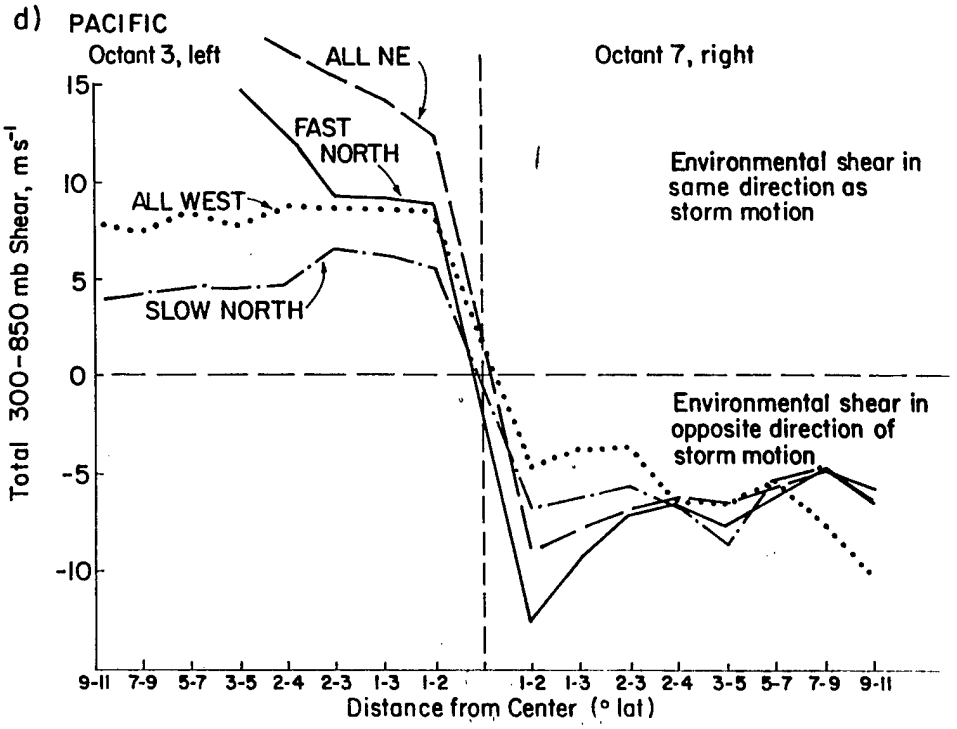

Figure 4.4: d.

to the warm core of the TC as well as the baroclinicity of the environment with the TC removed. Thus, an attempt to arrive at an environmental shear profile via subtracting tangential winds in the (ROTMOT) frame of reference from parallel winds in the (ROT) frame of reference on opposite sides of the TC track will not be successful. Because the winds in the TC's surroundings respond to baroclinicity of any origin, any attempt to distinguish between wind shear caused by the TC from wind shear present in the environment before the TC arrived will fail.

Note that in any circumstance, the influence of the TC's vortex on the parallel winds in the (ROT) system becomes insignificant out away from the TC center in the 9-11° radial band. This means that wind shears computed at this distance from the TC center will be representative of the environment with no TC present. Figure 4.4 depicts significant shears of opposite sign in the 9-11° radial band, so a sign change must occur across the TC track. The shear pattern in Fig. 4.4 is relatively symmetric, so one can infer the position of zero environmental 300-850mb shear lies very close to the TC track.

The vertical wind shear profile to each side of the TC track also provides information as to how the TC moves faster than its mean surrounding flow. The vertical wind shear present as a result of environmental baroclinicity causes the wind components following the TC to be less to the right and left of the TC track. A glance at Fig. 4.5 will provide an idealized cross-sectional view of the tropical atmosphere in the vicinity of a TC's formation and initial movement area.

4.4 The "Warm Pocket"

The pattern of opposite shears to the left and right of TC tracks just discussed implies a thickness ridge right over the TC track by the thermal wind equation

$$\frac{\Delta U}{\Delta P} = -\frac{R}{f\bar{p}}\frac{\Delta T}{\Delta y} \tag{4.1}$$

Evidence for such a thermal ridge in the Northwest Pacific has already been found in the 10 year climatology data discussed in Chapter 3 (Fig. 3.4). Interestingly, the existence of

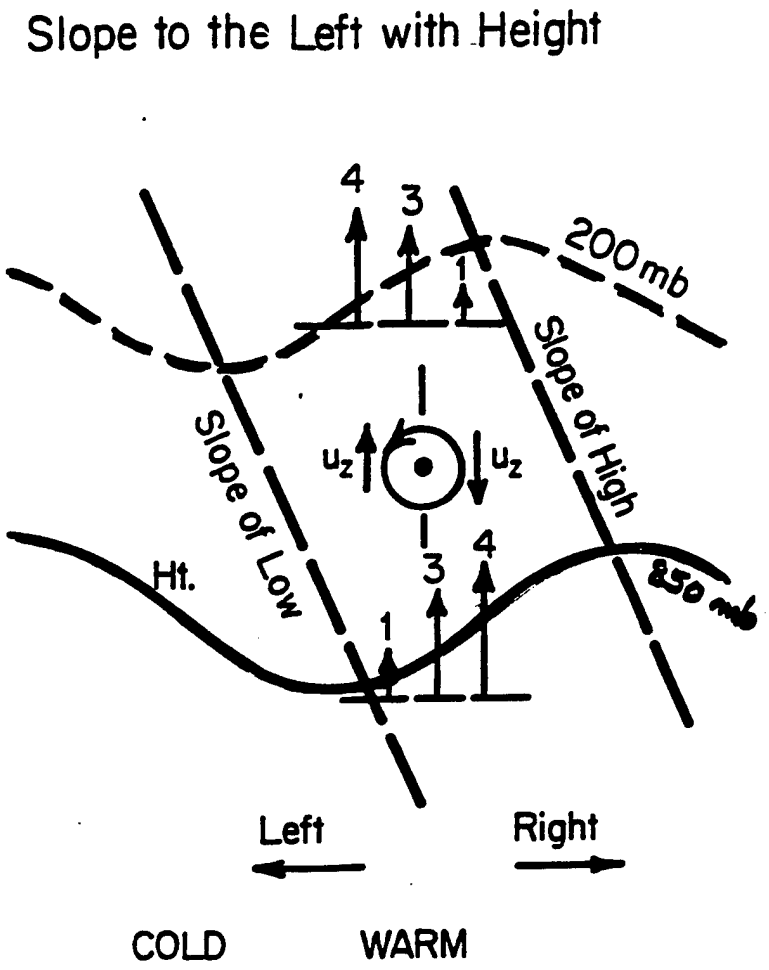

Figure 4.5: Idealized vertical cross section of the typical slope of the TC's left to right environmental 850 mb and 200 mb height fields with associated idealized environmental wind components parallel to the cyclone motion. Cyclone winds are not included. The cyclone and the winds are directed into the paper. This typical picture is valid for all cyclone direction orientations (Gray 1992).

this "warm pocket" or "tongue" of relatively warm air aligned along the axis of the TC track was postulated by Simpson (1946). Figure 4.6 provides an idealized cross-section of this "warm pocket". Note how the 850-200 mb thickness increases when a TC develops in the favorable "warm pocket" environment.

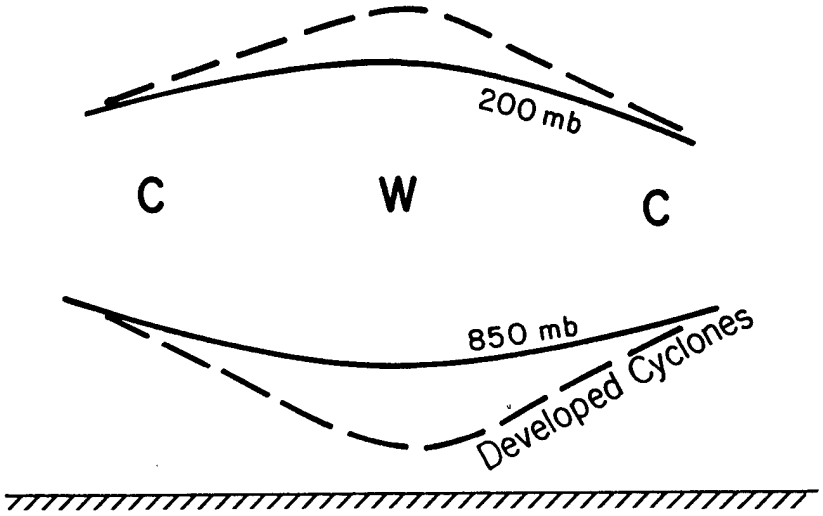

Figure 4.6: Idealized cross section of the "warm pocket" TCs form in. The TC track is perpendicular to the plane of the page.

4.5 Similarities Between the Motion and Genesis Environments

When a TC forms the environmental conditions conducive to its formation do not go away, but persist and remain influential in guiding the newly formed TC. Quite a bit of work has been done in determining what conditions are favorable for TC genesis. Required conditions for TC genesis which have been uncovered by past researchers will be recalled. Then they will be compared to the environmental conditions which govern the TC's motion.

When McBride and Zehr (1981) analyzed the differences between developing and non-developing tropical systems in the Atlantic and Northwest Pacific, they identified two conditions which must be satisfied a priori for development to occur. Development depended upon 1) a strong north-south gradient of vertical shear of the zonal wind. Development also depended upon 2) the system being situated right on the zero shear line between the regions of positive and negative shear as depicted earlier in Fig. 3.3.

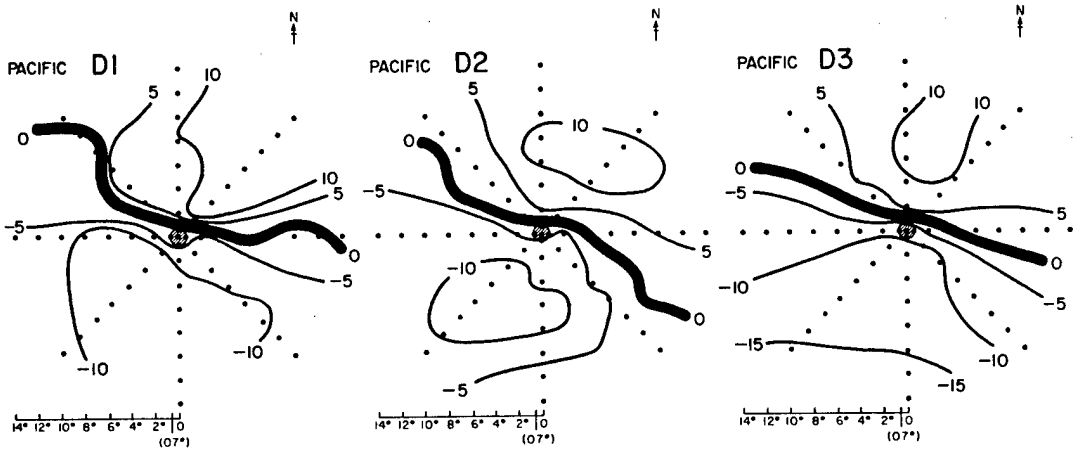

Figure 4.7: Plan views of zonal shear, $U_{200mb} - U_{900mb}(ms^{-1})$ for Pacific data sets. D1, D2 and D3 denote three stages of TC development. These are the early pretyphoon cloud cluster, pretyphoon cloud cluster, and intensifying cyclone, respectively (from McBride, 1979)

.

Both of these genesis conditions are present in the environments which steer TCs (see Fig. 4.7), especially before recurvature. Tropical cyclone tracks in the deep tropics during and shortly after formation are almost universally aligned east/west. Thus, the vertical wind shear present will be almost entirely zonal. Vertical shears of $\pm 10ms^{-1}$ which were discussed in Section 4.3 are significant, hence the first genesis condition discussed here persists in the environment which guides the TC after it has formed. The second condition required for genesis has already been shown to exist in Section 4.3.

McBride and Gray (1979) noted that Northwest Pacific TCs needed a "warm pocket" for formation, but the Atlantic TCs did not require a "warm pocket" for formation. McBride and Gray attribute this difference to Northwest Pacific TCs forming in a monsoon trough environment, whereas Atlantic TCs form in a trade wind environment. This mirrors the environmental conditions encountered in this study and discussed in Section 4.4. Outflow channels for TCs in the Northwest Pacific and Atlantic reflect TCs which have formed in these two different environments. McBride and Gray (1979) show the environmental shear patterns which support outflow channels to the north and south for Northwest Pacific TCs are reflective of a "warm pocket" environment. A single outflow

channel to the north for Atlantic TCs is reflective of location in the absence of a distinct, relatively symmetric "warm pocket."

Basically, there is continuity between TC genesis and motion environments. Fundamental environmental parameters such as wind shear profiles which are reflective of a baroclinic environment, height profiles, and thickness profiles remain strikingly similar to their genesis values as a TC proceeds from formation to being advected along by the deep-layer flow.

Chapter 5

PROPAGATION OF TROPICAL CYCLONES (TC) TO THE LEFT OR RIGHT OF DEEP LAYER TROPOSPHERIC STEERING FLOWS

This chapter seeks explanations for known tendencies of TCs to propagate to the left or right of the deep layer environmental flow centered on the disturbance. A point of clarification would be helpful before proceeding into the heart of this chapter. Propagation can also be attributed to tropical cyclone centers outrunning the average deep layer environmental flow in their vicinity. This forward propagation will not be examined in this chapter. Only left/right propagation will be looked into as this chapter proceeds. Also, propagation caused by differing local absolute vorticity tendencies within the TC vortex will not be examined here but will be looked into in the next chapter.

5.1 Best Measures for TC Steering Flow

Elsberry and Abbey (1991, 1992) found the most consistent representation of a TC steering vector in their study to be a deep layer vertical average through a 850-300 mb depth. This represents the layer of the troposphere between the boundary and outflow layers of the TC . Fitzpatrick (1992) determined from composite sounding analysis that the deep layer winds at a radius of 5-7° through the same layer as Elsberry and Abbey provide a good rule of thumb for TC steering flow as well. Accordingly, the 850-300 mb, as well as the 1000-100 mb deep layer flows will be used to examine left/right propagation.

5.2 Observed TC Propagation

George and Gray (1976) observed a consistent propagation of tropical cyclones in the Western Pacific in a range between 12 and 23 degrees to the left of the mean surrounding

winds at 500 mb. Soon afterward, Gray (1977) studied TCs in the Atlantic. He showed the same general behavior(between 3 and 17 degrees leftward propagation) as that observed for TCs in the Western Pacific, with one major exception. This exception is the west moving category of TCs, which propagated about 8 degrees to the right of the deep layer winds at a radius of 5 to 7 degrees. A goal here will be to provide at least one viable explanation for this propagation dichotomy.

In fact, two explanations using environmental winds will be offered to explain left/right propagation. The first will employ an approach using "normal wind blow through" in the (ROT) frame of reference. The second will take a look at "thermal wind blow through" as a cause of TC propagation to the left or right of the deep layer steering flow.

5.3 "Normal Wind Blow Through" Explained

One way to conceptualize TC left/right propagation is to view it as a reflection of the normal component of environmental winds in the (ROT) frame of reference which impinge on and pass through it. The normal component of the environmental winds in the (ROT) frame of reference blow from left to right across the path of the TC when facing the direction of TC motion. In other words, TCs appear to move to the left or right of the deep layer environmental flow within a certain radius. This happens because leftward or rightward blowing winds at that same radius will "blow through" the TC. The TC will then appear to propagate in an opposite sense(i.e., to the right or left, respectively) relative to the "blow through" winds.

Specifically, all octant averages in the (ROT) frame of reference for the normal wind blowing within a 5 to 7 degree radial band were vertically graphed from 1000 to 100 mb. Graphs for two Northwest Pacific cases (Fig. 5.1) and five Atlantic cases (Fig. 5.2) are provided. Note the overall reversal in normal winds for the Atlantic west moving cases versus the other cases illustrated. From the same deep layer flow data just discussed, deep layer flow averages were retrieved from the composite data set for two layers. These were 1000-100 mb and 850-300 mb (Table 5.1). Thirteen different TC cases were graphed,

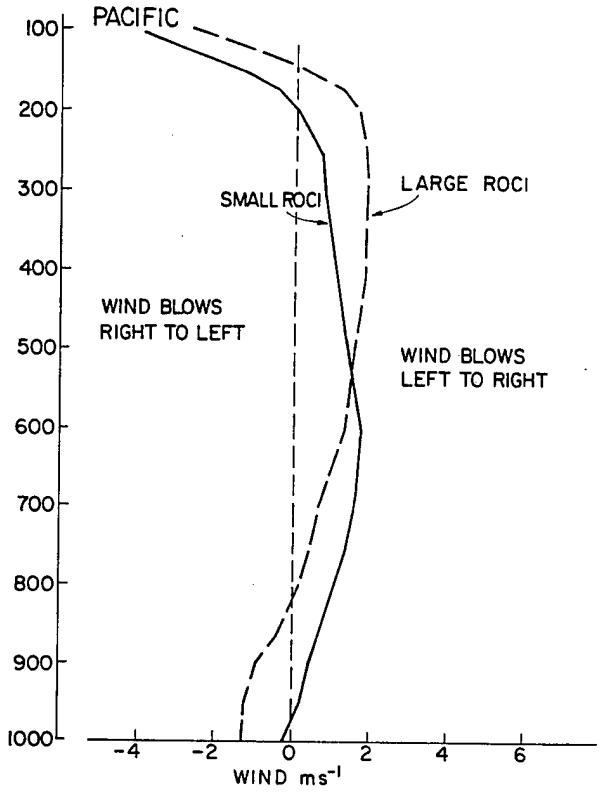

Figure 5.1: (a-b) Vertical graphs of the normal wind in the ROT frame of reference for the NW Pacific. The wind is all octant averaged within a 5-7° radial band. Normal winds blowing through the TCs from left to right indicate propagation to the left.

using 18 levels(100, 125, 150, 175, 200, 250, 300, 350, 400, 500, 600, 700, 750, 800, 850, 900, 950, and 1000 mb). As one might anticipate from section 5.1 of this chapter, the 850-300 mb deep layer normal wind flows were a better indicator of the direction of "normal wind blow through" than the 1000-100 mb deep layer normal wind flow. For all 14 cases analyzed, the direction of the 850-300 mb deep layer normal wind flow indicated the observed direction of "normal wind blow through." In all the 850-300 mb cases except the Atlantic west movers, "normal wind blow through" from left to right(rightward) reflected actually observed leftward propagation. The Atlantic west movers exhibited a right to left "normal wind blow through."

The 1000-100 mb deep layer normal wind flow was not as good an indicator for the direction of "normal wind blow through" (see Table 5.1). For 3 TC stratifications (Pacific Fast West, Pacific All West, and Pacific All North), the 1000-100 mb deep layer normal

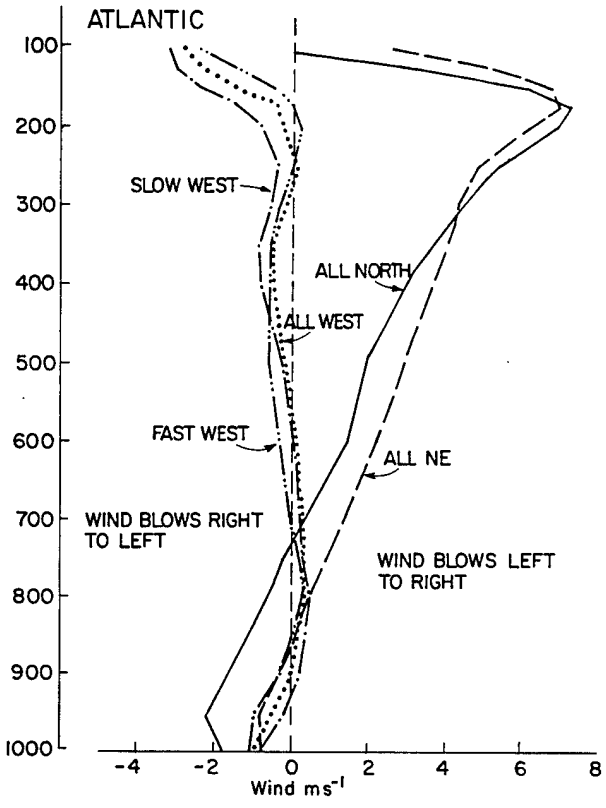

Figure 5.2: Vertical graphs of the normal wind in the ROT frame of reference for the Atlantic. The wind is all octant averaged within a 5-7° radial band. Note how "normal wind blow through" is reversed between the west moving TCs and all other categories.

Table 5.1: Deep layer all octant averaged normal winds in the 5-7° radial band. ROT frame of reference is used. Negative values denote a normal wind blowing from right to left, with positive values signifying a normal wind blowing from left to right. Note 850-300 mb deep layer normal winds are better at exclusively predicting propagation to the right for Atlantic west movers without any false indications for other directions of movement.

Deep Layer Normal Winds 1000-100 mb

Description	Normal Wind, ms^{-1}
Atlantic Slow West	-0.42
Atlantic Fast West	-0.38
Atlantic No Motion	0.57
Atlantic All West	-0.21
Atlantic All North	1.75
Atlantic All Northeast	2.52
Pacific Slow West	0.14
Pacific Fast West	-0.15
Pacific No Motion	0.05
Pacific All West	-0.04
Pacific All Northeast	2.01
Pacific Small ROCI	0.73
Pacific Large ROCI	0.77

Deep Layer Normal Winds 850-300 mb

Description	Normal Wind, ms^{-1}
Atlantic Slow West	-0.17
Atlantic Fast West	-0.31
Atlantic No Motion	0.47
Atlantic All West	-0.03
Atlantic All North	1.35
Atlantic All Northeast	2.25
Pacific Slow West	1.04
Pacific Fast West	0.68
Pacific No Motion	0.21
Pacific All West	0.83
Pacific All Northeast	1.98
Pacific Small ROCI	1.31
Pacific Large ROCI	1.15

wind flow did not indicate the observed motion correctly due to strong right to left winds occurring between 300 and 100 mb. This pressure interval lies above the top of the best steering layer of 850-300 mb, so the reason for the failure of the 1000-100 mb deep layer normal wind flow to perfectly indicate the direction of deep layer "normal wind blow through" would be the existence of strong winds counter to the direction of the deep layer "normal wind blow through" at a level where their influence on the TC's motion is lessened.

5.4 "Thermal Wind Blow Through" Explained

A second approach to explaining left/right propagation is to employ a "thermal wind blow through" argument. The thermal wind blows along thickness(e.g., 850-300 mb) contours for a given pressure layer, with cold air lying to the left of the thermal wind vector when facing the same direction it points (see Fig. 5.3). "Thermal wind blow through" happens when a TC moves within a baroclinic environment(which is always!). For example, when a TC moves from relatively warm air toward relatively cold air, it encounters a thermal wind component from left to right across its path. This thermal wind component from left to right is felt by the TC as "thermal wind blow through" in the same direction. Now, relative to the "thermal wind blow through" from left to right, the TC moves from right to left. This right to left TC movement with respect to the thermal wind component can be viewed as leftward propagation. For all the TC stratifications, this is the usual situation encountered. Only the Atlantic west moving TCs display rightward propagation behavior. One might anticipate that this class of TCs moves from relatively cold air toward relatively warm air. This would reverse the direction of "thermal wind blow through" and, consequently, the direction of left/right propagation.

The best evidence available to support this second approach is a set of 40 850-300 mb average height change profiles done in the (ROT) frame of reference with plot points 0.5, 1.5, 2.5, 3.5, 4.5, 5.5, 6.5, 8.0, 10.0, 12.0, and 14.0 degrees latitude from the center taken with the rear of the TC to the left and the front of the TC to the right. Atlantic west movers show a tendency to have greater overall thicknesses in their forward direction

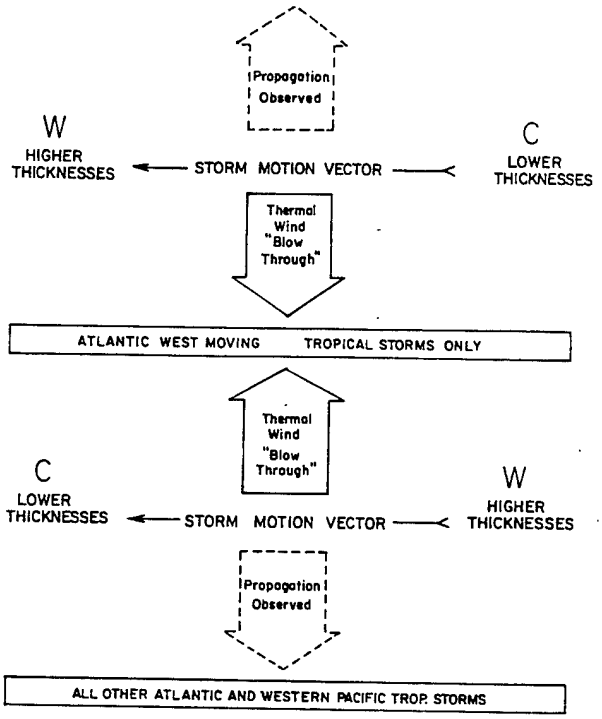

Figure 5.3: Tropical cyclone propagation explained using a schematic diagram of "thermal wind blow through" for a deep layer such as 850-300 mb.

of motion, while all the other cases show a clear tendency for lower overall thicknesses to reside in the forward flank of the TC. An Atlantic All West case and Atlantic All North case are provided in Figs. 5.4a and 5.4b as examples of Atlantic TCs. Figure 5.4c provides an All West case as an example of a NW Pacific TC.

The second best evidence available in support of "thermal wind blow through" is a collection of temperature plots on a constant 850 mb pressure surface for 11 different Western Pacific TC stratifications. For 10 of the 11 stratifications, the TC motion vector carries it toward cooler air at 850 mb. This would support "thermal wind blow through" from left to right, leading to leftward propagation. The assumption being made here is that the thickness gradient between 850 and 300 mb would follow the same pattern as the observed temperature gradient at 850 mb. Figure 5.5 is provided using the Northwest Pacific Slow North moving TC stratification as an example.

No clear, consistent evidence to support "thermal wind blow through" can be found in the 10 year climatology for the Atlantic and Western Pacific 850-200 mb thicknesses.

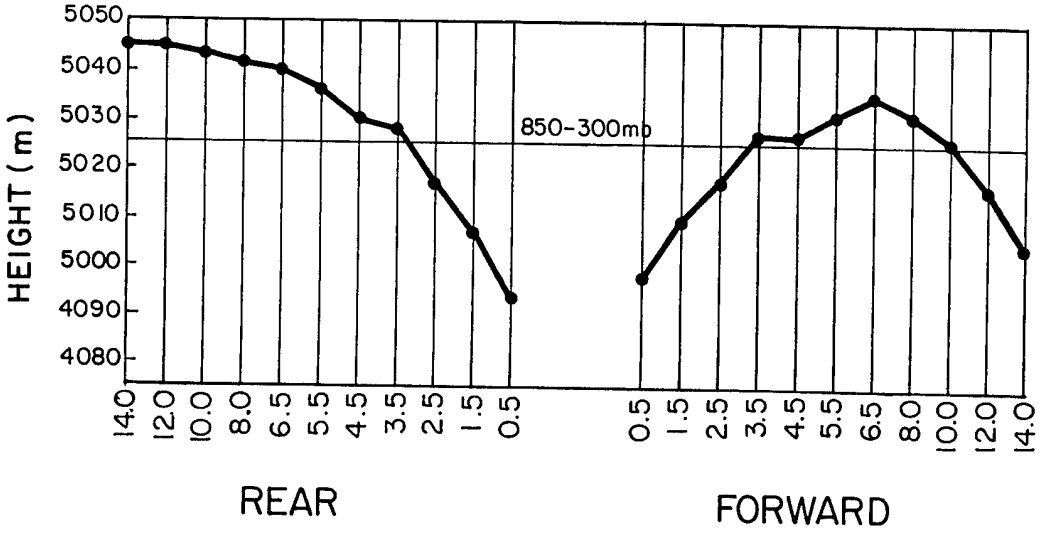

Figure 5.4: a. Average height change profile for nine pressure levels in a 850-300 mb inclusive interval (850, 800, 750, 700, 600, 500, 400, 350 and 300 mb). Plot points represent values from the 0-1, 1-2, 2-3, 3-4, 4-5, 5-6, 6-7, 7-9, 9-11, 11-13, and 13-15 degrees latitude radial bands for both the forward and rear portions of the TC. This height profile is plotted for the Atlantic All North TC category.

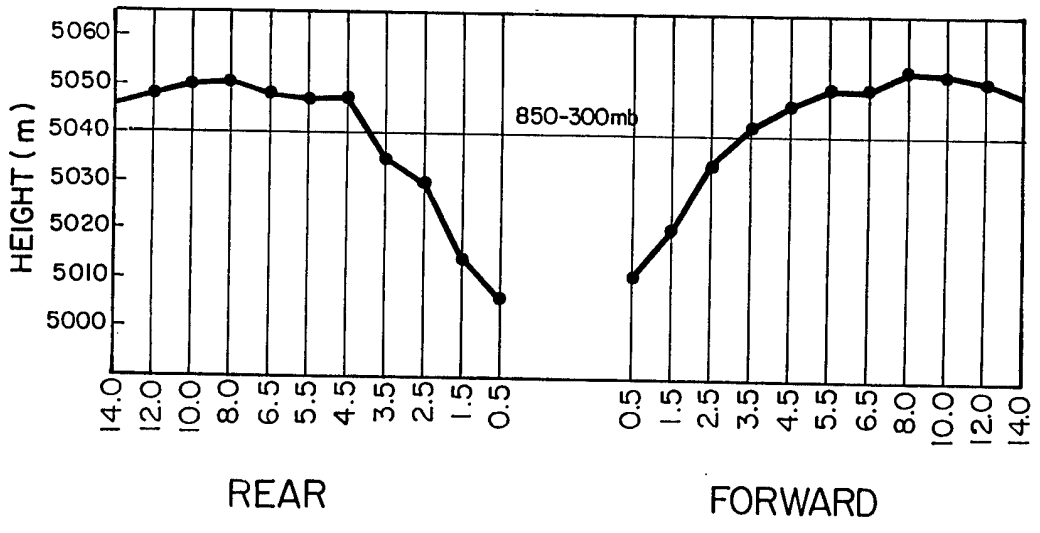

Figure 5.4: b. Same as Fig. 5.4a, except this height profile is plotted for the Atlantic All West TC category.

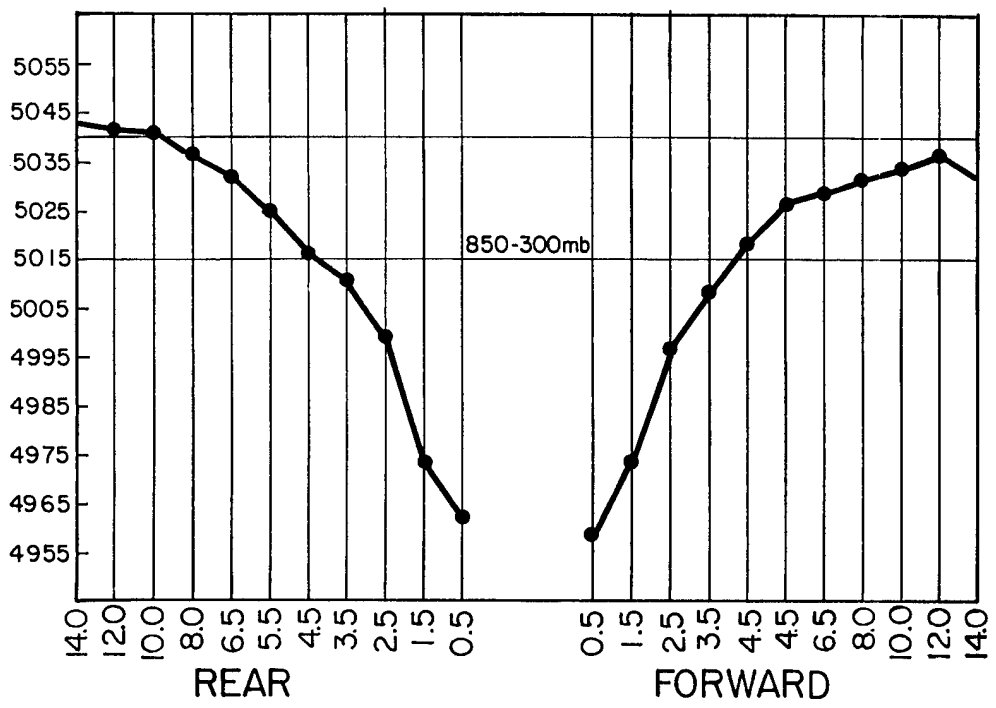

Figure 5.4: c. Same as Fig. 5.4a, except this height profile is plotted for the Northwest Pacific All West TC category.

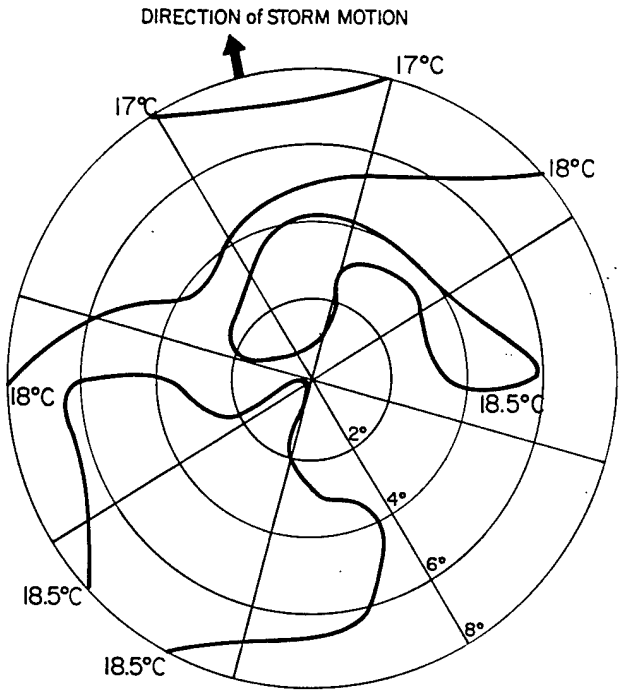

Figure 5.5: Temperature analysis in °C on a constant 850 mb pressure surface, with plot points for each octant at radii of 2, 4, 6, and 8 degrees latitude. The motion frame of reference used is the NAT frame, with north toward the top of the figure. The specific TC category illustrated here is the Northwest Pacific Slow North moving TC. The direction of TC motion is toward 352.61° as shown by the arrow.

Monthly mean TC tracks overlaid on the 850-200 mb thickness field for the same month did not consistently show movement toward warm air for Atlantic west moving TCs, nor did it consistently show movement toward cold air for all other TC stratifications.

5.5 Synoptic Environments Used to Explain "Thermal Wind Blow Throughs" in Opposite Directions

The Atlantic west moving TC experiences "thermal wind blow through" in the opposite direction from all other TC motion direction categories. A comparison of the synoptic environment of the Atlantic west moving TC to the synoptic environment of all the other TC motion categories in may shed some light on why the Atlantic west moving TC experiences "thermal wind blow through" from right to left and why all the other TC motion categories experience "thermal wind blow through" from left to right. The synoptic environment the Atlantic west moving TC moves through is a trade wind environment. As the Atlantic west moving TC crosses the ocean from east to west, it travels from relatively cool waters off Africa to relatively warm ocean waters in the Caribbean. Air which comes in contact with these waters becomes relatively cool to warm from east to west as a consequence. The prevailing trade winds which guide this TC category west also prevent advection of relatively warm air to the front of the TC from its source region. The same trades also inhibit advection of relatively cold air behind the TC from its source region(see Fig. 5.6b). Thus, relatively warm air remains in front of the Atlantic west moving TC, and relatively cool air remains behind it. This is the thermal wind environment shown at the top of Fig. 5.3.

As the Atlantic west moving TC recurves north, then northeast, it begins to move toward colder waters. This sets up a thermal wind environment shown at the bottom of Fig. 5.3.

In the Northwest Pacific Ocean, the synoptic environment is different. It is characterized by the presence of a monsoon trough. Relatively warm waters lie equatorward of the trough, and relatively colder waters lie poleward of it. In contrast to the Atlantic trade wind environment, the monsoon trough environment allows advection of different

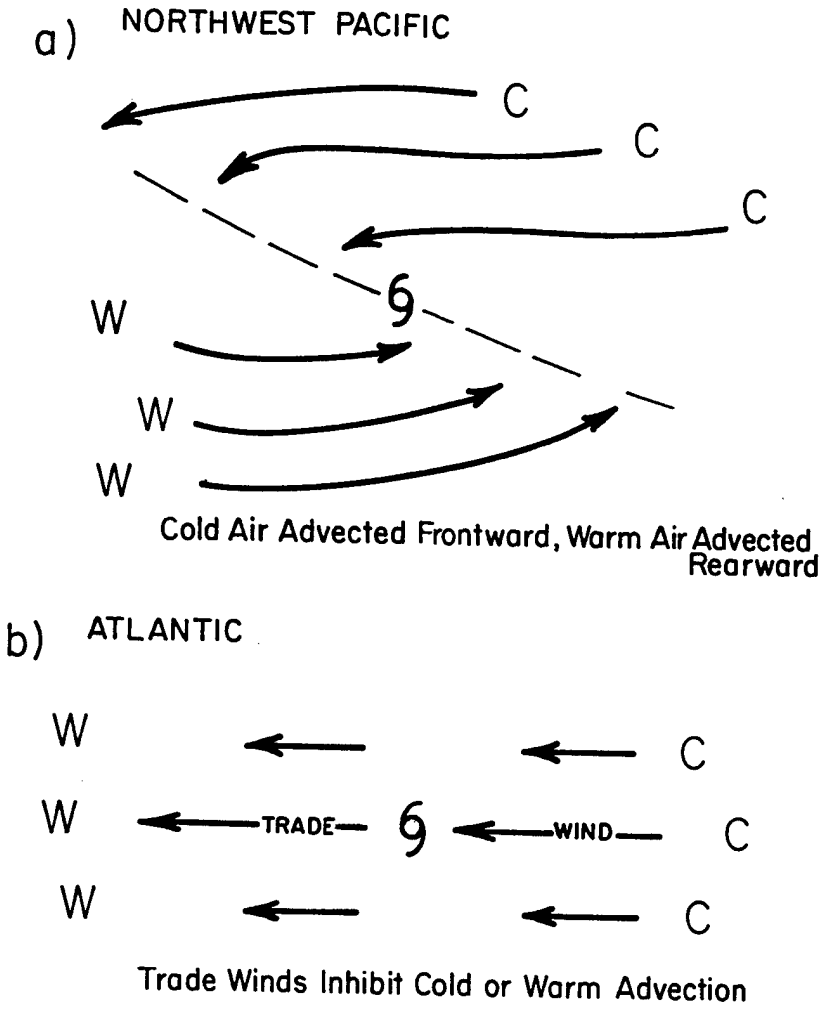

Figure 5.6: Idealized synoptic overview of opposing "thermal wind blow through" environments for the Atlantic and Northwest Pacific. Note how the prevailing trade wind environment in the Atlantic prevents both advection of cold air in front of the TC as well as warm air to the rear of the TC. In contrast, the monsoon trough environment in the Northwest Pacific permits such advections to take place.

air masses to occur from their source regions. Prevailing westerlies to the south of the monsoon trough advect relatively warm air to the rear of the TC, while prevailing easterlies to the north of the monsoon trough advect relatively cool air to the front of the TC(see Fig. 5.6a). As a consequence of this circulation pattern, the Pacific west moving TC moves toward relatively cool air. Therefore, a "thermal wind blow through" from left to right happens as is shown at the bottom of Figure 5.3.

As Northwest Pacific TCs recurve and move north, then northeast, they also move toward colder waters like their Atlantic counterparts. Again, the thermal wind setup depicted at the bottom of Figure 5.3 applies.

To summarize, it takes a trade wind environment with relatively warm waters ahead of a TC to provide the proper conditions for "thermal wind blow through" from right to left. Rightward propagation will then be observed. All other synoptic environments have the TC moving towards colder waters already, or allow differential advection of relatively cold and relatively warm air to create a situation where the TC moves toward colder air. Accordingly, every TC motion category except the Atlantic west moving TC will experience "thermal wind blow through" from left to right. As a consequence, all these cases will exhibit propagation to the left.

In summary, evidence in the environmental data exists to support both the concept of left/right propagation as a reflection of "normal wind blow through" and also left/right propagation as a reflection of "thermal wind blow through." Evidence for "normal wind blow through" exists in its best form as vertical graphs of all octant averaged normal winds in the (ROT) frame of reference within the 5-7° radial band. Evidence for "thermal wind blow through" can best be found in the form of 850-300 mb thickness profiles plotted with the rear/front of the TC on the left/right, respectively. Perhaps "normal wind blow through" and "thermal wind blow through" are synonymous. The magnitude of the "thermal wind blow through" could be determined using the thermal wind relation. In this study, only the direction of the "thermal wind blow through" was ascertained. Finally,

left/right propagation is a relative phenomenon, with the observed TC propagation being in the opposite direction as the measured "normal/thermal wind blow through."

Chapter 6

GEOSTROPHIC IMBALANCE THEORY AS A CAUSE OF SOUTHERN CONVERGENCE

6.1 North/South Asymmetry of Convergence

In the past it has been noted that the divergence pattern is not symmetric between the north and south halves of the TC cases on the average. Figure 6.1 shows a clear tendency for convergence to the south of TCs. Note that this inflow occurs throughout the 850-300 mb deep layer radial winds inside 10° radius. In this chapter, only the 850 mb pressure level will be examined, but in later chapters the 850-300 mb deep layer will be the focus of study. One possible mechanism for this asymmetry could be the development of a geostrophic imbalance in the tangential winds as they circulate around the TC vortex from north to south.

6.2 Diagnosing Geostrophic Imbalance

A way to diagnose the development of such an imbalance in the tangential wind flow is to employ the geostrophic wind equation in cylindrical coordinates. The equation is expressed as $V_\theta = g\partial z/f\partial r$, where V_θ is the tangential wind on a constant pressure surface, g is the acceleration due to gravity, f is the Coriolis parameter, and $\partial z/\partial r$ is the height gradient on a constant pressure surface. The level of 850 mb was chosen as the diagnostic level, and an interval of 5.5° latitude was chosen for evaluating the height gradient at specific locations 6° latitude to the north and south of the TC center. A point to note here is that the geostrophic wind approximation will be valid at this radius. This means the gradient wind equation $fV_t + V_t^2/r = g\frac{\partial z}{\partial r})_p$ will approximate the geostrophic wind equation very well. A scale analysis of the 2 terms to the left of the equality sign in

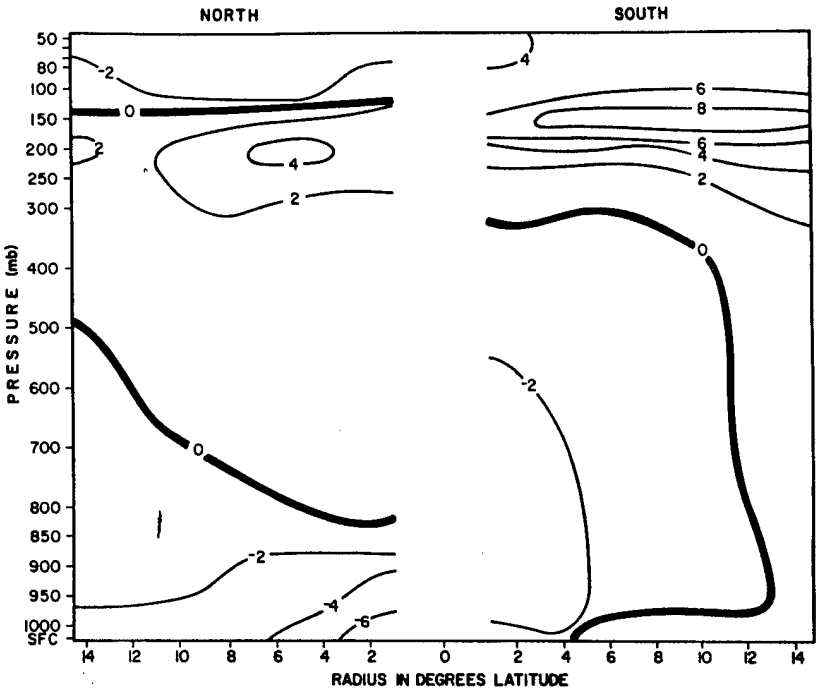

Figure 6.1: North/South cross section of V_r with TC motion vectors subtracted from winds (MOT), (ms^{-1}) (from Frank, 1976)

the gradient wind equation gives the first term an order of 10^{-4}, and the second one an order of 10^{-7}. Thus, the geostrophic wind approximation holds.

Height data were readily available for 14 different TC stratifications. Two height cross section formats were available. These were left/right and front/rear. Six of the 14 cases were chosen for scrutiny here in Table 6.1. Since these height data were not in the (MOT) system, an effort had to be made to select the height profile which most closely matches a north/south cross section. Accordingly, left/right or front/rear height data were selected based upon the TC's heading. For example, a straight west moving TC would have left/right height data chosen as south/north height data. Since nature does not cooperate perfectly and direct TCs straight west, north, etc., an error is generated by choosing the height data in this way. The average height data deviation from directly north/south for the six TCs examined here is roughly 22°. No effort was made to quantify the effect of this error. The Coriolis parameter was calculated at both 6° to the north and south of the average latitude for each TC case. Actual tangential winds in the (MOT) system were compiled 6° to the north and to the south of each TC system. The average tangential winds at 850 mb 6° to the north and south of all six TC centers were 5.93 ms^{-1} and 5.26 ms^{-1}, respectively. The average height change between 2.5° and 8.0° radius to the north and south of the same six TC centers was 40.9 m and 42.3 m, respectively. These serve as estimates of the height gradient at 6° to the north and south of this group of TCs. Because g and r are constants in the geostrophic wind equation as it is used here, there is an easier way to see if the height gradient relaxes in concert with the southward weakening of f. This way compares the ratio of total height changes between 6° north and south of the TC center for all six cases to the ratio of total changes in f for all six cases between 6° north and south of the TC center. When this is done, the ratio of height change at 6°N to height change at 6°S is about 1.02 (see Table 6.1). In comparison, the f change ratio is about 1.68. Note the predominance of higher f change ratios relative to height change ratios.

Table 6.1: Comparison of north versus south 850 mb height gradients to north/south Coriolis parameter change. Radial height gradients are measured from 2.5-8.0° in a poleward 45° octant versus an equatorward 45° octant.

North of TC to TC Stratification	Ratio of $\vec{\nabla}z$ vs f at 6° $\vec{\nabla}z$ South of TC	Ratio of f at 6° to the North N-S $\vec{\nabla}z$ to to the South	Ratio of N-S Δf
Atlantic All West	1.37	1.91	0.72
Atlantic All North	1.23	1.53	0.80
Atlantic All Northeast	0.58	1.39	0.42
Pacific All West	1.04	2.12	0.49
Pacific All North	1.02	1.63	0.63
Pacific All Northeast	0.85	1.48	0.57
Averages	1.02	1.68	0.61

6.3 Convergence Asymmetries Explained Using Geostrophic Imbalance

Table 6.1 suggests that as the tangential winds at 850 mb circulate from north to south around TCs, they encounter a height gradient which becomes too strong for the ever weakening Coriolis force to resist. Another way to state this is that the height gradient is more symmetric than the distribution of f across the TC from north to south. Thus, on the south side of an average TC, one would expect convergence to occur as the pressure gradient force pushes the tangential winds at 850 mb inward against the relatively weak Coriolis force there. See Fig. 6.2 for an illustration of this process.

Height gradients are also relatively symmetric from west to east at 850 mb. See Table 6.2 for ratios of west versus east 850 mb height gradients. Tables 6.1 and 6.2 show the TC vortex to have a symmetric height gradient in all four quadrants relative to f.

Another way to explain the predominance of south side convergence uses the tangential wind profile around the average TC and f. One can recall that the tangential winds are approximately equal around the average TC from north to south. The same tangential wind blowing on the south side of the TC is pulled to the right less than the same tangential wind on the north side. Again, south side convergence prevails under the explanation.

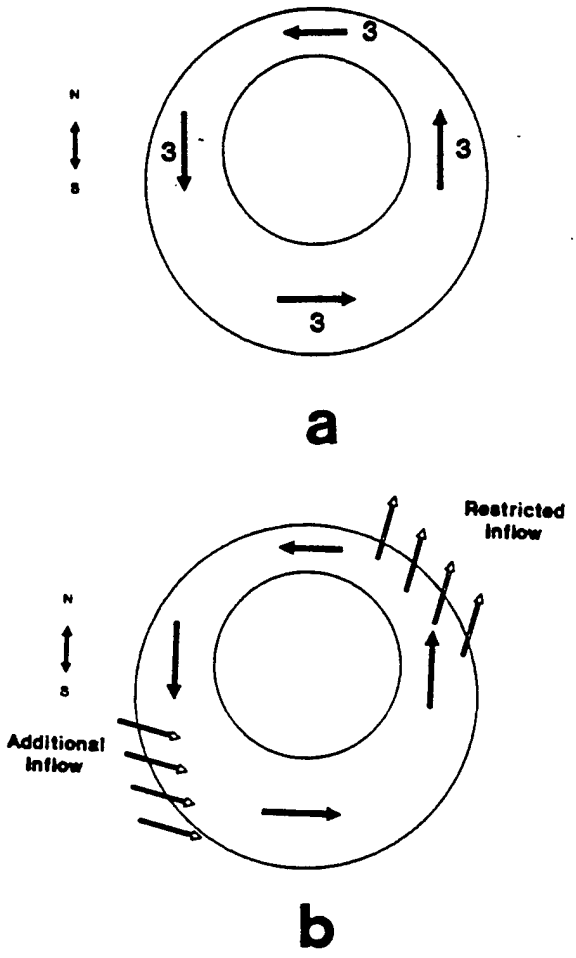

Figure 6.2: Conceptualization of the process that produces more convection in the southwest quadrant. (a) Shows an exaggeration of the pressure gradient required to maintain three units of tangential wind (MOT coordinate system) in each quadrant. (b) Shows the extra radial inflow that is required to mass balance the tangential circulation due to the extra mass in the southwest quadrant (Hallin 1991).

Table 6.2: Ratio of west versus east 850 mb height gradients. Radial height gradients are measured from 2.5-8.0° in a 45° octant facing west versus a 45° octant facing east.

TC Stratification	Ratio of $\vec{\nabla}z$ West of TC to $\vec{\nabla}z$ East of TC
Atlantic All West	0.94
Atlantic All North	0.54
Atlantic All Northeast	1.08
Pacific All West	0.95
Pacific All North	0.68
Pacific All Northeast	1.07
Averages	0.88

Another factor to consider in explaining the dominance of south side convergence is that the Rossby radius of deformation is roughly 2 times larger 6° to the south versus 6° to the north of the average TC center. Thus, the geostrophic adjustment process would be about 2 times slower on the south sides of TCs at this radius.

Chapter 7

SATELLITE IMAGERY OF ENHANCED EQUATORIAL VERSUS POLEWARD DEEP CONVECTION

It is one thing to show in theory that convergence in TCs tends to predominate in the southmost octants versus the (northmost) octants; it is another to find visible natural signs that such a bias really exists. One way to seek evidence for such convergence on the south side of TCs is to search for a local maximum in deep convection in the area where it is predicted to occur in theory.

7.1 Relative Importance of Geostrophic Imbalance Versus "Blow Through" in Determining Convergence

Geostrophic imbalance, which was discussed in the previous section, appears to be the primary cause for this asymmetry in convergence. In west moving TCs, "blow through" convergence/divergence contributes as well in octants 4 and 8, respectively. The north moving TC cases still show divergence in octant 8, where one would expect "blow through" convergence. This information lends itself to the conclusion that convergence caused by ageostrophy dominates convergence caused by the TC's motion relative to the surrounding wind field ("blow through" convergence).

7.2 Asymmetries in Deep Convection

If this relationship holds in nature, an asymmetry in deep convection should exist between octants 4 and 8 in the (ROT) frame of reference. Furthermore, the asymmetry should maximize along an axis which passes through both of these octants. Accordingly, the next step will be to look for a local maximum of deep convection in an azimuthal range between directly south and directly south-southwest of the TC center in satellite

imagery. A coincident minimum in deep convection should exist in the opposite direction. Evidence for this has already been compiled by Hallin(1991), as shown in Figs. 7.1 and 7.2. Gray and Shoemaker (1989) discussed the dominance of deep convection on the south sides versus the north sides of Pacific typhoons as well.

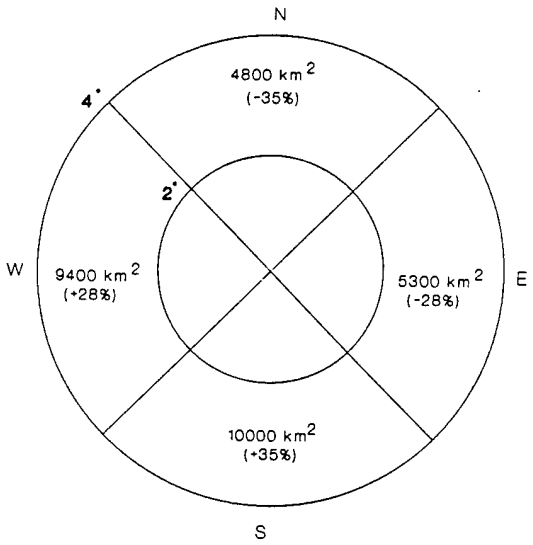

Figure 7.1: Average area of deep convection with cloud tops colder than -75°C in each quadrant at 2-4° radius. The quadrant deviation from the symmetric area average is shown in parenthesis (Hallin, 1991).

A composite GMS IR satellite image of Supertyphoon Vanessa in the Northwest Pacific Ocean(see Fig. 7.3) shows just such an asymmetry. A maximum in deep convection is clearly seen oriented to the WSW. The color enhancement scheme from Table 2.1 shows the cloud top temperatures depicted from the outermost white contour to dark red at the center to be in the range of –50 °C to –79 °C. Cloud top temperatures less then –50°C can be found on black and white satellite images on and inside the third white contour from the center of the TC. Every white contour crossed toward the center of the TC indicates a 10°C drop in cloud top temperature. This range of temperature can only be attributable to deep convection(Zehr, personal conversation). A minimum can be seen in the NNE direction.

Composite GMS IR imagery of 10 typhoons in the Northwest Pacific during 3 different life cycle stages is used for the next example. These 3 stages represent the middle of the

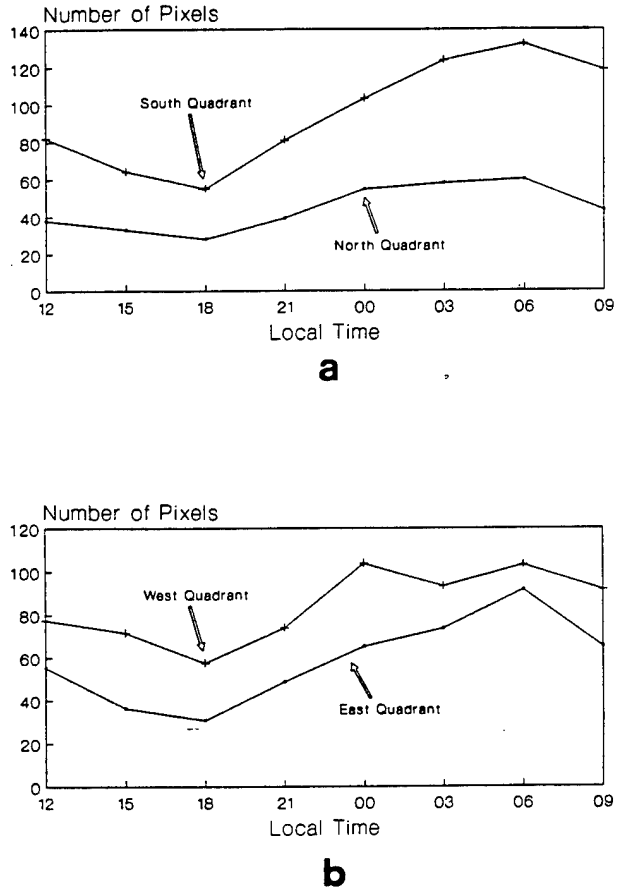

Figure 7.2: Diurnal variation in convective asymmetries as shown in the number of pixels colder than -75°C in the 2-4° radial belt for (a) the north and south quadrants and (b) the east and west quadrants (Hallin, 1991).

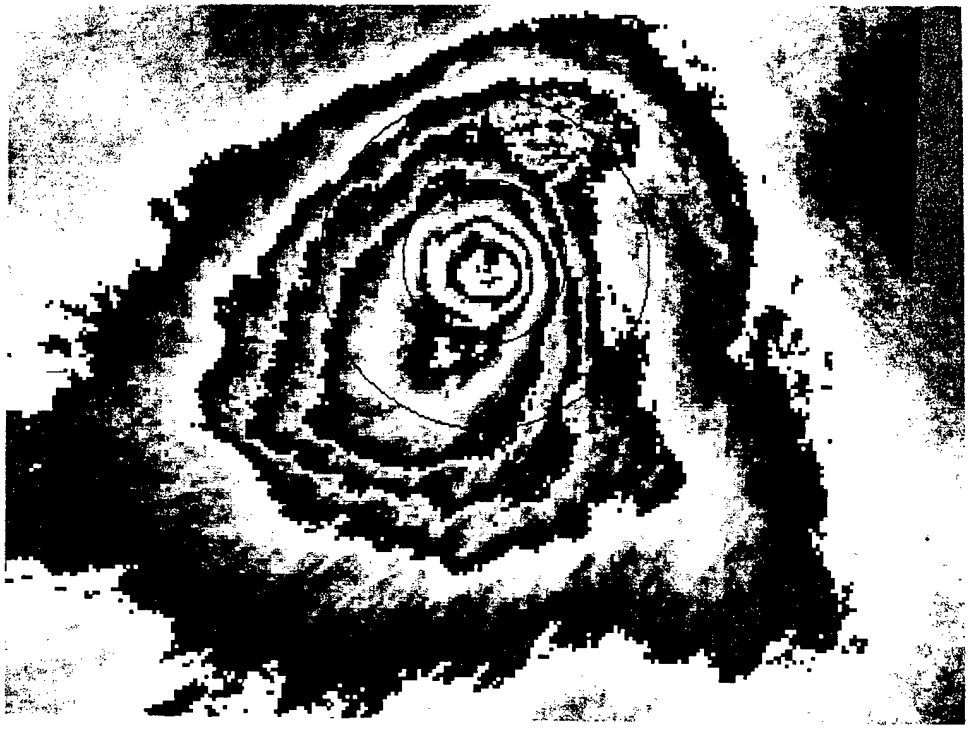

Figure 7.3: A 64 picture composite average of GMS IR imagery during an 8 day period for Supertyphoon Vanessa in the Northwest Pacific. Circles denote radii of approximately 2 and 4 degrees latitude. North is toward the top of the image. Note the prevalent deep convection in the SSW portion of this image.

typhoon's life cycle. The beginning and ending stages are omitted to limit the imagery analyzed to that for mature typhoons. Temperatures below –50°C indicate the presence of deep convection for this imagery as well. The interval of –50°C to –70°C will then be chosen to measure deep convection asymmetries.

Figure 7.4a is a composite image of a particular stage of a typhoon's life cycle, known as the Intensifying Least Typhoon stage (Weatherford, 1989). The -50°C isotherm has its maximum radial extent of 3.0 degrees latitude on the border of octants 4 and 5. The minimum radial extent for the -50°C isotherm occurs in octant 8. The –70°C isotherm has its maximum radial extent at 1.3° latitude in octant 5. The minimum radial extent is 0.8° latitude in octant 2.

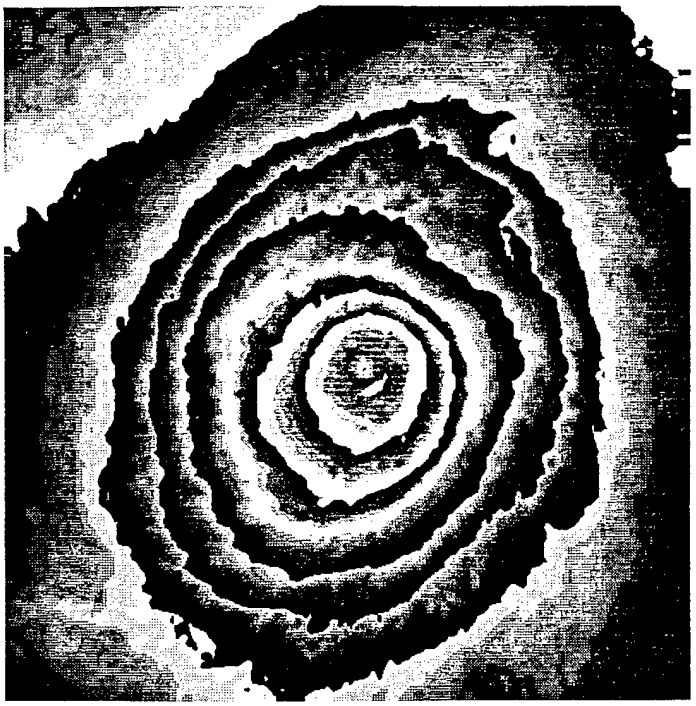

Figure 7.4: a. An averaged picture of GMS 10 km resolution IR imagery for 10 typhoons in the Northwest Pacific. Satellite imagery is compiled using only Weatherford (1989) Typhoon Life Cycle Stage 2 (Intensifying Least Typhoon, 976-930 mb) TCs. North is toward the top of the image. Note the deep convection maximum oriented SSW.

Figure 7.4b composes images from Stage 3 of the typhoon's life cycle, which is the Intensifying Intense Typhoon stage (Weatherford, 1989). The -50°C isotherm has its maximum radial extent of 3.8 degrees latitude in octant 4. The minimum extent for the

-50°C isotherm can be found in octants 7 and 8 at a radius of 2.0° latitude. The –70°C isotherm has its maximum radial extent at 2.0° latitude on the border of octants 4 and 5. The minimum radial extent is located at 1.2° latitude in octant 8.

Figure 7.4: b. Same as in Fig. 7.4a, but for Stage 3(Intensifying Intense Typhoon, 930-870mb).

Figure 7.4c depicts Stage 4 of the typhoon's life cycle, the Filling Intense Typhoon stage (Weatherford, 1989). The -50°C isotherm extends farthest outward(3.3° latitude) on the border of octants 4 and 5. The minimum extent of 1.5° latitude for the –50°C isotherm occurs in octant 8. The -70°C isotherm is 1.7° latitude from the center of the composite image on the boundary of octants 4 and 5. The –70°C isotherm is only 0.8° latitude away from the center in both octants 1 and 2.

Table 7.1 summarizes the convective asymmetries found in Fig. 7.2. Note the predominant SSW to NNE asymmetry in deep convection. This provides evidence that a convergence maximum does indeed exist on the south sides of TCs, at least in the Northwest Pacific.

Figure 7.4: c. Same as in Fig. 7.4a, but for Stage 4 (Filling Intense Typhoon, 870-930mb).

Table 7.1: Summary of convective asymmetries from IR composite imagery for 10 combined typhoons in the Northwest Pacific. Note the asymmetry of the -50°C isotherm is aligned SSW to NNE, and the -70°C isotherm asymmetry is aligned S to N. The radial asymmetries for both the -50°C and -70°C isotherm are both very close to 2 to 1.

Convective Asymmetries by Typhoon Life Cycle

Life Cycle Stage	Octant of -50°C Maximum Extent	Octant of -50°C Minimum Extent	Octant of -70°C Maximum Extent	Octant of -70°C Minimum Extent
2	4(SW) & 5(S)	8(NE)	5(S)	2(NW)
3	4(SW)	7(E) & 8(NE)	4(SW) & 5(S)	8(NE)
4	4(SW) & 5(S)	8(NE)	4(SW) & 5(S)	1(N) & 2(NW)
Averages	4(SW)	8(NE)	5 (S)	1(N)

Table 7.1: Continued

Life Cycle Stage	Maximum Radial Extent of -50°C Lat	Minimum Radial Extent of -50°C Lat	Ratio of Maximum to Minimum Radial Extent of –50°C	Maximum Radial Extent of -70°C Lat	Minimum Radial Extent of -70°C Lat	Ratio of Maximum to Minimum Radial Extent of –70°C
2	3.0	1.7	1.76	1.3	0.8	1.63
3	3.8	2.0	1.90	2.0	1.2	1.67
4	3.3	1.5	2.20	1.7	0.8	2.13
Averages	3.4	1.7	2.0	1.7	0.9	1.89

In review, the orientation of convective asymmetries measured from composite IR satellite imagery for Northwest Pacific typhoons closely agrees with the orientation of the convergence asymmetry predicted by geostrophic imbalance in Chapter 6. This convergence asymmetry occurs (refer back to Fig. 6.2) as a result of ageostrophies which arise because the height field surrounding TCs is more symmetric from north to south than Earth's vorticity field.

7.3 Vortex Propagation Caused by Asymmetric Convective Heating

Finally, note that Flatau(1992) showed asymmetric heating caused by convection on the south sides of vortices on a Beta plane(see Fig. 7.5) can cause vortex propagation in directions well to the south of what would occur under the influence of Beta alone.

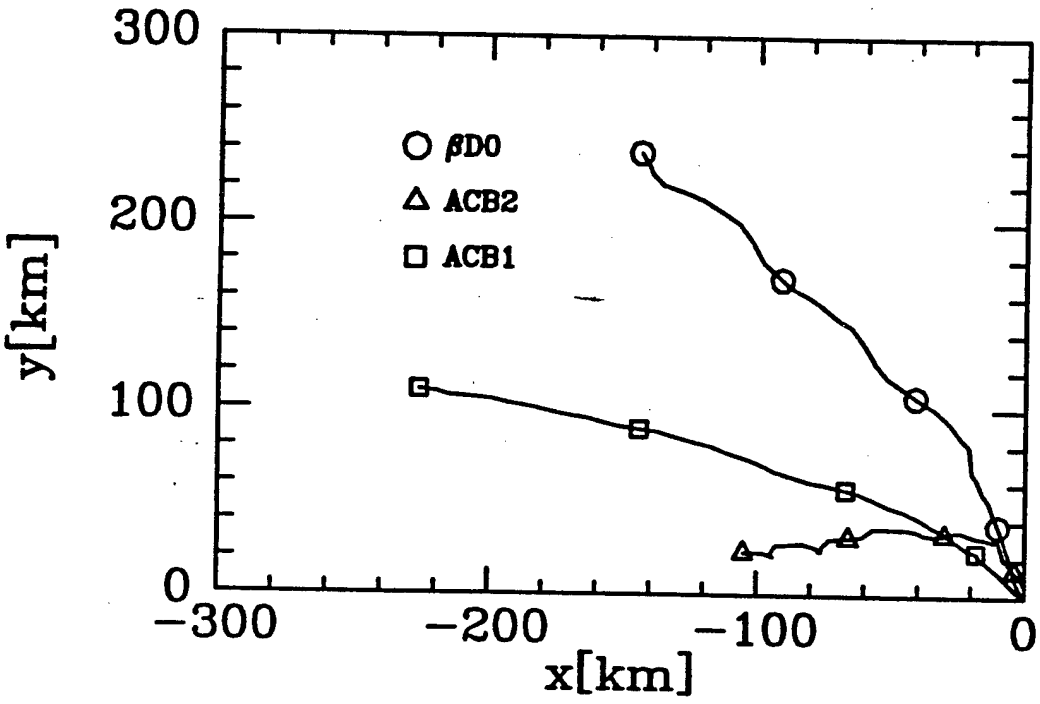

Figure 7.5: Trajectories of vortices in experiments ACB1, ACB2 (asymmetric heating in the southeastern quadrant of the vortex on the β plane, and in the southeastern quadrant of the vortex on the β plane, respectively) and βDO (symmetric heating on the β plane) (Flatau 1992).

Chapter 8

USE OF COMPOSITE SOUNDING DATA TO EXAMINE LOCAL VORTICITY TENDENCIES IN TROPICAL CYCLONES

Tropical cyclone Beta-induced propagation is a topic which has been studied extensively. Recently, there has been much work done with Beta drift as an influence on TC propagation to the northwest of the deep layer environmental flow. Basically, positive earth vorticity advection (PVA) induces propagation toward the northwest, where PVA is the strongest. In nature, however, there are other factors at work which influence the local vorticity tendency, $\frac{\partial \zeta_a}{\partial t}$.

8.1 Absolute Vorticity Tendency Equation Discussed

In this chapter, an absolute vorticity tendency equation will be examined to see what other factors besides Beta have an influence on TC propagation. The absolute vorticity tendency $\frac{\partial \zeta_a}{\partial t}$ is expressed in pressure coordinates by Holland (1983) as $\frac{\partial \zeta_a}{\partial t} = -\vec{V} \bullet \nabla(\zeta_r + f)$ $-\omega \frac{\partial \zeta_a}{\partial p} - (\zeta_r + f)\vec{\nabla} \bullet \vec{V} + \hat{k}(\frac{\partial \vec{V}}{\partial p} \times \vec{\nabla}\omega) + \hat{k}(\vec{\nabla} \times \vec{F})$. Because vertical advection, vorticity tilting, and friction are difficult to calculate in the TC environment, terms 2, 4 and 5 from left to right on the right hand side of the equation will be ignored. A scale analysis of the same equation by Chan (1982) supports the neglect of vertical advection, vorticity tilting, and friction as well. This reduces the absolute vorticity tendency equation to 3 terms, which are:

$$\frac{\partial \zeta_a}{\partial t} = -\vec{V} \bullet \vec{\nabla}(\zeta_r + f) - (\zeta_r + f)\vec{\nabla} \bullet \vec{V}, \quad or$$

$$\frac{\partial \zeta_a}{\partial t} = -\vec{V} \bullet \vec{\nabla}\zeta_a - (\vec{\nabla} \bullet \vec{V})\zeta_a.$$

Examination of this abbreviated vorticity equation (VE) $\frac{\partial \zeta_a}{\partial t} = -\vec{V} \bullet \vec{\nabla}\zeta_a - (\vec{\nabla} \bullet \vec{V})\zeta_a$ reveals three terms. The first, $\frac{\partial \zeta_a}{\partial t}$, is merely the local absolute vorticity tendency at a given point. The second, $-\vec{V} \bullet \vec{\nabla}\zeta_a$, is the absolute vorticity advection which gives rise to the well known Beta drift. The third and last term, $-(\vec{\nabla} \bullet \vec{V})\zeta_a$, explains the local change in absolute vorticity in terms of divergence times absolute vorticity at that same point.

8.2 Vorticity Equation Role in Understanding TC Propagation

A glance at the VE will lead one to at least infer that both convergence and vorticity advection need to be analyzed in order to fully understand what tendency the local change in absolute vorticity has for a given point in a TC vortex's deep layer flow. One goal of this chapter will be to show that it is this divergence term, and not the vorticity advection term, which is the dominant player in determining the local vorticity tendency. In other words, TC propagation cannot be explained by Beta drift alone. Frequently, natural processes take place within a TC vortex which can cancel Beta drift out. Therefore, to completely understand propagation at a certain location within a tropical TC, one must examine the local vorticity tendency itself. An explanation which uses only vorticity advection will be incomplete.

8.3 Vorticity Equation Term Computation Procedures

The starting point in computing both the divergence and advection terms in the VE was to compile both the radial and tangential wind fields in the (MOT) system. In the (MOT) system, TC motion is subtracted out, and octant 1 always faces north(natural coordinate system). Both wind fields for each TC case formed an annulus with inner and outer radii of 4° and 10° latitude, respectively. Specific point values for each octant were plotted in radial bands with radii of 3-5, 5-7°, 7-9°, and 9-11° latitude. Radial wind values in the 1-3° radial band were used in computations involving radial winds. No calculations were performed for radii inside 4° because data become relatively sparse there and statistical significance comes into question. This means isoplethed data fields were analyzed without using data inside 4° radius.

Once the radial and tangential wind fields in the (MOT) system were compiled, both absolute vorticity and divergence needed to be computed in cylindrical coordinates. The formula for divergence in cylindrical coordinates is $\frac{V_r}{r} + \frac{\partial V_r}{\partial r} + \frac{\partial V_\theta}{r\partial\theta}$, with the $\frac{V_r}{r}$ term representing divergence due to curvature, the $\partial V_r/\partial r$ term representing radial divergence, and the $\partial V_\theta/r\partial\theta$ term representing tangential divergence.

Point calculations involving tangential directions used an interval 2 octants wide centered upon the octant and radius in question. Radial calculations using $\partial/\partial r$ were performed over an interval 4° of latitude wide centered upon the octant and radius in question. Radial calculations employing r used the actual radius for the point calculation in question. Radial calculations done at the innermost and outermost radii were done over an interval 2° wide ending on the inner or outer boundary of the annulus, respectively. For simplicity, gradients were always measured and assumed to be normal to the advecting wind.

8.4 Analysis of Divergence Fields

An examination of the divergence fields for six individual cases (Atlantic and Pacific All West, Atlantic and Pacific All North, and the Atlantic and Pacific No Motion) reveals patterns in these fields (see Fig. 8.1). Convergence predominates in octant 2, while divergence predominates in octant 8. For TCs with a significant westward component of motion (with All West and both No Motion cases), this pattern of convergence and divergence can be explained by "relative wind blow through" which is observed when following a TC in the (MOT) system. Basically, this is just a consequence of the TC being embedded in a deep layer flow maximum as discussed in an earlier chapter. If one follows a TC in the (MOT) system, any environmental winds to the TC's right and left flanks will be perceived as negative due to the deep layer flow maximum near the TC's center approximating the TC's speed of forward motion. For example, a TC moving west would experience maximum convergence in octants 2 and 4 when its winds are being measured in the (MOT) system. Note the divergence in octant 8 for the north moving cases. This occurs in defiance of what "relative wind blow through" would predict. Chapter 6, as well

as Section 1 of Chapter 7, shows the predominant divergence in octant 8 to be caused by geostrophic imbalance.

Now, a sign for divergence consistent with a "relative wind blow through" explanation is not observed between octants 4 and 6 for all six of these TC cases. This is also related to a geostrophic imbalance in the TC vortices. A relevant clue here is the tendency for convergence to happen in either octant 4 or 5. Reference back to Fig. 6.1 shows thee to be a deep layer inflow between 850 and 300 mb in a 4-10° annulus. Geostrophic imbalance within this layer appears to be the cause of this convergence in octants 4 and 5. Reference back to Fig. 6.1 shows there to be a deep layer inflow between 850 and 300 mb in a 4-10° annulus. Geostrophic imbalance within this layer appears to be the cause of this convergence in octants 4 and 5.

8.5 Analysis of Absolute Vorticity and Absolute Vorticity Advection Fields

The absolute vorticity and consequent absolute vorticity advection (AVA) patterns (see Figs. 8.2 and 8.3) are mostly as one would expect, with PVA prevalent to the west side of the TC and NVA holding to the east side of the TC. The AVA patterns do not have perfect east-west symmetry because they are not pure Beta advection. Relative vorticity patterns are not perfectly symmetric and are unique as well for a given TC case, so this gives rise to an unbalanced vorticity advection pattern when advection of relative vorticity is included with advection of f.

8.6 Comparison of Convergence Term and AVA Fields

Another important item to observe is the relative strength of the convergence times absolute vorticity (hereafter referred to as the convergence term, $-(\vec{V} \bullet \vec{\nabla})\zeta_a$ fields for these six TC cases (see Fig. 8.3) when compared to the absolute vorticity advection ($-\vec{V} \bullet \vec{\nabla}\zeta_a$) fields. Both of these fields are graphed in units of $1 \times 10^{-11} s^{-2}$ and isoplethed every 10 units. It is readily apparent the convergence times absolute vorticity field has more isopleths than the absolute vorticity advection field. The relative field strength of the convergence term tends to prohibit the local absolute vorticity tendency from being

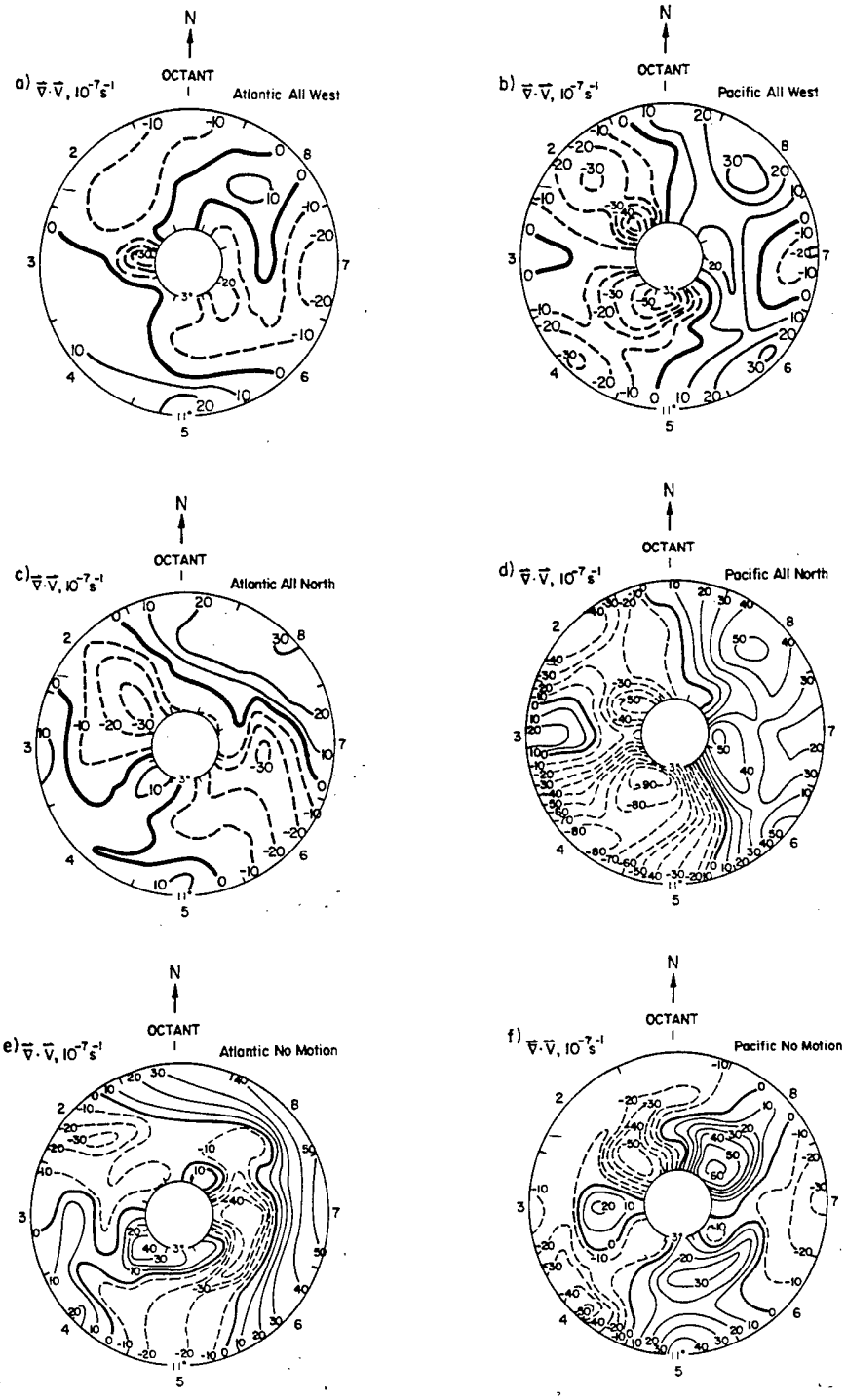

Figure 8.1: (a-f) Divergence field in a 4-10° annulus (3-5, 5-7, 7-9, 9-11° radial bands) within a 850-300 mb deep layer flow (MOT) for Atlantic and Northwest Pacific TCs.

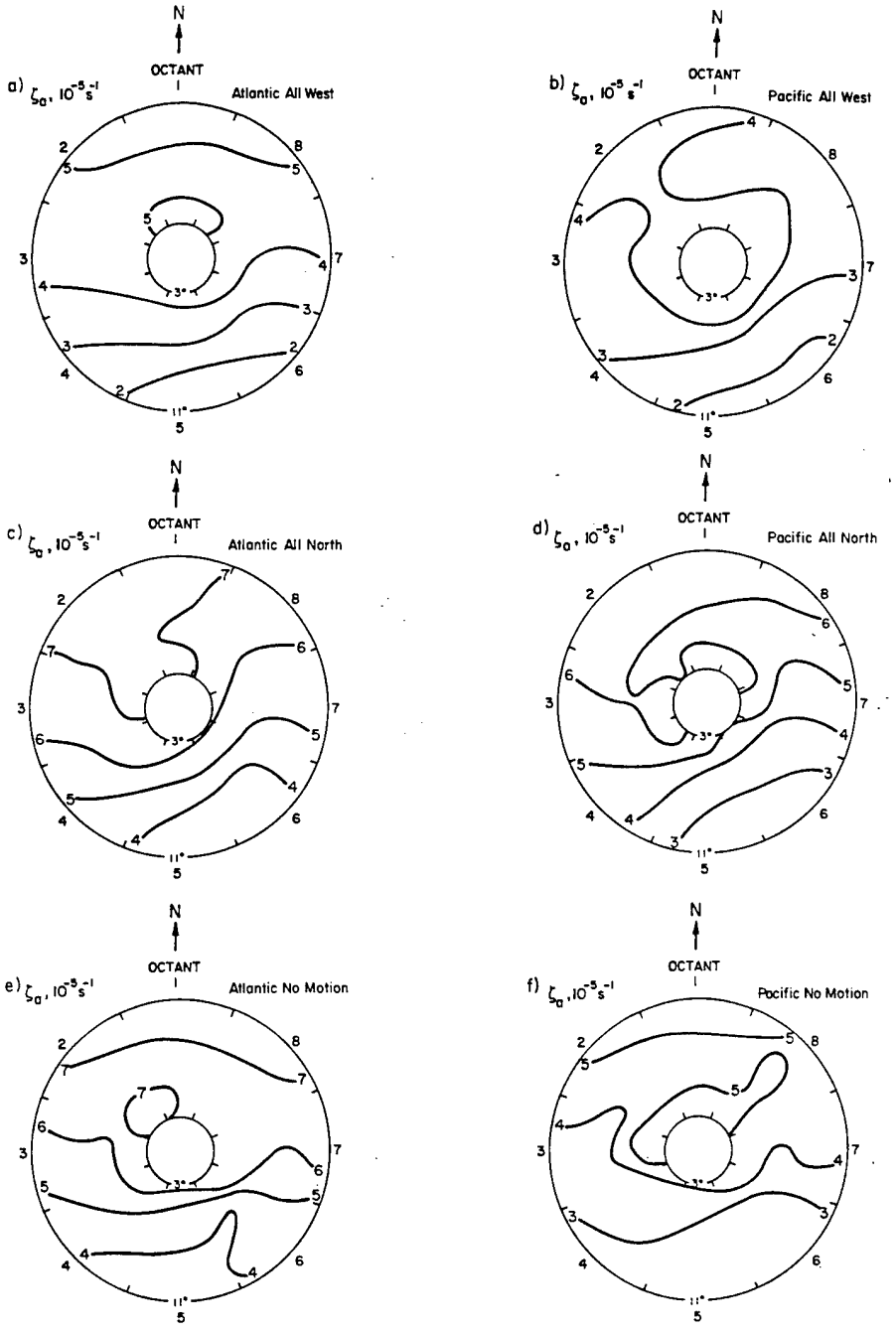

Figure 8.2: (a-f) Absolute vorticity field in a 4-10° annulus (3-5, 5-7, 7-9, 9-11° radial bands) within a 850-300 mb deep layer flow (MOT) for Atlantic and Northwest Pacific TCs.

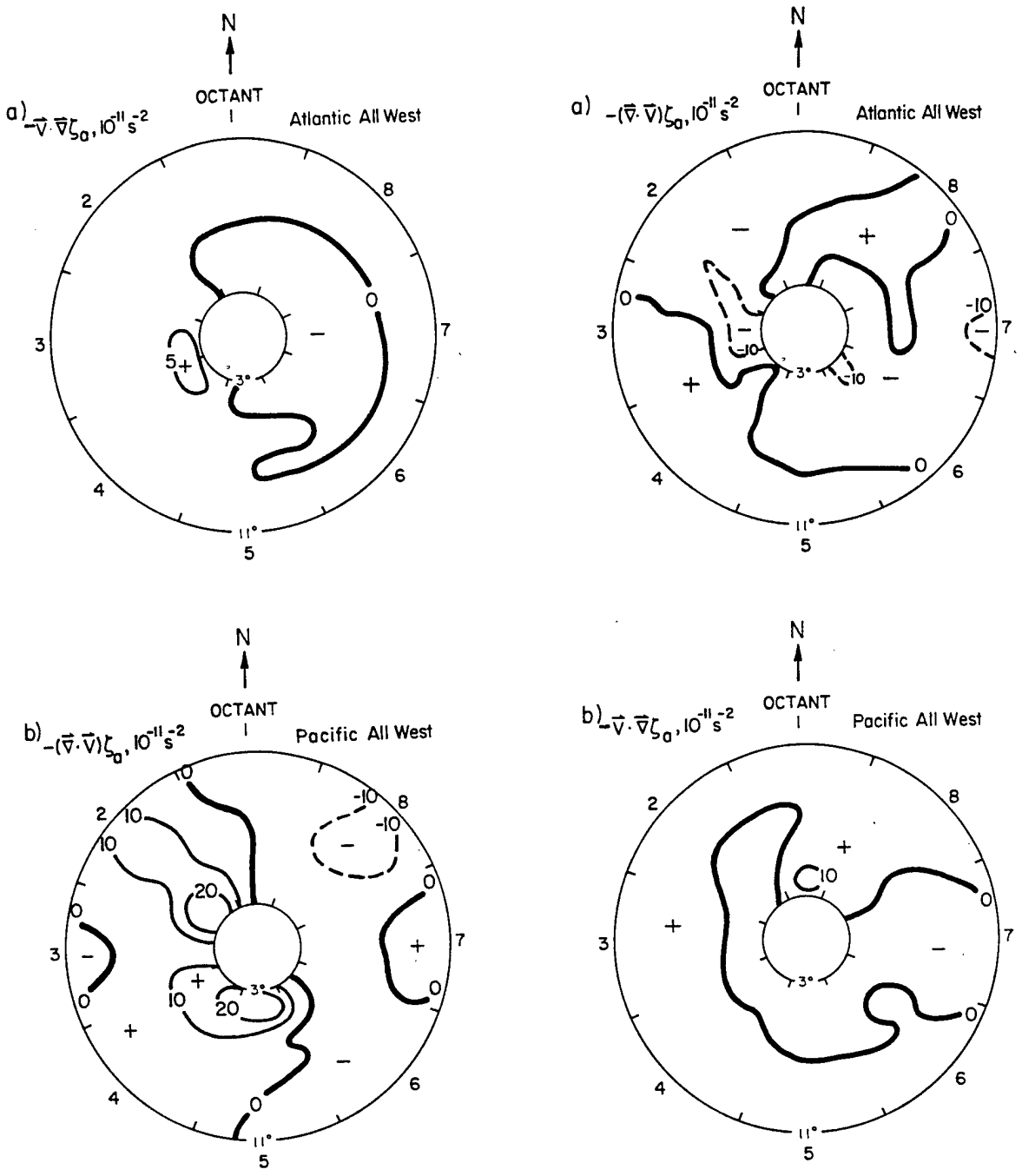

Figure 8.3: a-b. (a-f) Absolute vorticity advection field compared to the absolute vorticity times convergence (convergence term) field in a 4-10° annulus (3-5, 5-7, 7-9, 9-11° radial bands) within a 850-300 mb deep layer flow (MOT) for Atlantic and Northwest Pacific TCs.

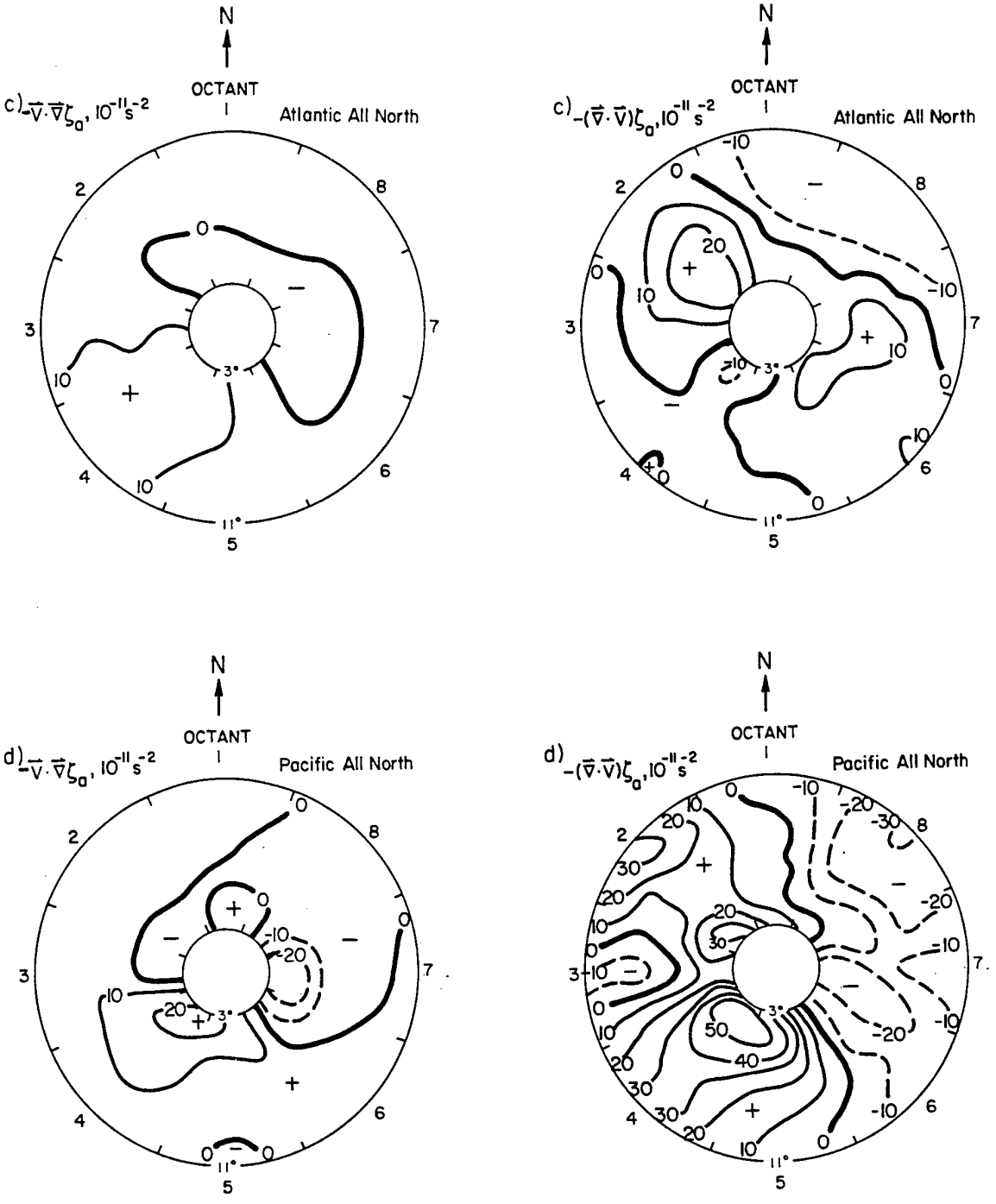
N
OCTANT
1
c) $-\vec{V}\cdot\vec{\nabla}\zeta_a$, $10^{-11}s^{-2}$
Atlantic All North
2
8
3
7
4
6
5
11°
3°
0
10
20
−
+
c) $-(\vec{\nabla}\cdot\vec{V})\zeta_a$, $10^{-11}s^{-2}$
Atlantic All North
-10
-20
-30
d) $-\vec{V}\cdot\vec{\nabla}\zeta_a$, $10^{-11}s^{-2}$
Pacific All North
d) $-(\vec{\nabla}\cdot\vec{V})\zeta_a$, $10^{-11}s^{-2}$
Pacific All North
30
40
50

Figure 8.3: c-d.

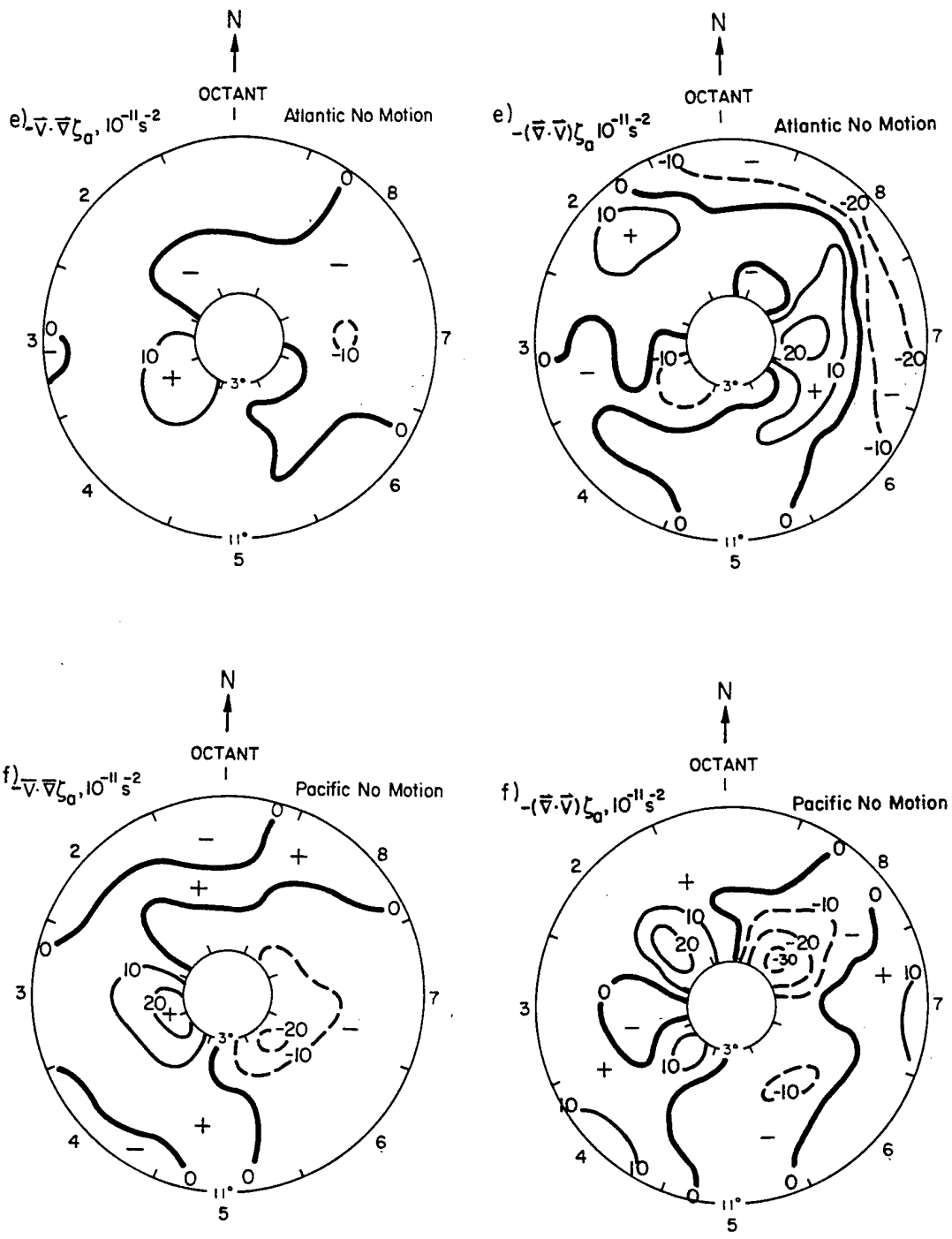
N
OCTANT
e) $-\vec{V}\cdot\vec{\nabla}\zeta_a$, $10^{-11}s^{-2}$
Atlantic No Motion
N
OCTANT
e) $-(\vec{\nabla}\cdot\vec{V})\zeta_a$ $10^{-11}s^{-2}$
Atlantic No Motion
N
OCTANT
f) $-\vec{V}\cdot\vec{\nabla}\zeta_a$, $10^{-11}s^{-2}$
Pacific No Motion
N
OCTANT
f) $-(\vec{\nabla}\cdot\vec{V})\zeta_a$, $10^{-11}s^{-2}$
Pacific No Motion

Figure 8.3: e-f.

dominated by AVA alone. As a matter of fact, when AVA and the convergence times absolute vorticity (hereafter the convergence term) are added together, a maximum in the local absolute vorticity tendency can occur in octants significantly distant from octant 2, where Beta alone would be expected to generate a local absolute vorticity tendency maximum.

Also, comparing the convergence fields with the convergence term fields will reveal a strong negative correlation between these fields, as would be expected.

8.7 Area Averaging Procedures for the Convergence Term and AVA Term

What happens when the two terms which constitute the local absolute vorticity tendency are added together will be discussed shortly. First, a data averaging procedure needs to be discussed. To simplify matters at this juncture, it was decided to average the AVA term and the convergence term by octants, using an area weighted average. This weighted average scheme more heavily weights point values of AVA and the divergence term at outer radii within an octant for which an average is computed.

8.8 Combining the Convergence and AVA to Obtain the Absolute Vorticity Tendency

The first exercise in utilizing the area weighted averaging procedure was to compute the individual octant averages for the AVA term and the convergence term. Averages for the same individual cases depicted in Fig. 8.3 were calculated, then averages were determined for the combined Atlantic and NW Pacific All West cases, combined Atlantic and NW Pacific All North cases, and the Atlantic and NW Pacific No Motion Cases. A four case average was done for the combined Atlantic and NW Pacific All West and All North Cases. Finally, an eight case average was calculated using the Atlantic and NW Pacific All West, All North, All Northeast, and No Motion cases.

The actual data fields for the AVA term and the convergence term have already been shown in Fig. 8.3. To avoid redundancy in this chapter, individual octant averages for

these two terms in single TC cases, as well as two and four case averages, will be illustrated in Appendix B exclusively as Figs. B.2 and B.3.

An eight case average will be examined here for overall trends in $-\vec{V} \bullet \nabla\zeta_a$ and $-(\vec{\nabla} \bullet \vec{V})\zeta_a$.

8.9 Patterns in Absolute Vorticity Tendency Discussed for Individual TC Cases

Combining the AVA and divergence terms in individual TC stratifications to compute the local absolute vorticity tendency (see Fig. 8.4) causes a maximum to occur in octant 2 as well as in an octant 4 through 7 interval. A consistent $\frac{\partial\zeta_a}{\partial t}$minimum was encountered in octant 8, with the exception that the minimum could be found in octant 7 for the Atlantic No Motion case. The variation in local absolute vorticity tendency patterns is a combination of spinup due to "blow through" convergence and convergence due to geostrophic imbalance. A particular case to note is the Atlantic All West moving TC stratification. A strong positive local absolute vorticity tendency is observed on the east-southeast side which is roughly equal to the local maximum found in octant 2. In effect, Beta drift is being almost directly opposed by vortex spinup on the TC's east side as a result of a local convergence maximum there.

8.10 Patterns in Absolute Vorticity Tendency Discussed for an Eight Case Average

An eight case average will be examined here for overall trends in $-\vec{V} \bullet \vec{\nabla}\zeta_a$ and $-(\vec{\nabla} \bullet \vec{V})\zeta_a$. The strongest convergence (see Fig. B.1 for area averages) which led to a maximum in the convergence term was found in octant 2, with a secondary maximum occurring in octant 4. The highest value for AVA happened in octant 4. Adding the AVA and convergence terms together to obtain the local absolute vorticity tendency (see Figs. 8.4 and 8.5) resulted in a primary maximum in octant 2, with strong secondary maxima in octants 4 and 5.

When a three contiguous octant average of $\frac{\partial\zeta_a}{\partial t}$ centered on a given octant is taken which combines all eight cases above, a strong local absolute vorticity tendency is noted.

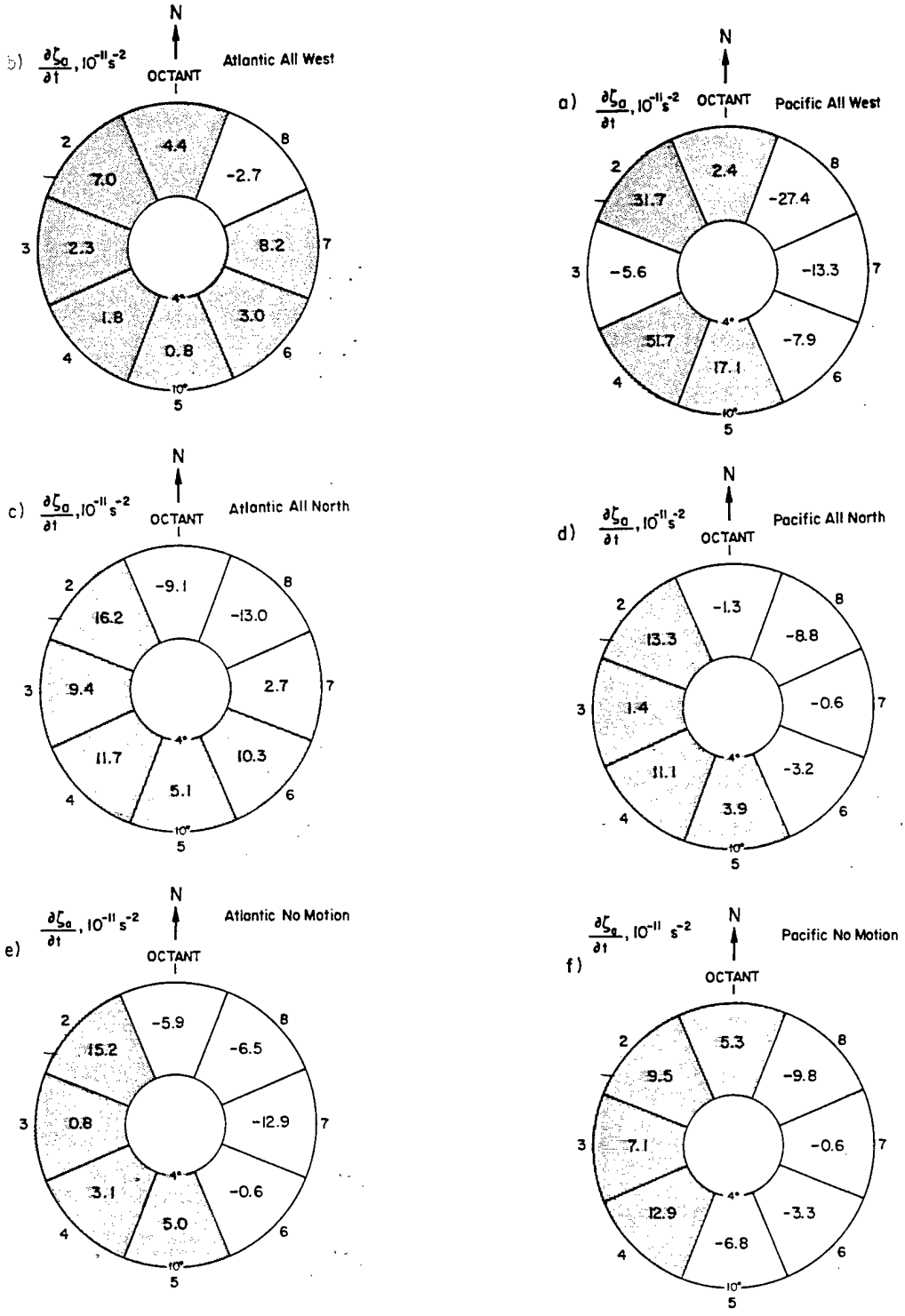

Figure 8.4: Area averaged absolute vorticity tendencies for both Atlantic and Northwest Pacific TCs. Numbers come from the equation $\frac{\partial \zeta_a}{\partial t} = -\vec{V} \bullet \vec{\nabla}\zeta_a - (\vec{\nabla} \bullet \vec{V})\zeta_a$. Terms on the right hand side of the equation are calculated using the 850-300 mb deep layer flow in the (MOT) frame of reference.

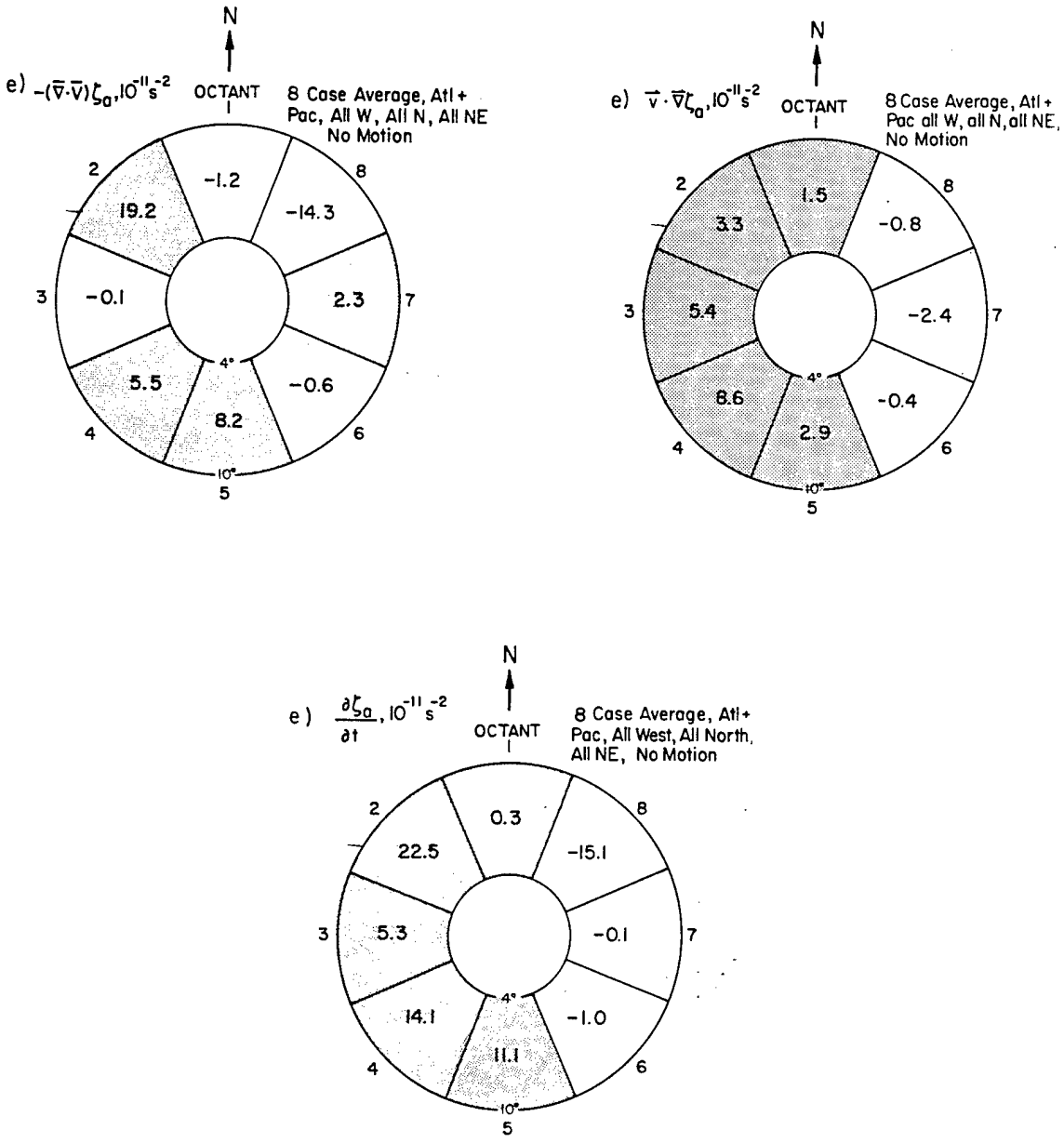

Figure 8.5: Area averages for absolute vorticity advection convergence times absolute vorticity, and local absolute vorticity tendency in the 850-300 mb deep layer wind flow (MOT) for combined TC cases in the Atlantic and NW Pacific.

This tendency is directed in a west-southwesterly direction (see Fig. 8.6). A subsequent step of averaging opposing octants clarifies this trend even further. See Fig. 8.7, which depicts this tendency for the deep layer 850 to 300 mb vortex to propagate WSW, with the greatest positive values of $9.7 \times 10^{-11}s^{-2}$ and $7.6 \times 10^{-11}s^{-2}$ situated in octants 3 and 4, respectively.

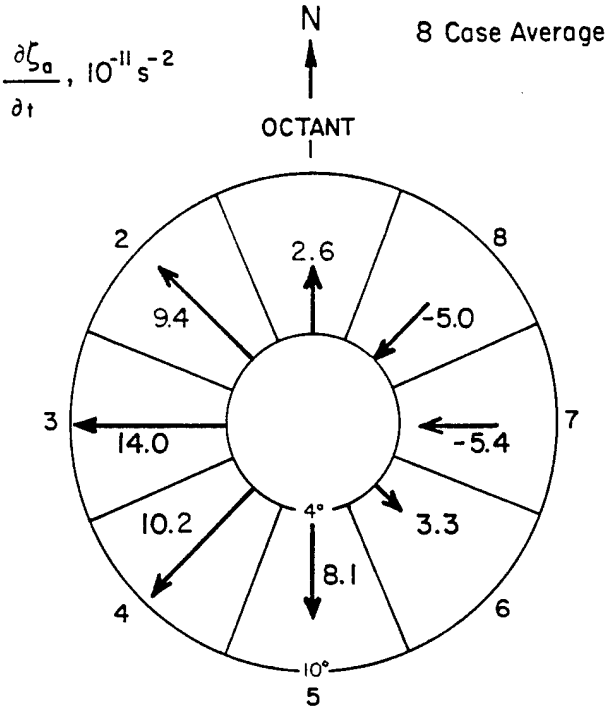

Figure 8.6: Three contiguous octant averaged local vorticity tendencies ($\partial\zeta_a/\partial t$) for eight combined Atlantic and Northwest Pacific tropical TC stratifications. The Atlantic and Pacific All West, All North, All Northeast and no Motion TC motion stratifications were the TC stratifications used.

Table 8.1 was constructed to summarize two different local absolute vorticity tendencies: south minus north(S-N) and northwest minus southeast(NW-SE). The S-N tendency was figured by subtracting the average of the northmost 3 octants from the average of the southmost 3 octants in Fig. 8.4. The NW-SE tendency was determined in an analogous fashion. A look at Table 8.1 reveals two trends. Both the S-N and NW-SE absolute vorticity tendencies tend to be positive. This means the deep layer 850 to 300 mb vortex for these six cases tends to propagate due to local absolute vorticity tendency south versus north, and northwest versus southeast.

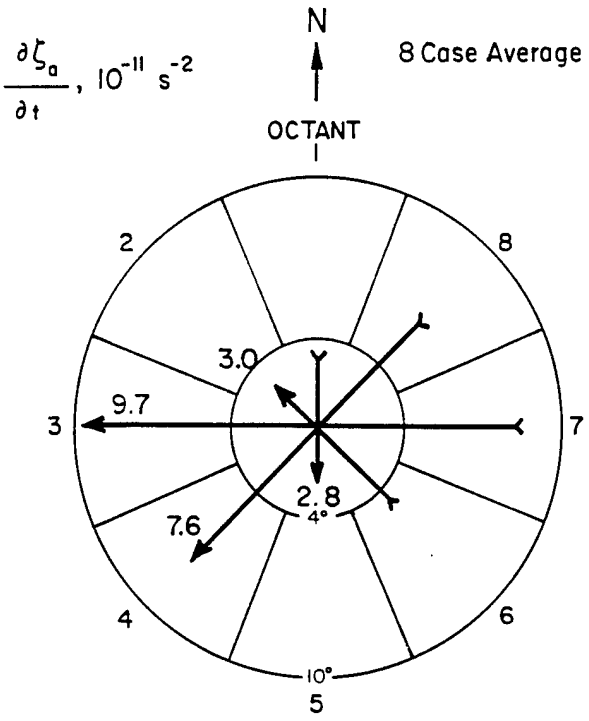

Figure 8.7: Same as Fig. 8.6 except opposing octants are netted and averaged to obtain a clear local vorticity tendency toward the west-southwest.

Table 8.1: Absolute vorticity tendencies for Atlantic and Northwest Pacific TCs computed using the equation $\partial\zeta_a/\partial t = -\vec{V} \bullet \nabla\zeta_a - (\vec{\nabla} \bullet \vec{V})\zeta_a$, with individual terms on the right hand side of the equation being calculated using the 850-300mb deep layer flow in the (MOT) frame of reference. Positive numbers for the NW-SE and S-N categories signify tendencies to propagate NW and S, respectively.

Absolute Vorticity Tendencies for Atlantic and Northwest Pacific TCs
Units of 1 $\times 10^{-11} s^{-2}$

NW - SE Denotes Tendency to Propagate Northwest
S - N Denotes Tendency to Propagate South

Stratification	Propagation Tendency	Atlantic	Pacific	Two Ocean Average
All West	NW - SE	0.6	10.9	5.8
	S - N	-1.0	18.1	8.6
All North	NW - SE	-0.5	4.5	2.0
	S - N	11.0	2.8	6.9
No Motion	NW - SE	6.2	10.9	8.6
	S - N	1.6	-0.8	0.4
Combined All West & North	NW - SE	0.1	7.7	3.9
	S - N	5.0	10.5	7.8

Chapter 9

TANGENTIAL WIND ASYMMETRIES RELATIVE TO THE MOVING CYCLONE SYSTEM

Another natural process may be present in the tangential wind fields of TCs which acts to resist Beta drift. When the tangential winds at a radius of 6° latitude for the 850 to 300 mb deep layer wind flow are observed using the (MOT) system to remove the TC's motion from the wind field, asymmetries are noted between the east/west and north/south octants. Reference to Fig. 9.1 reveals the west minus east tangential wind total is always positive for a set of 16 individual and averaged TC cases. The south minus north tangential wind total is always positive with the exception of the Atlantic No Motion case and the two case average for the NW Pacific and Atlantic No Motion cases.

9.1 Tangential Wind Asymmetries in the No Motion Cases

Tangential winds in the 850-300 mb deep layer within the 5-7° radial band measured in the (MOT) frame of reference tend to be relatively low in the No Motion cases when compared to tangential winds in the All West, All North, and All Northeast moving TC stratifications. A more important item to notice is that the tangential winds on the east and west sides of TCs exhibiting slow motion are nearly equal, especially when both Atlantic and NW Pacific No Motion cases are averaged. The No Motion class of TCs shows very little east/west tangential wind asymmetry because there is virtually no 850-300 mb deep layer wind flow differential between the TC center and its flanks (see Fig. 9.1).

In contrast, note that a significant north south tangential wind asymmetry persists in the No Motion class of TCs. This asymmetry can be explained using the geostrophic

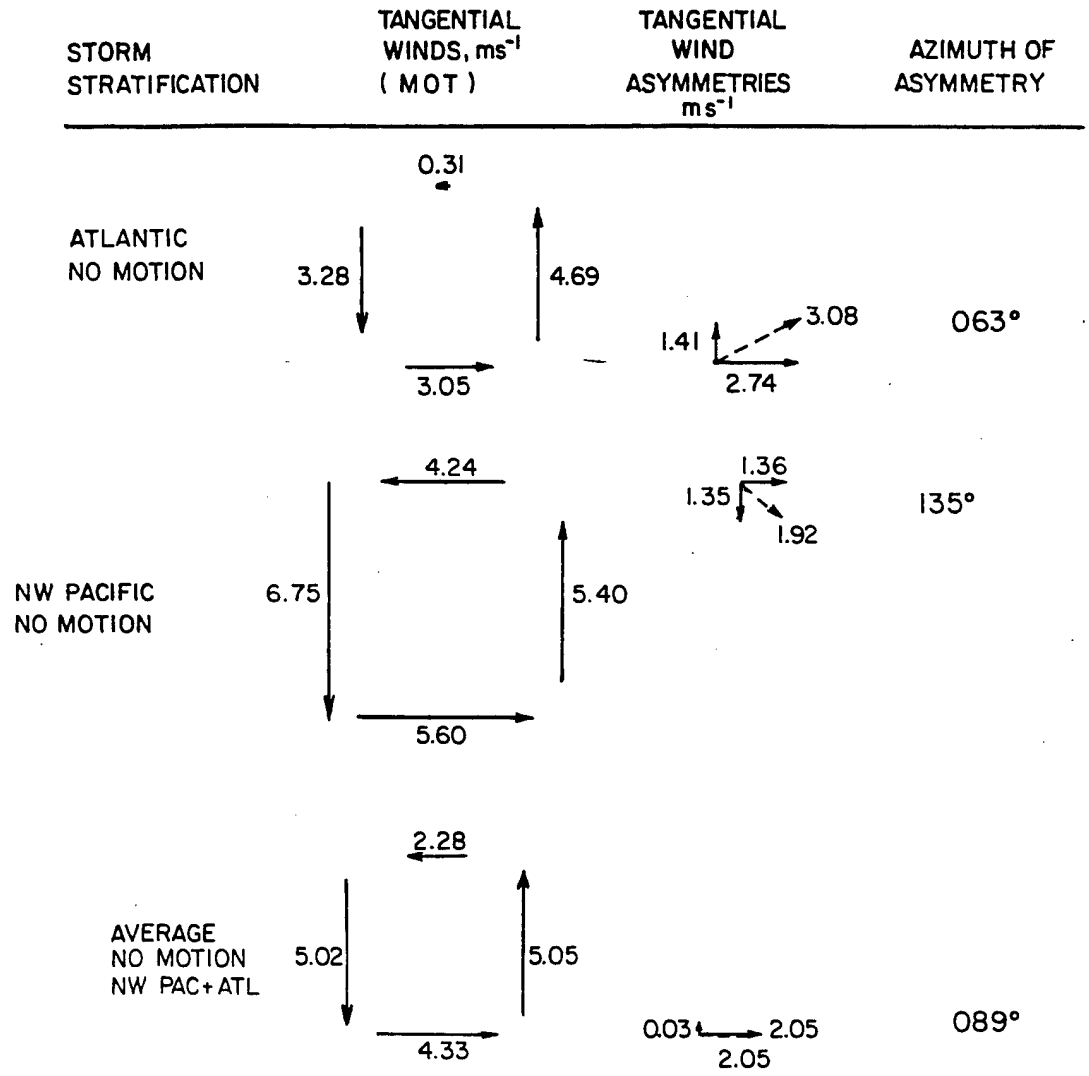

Figure 9.1: Analysis of north/south and east/west 850-300 mb deep layer tangential wind asymmetries in the (MOT) frame of reference. The left column depicts the actual tangential winds in the 5-7° radial band in the north, east, south and west facing TC octants. The right two columns show the net north/south and east/west asymmetries with the resultant wind asymmetry vector and azimuth. Note an almost uniform southeasterly net tangential wind asymmetry, a direction which opposes Beta drift.

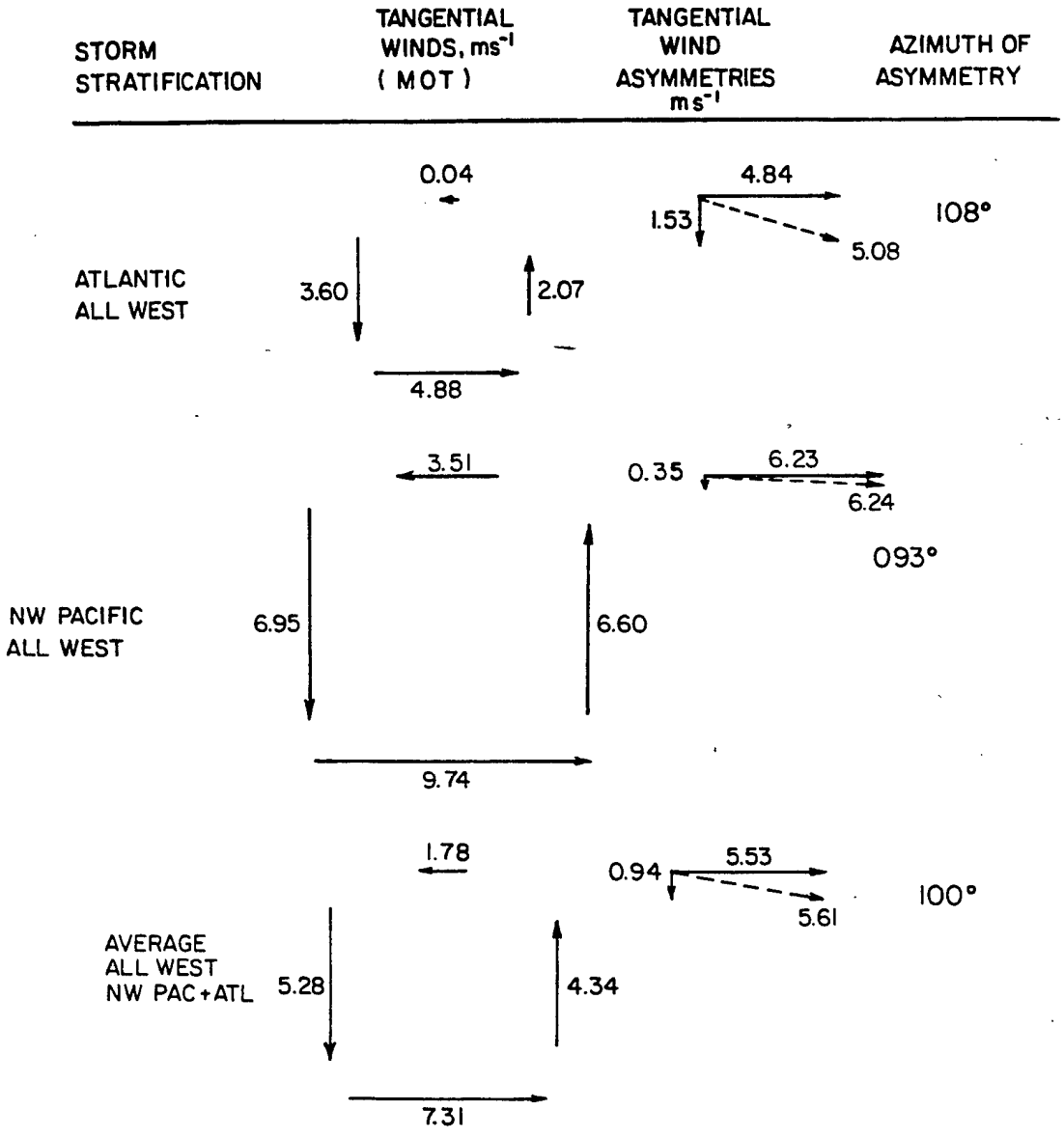

Figure 9.1: Continued.

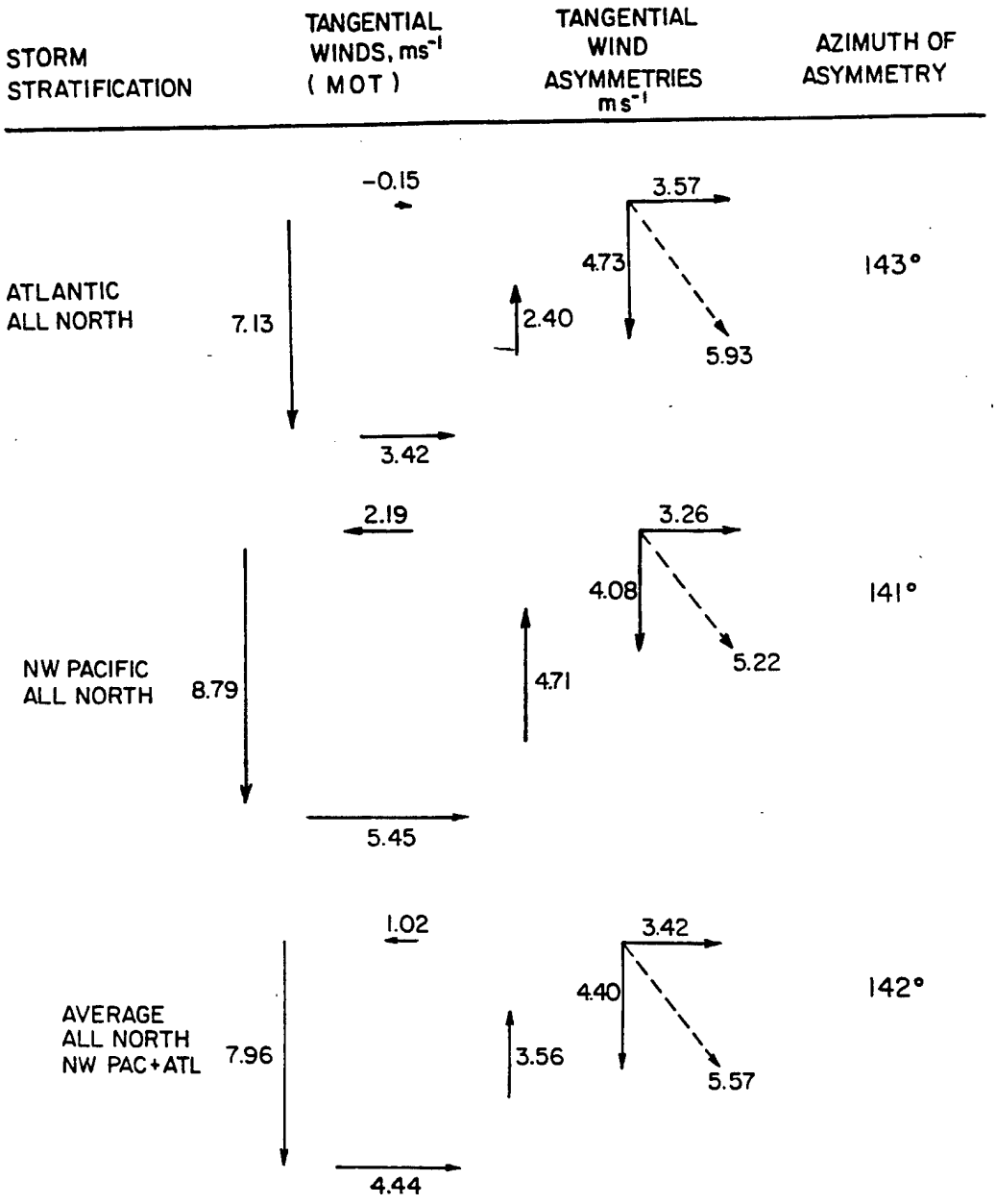

Figure 9.1: Continued.

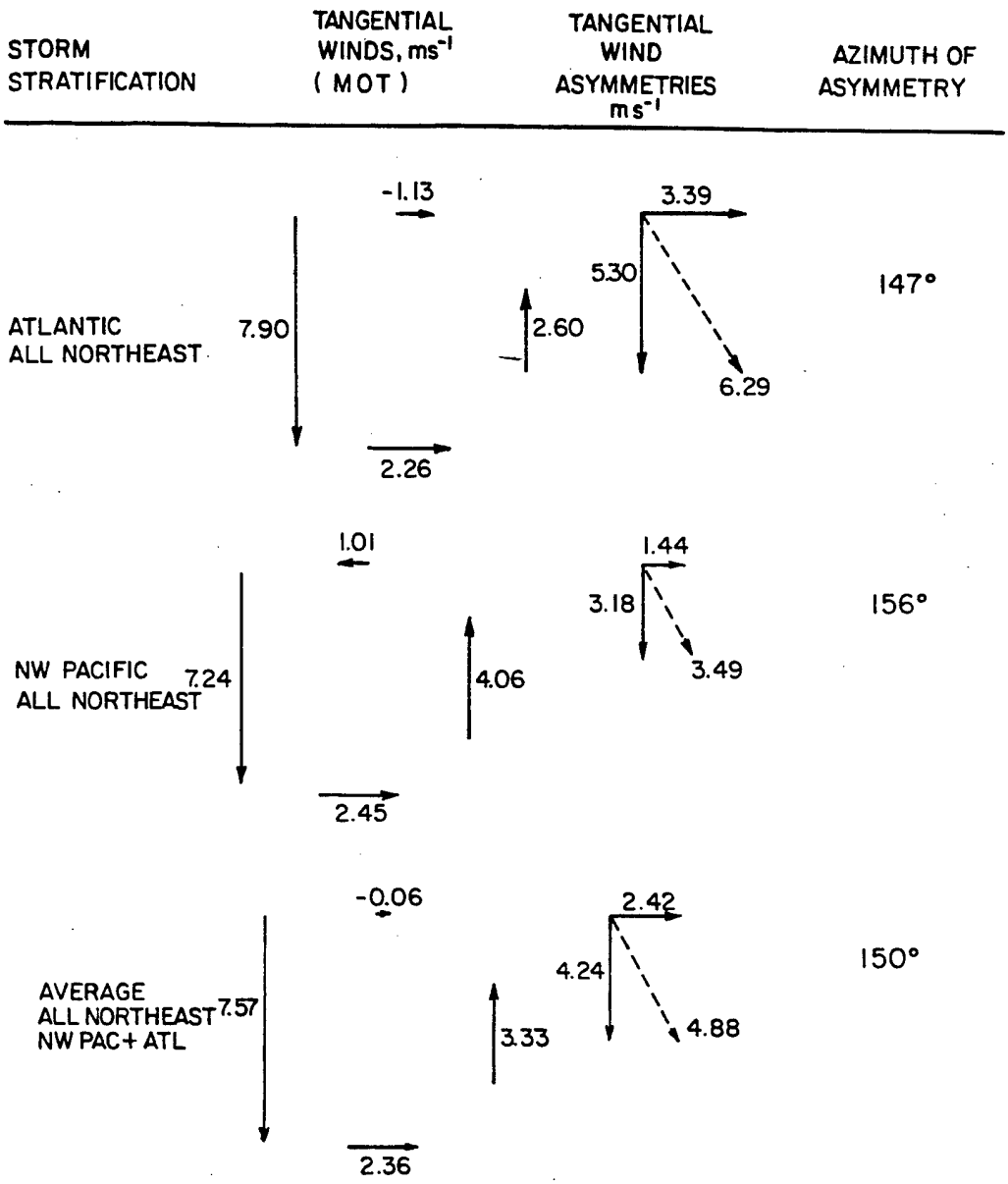

Figure 9.1: Continued.

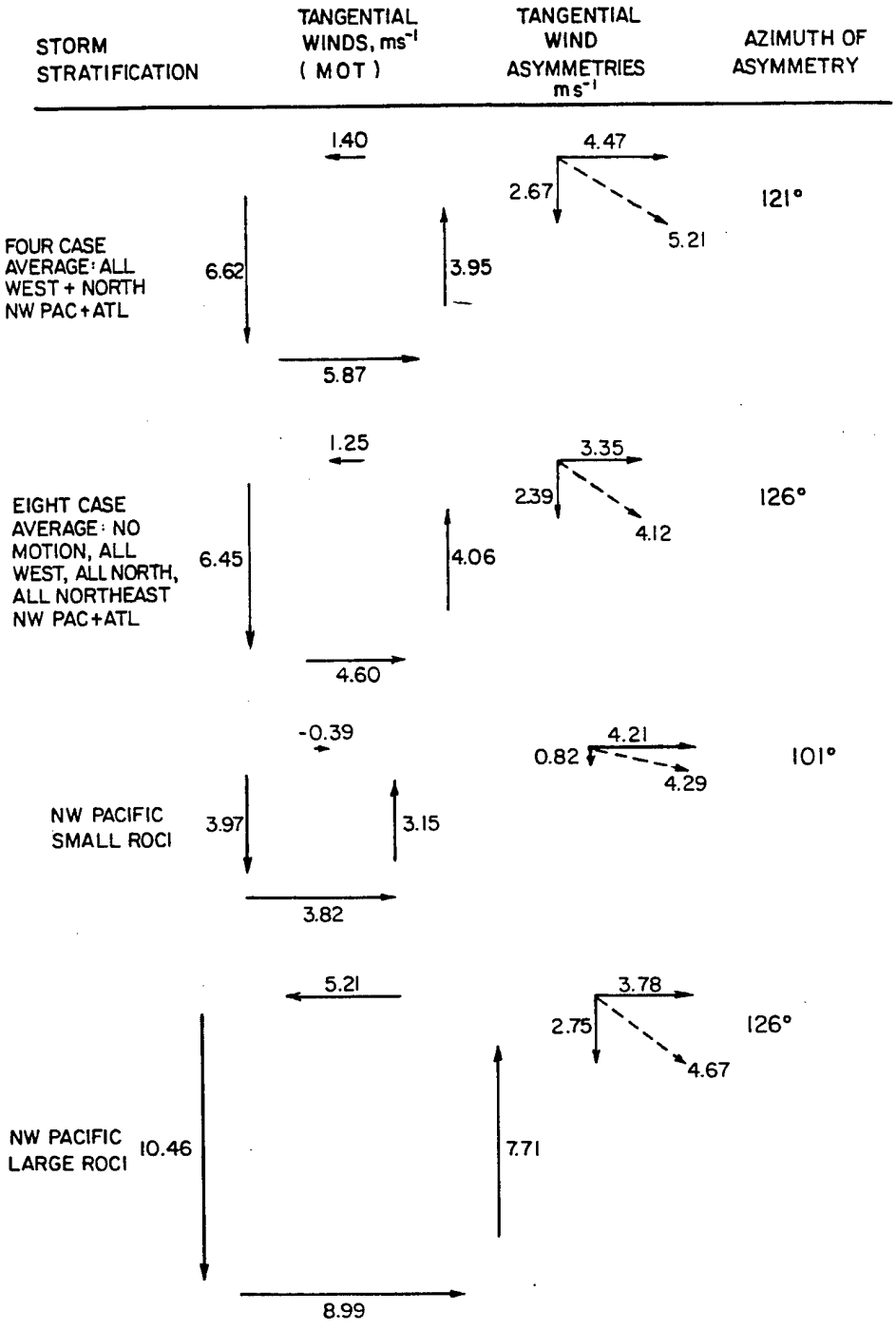

Figure 9.1: Continued.

wind relation. It has been shown in Chapter 6 that the variation of height gradient in the 5-7° radial band around TCs is less than the total north/south variation of f in the same radial band. Accordingly, the strongest geostrophic wind in the 5-7°radial band must blow 6° to the south of a TC to maintain geostrophic balance if the average height gradient in the 850-300 mb layer is held nearly constant.

9.2 Tangential Wind Asymmetries in the All West Cases

The All West TC motion case displays a relatively small east/west tangential wind asymmetry because there is very little deep layer wind flow component over the TC center from the north or south. However, the north/south tangential wind asymmetry for this case is more pronounced than in the No Motion TC stratification - see Fig. 9.1. A TC with a significant westward component of motion will have a relatively large north/south tangential wind asymmetry because westerly "tangential wind blow through" will reinforce TC tangential winds to the south of the TC center, while the same westerly "tangential wind blow through" will cancel out tangential winds on the north side attributable to the TC vortex. "Tangential wind blow through" is observed in the (MOT) system when a deep layer wind flow maximum over the TC center which approximates the TC's speed occurs. Weaker winds to each side of the TC center appear to blow from front to rear through the TC's flanks from the frame of reference of following the TC.

Figures 9.2 and 9.3 show how the tangential wind asymmetries increase as a TC's forward speed increases. This suggests that "relative wind blow through" increases as the TC's speed increases. Recall from Fig. 4.3 that the NE moving TCs had deep layer flow graphs which were the most peaked of the TC motion categories depicted in that figure. The NE moving TCs were the fastest moving TCs illustrated in Fig. 4.3 as well. The peakedness of the All NE deep layer flow profiles, combined with the fast movement of these TCs would give them strong "relative wind blow through". Figure 9.1 shows this class of TC to have large N/S V_θ asymmetries. Superposition of a deep layer wind flow maximum directly over the center of the TC vortex with weaker deep layer winds to each

side of the TC center will create tangential wind asymmetries along an axis normal to the TC direction of motion.

Table 9.1: Plot Points for Fig. 9.2.

Plot Point	TC Motion Stratification
1	NW Pacific No Motion
2	Atlantic No Motion
3	Atlantic All West
4	NW Pacific All West
5	NW Pacific Slow North
6	Atlantic All Northeast
7	Atlantic All North
8	NW Pacific Small ROCI
9	NW Pacific Large ROCI
10	NW Pacific All Northeast
11	NW Pacific All North
12	NW Pacific Fast North

Table 9.2: Plot points for Fig. 9.3.

Plot Point	TC Motion Stratification
1	NW Pacific All West
2	Atlantic All West
3	NW Pacific Small ROCI
4	NW Pacific Large ROCI
5	NW Pacific Slow North
6	Atlantic All North
7	NW Pacific All North
8	Atlantic No Motion
9	NW Pacific No Motion
10	NW Pacific Fast North
11	Atlantic All Northeast
12	NW Pacific All Northeast

The north/south tangential wind asymmetry in the All West TC motion case has a component which is caused by the variation of f across the TC from north to south. As a matter of fact, All TC motion stratifications have north/south tangential wind asymmetry caused by the geostrophic wind's adjustment to Beta.

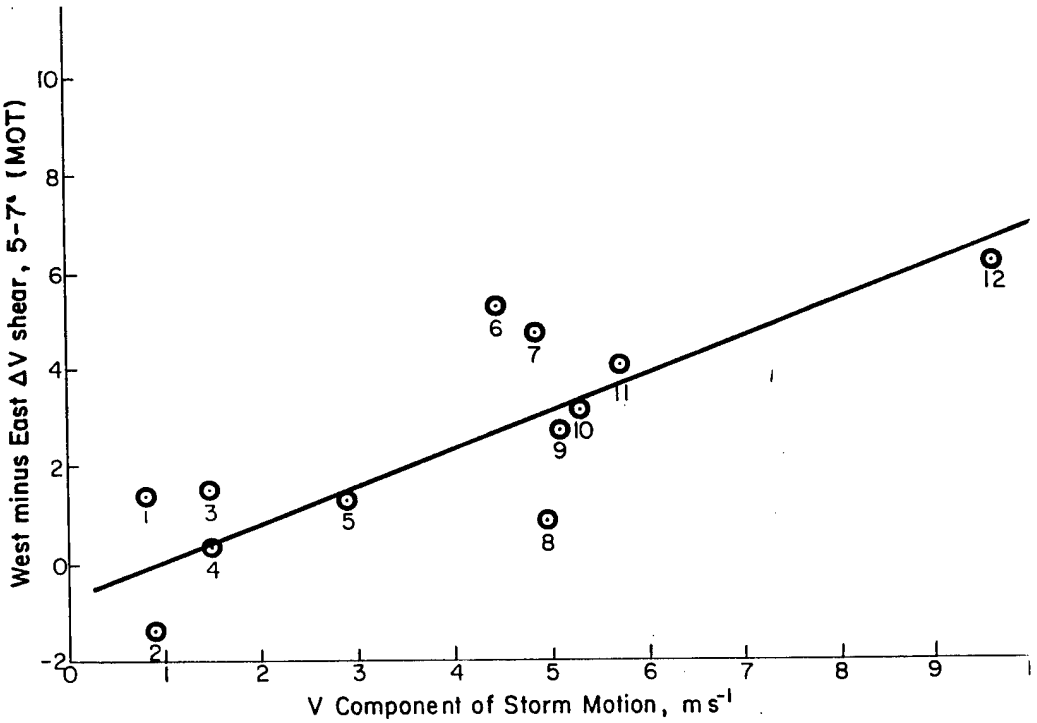

Figure 9.2: Scatterplot showing the correlation of a tropical cyclone's northward speed with its N/S tangential wind asymmetry in the 5-7° radial band as measured in the (MOT) system. The abscissa denotes the TC's northward component of motion, while the ordinate indicates the N/S tangential wind asymmetry. A positive number for the ordinate means the magnitude of the north winds on the west side of the TC exceeds the magnitude of the south winds on the TC's east side. Plot points for Fig. 9.2 are detailed in Table 9.1.

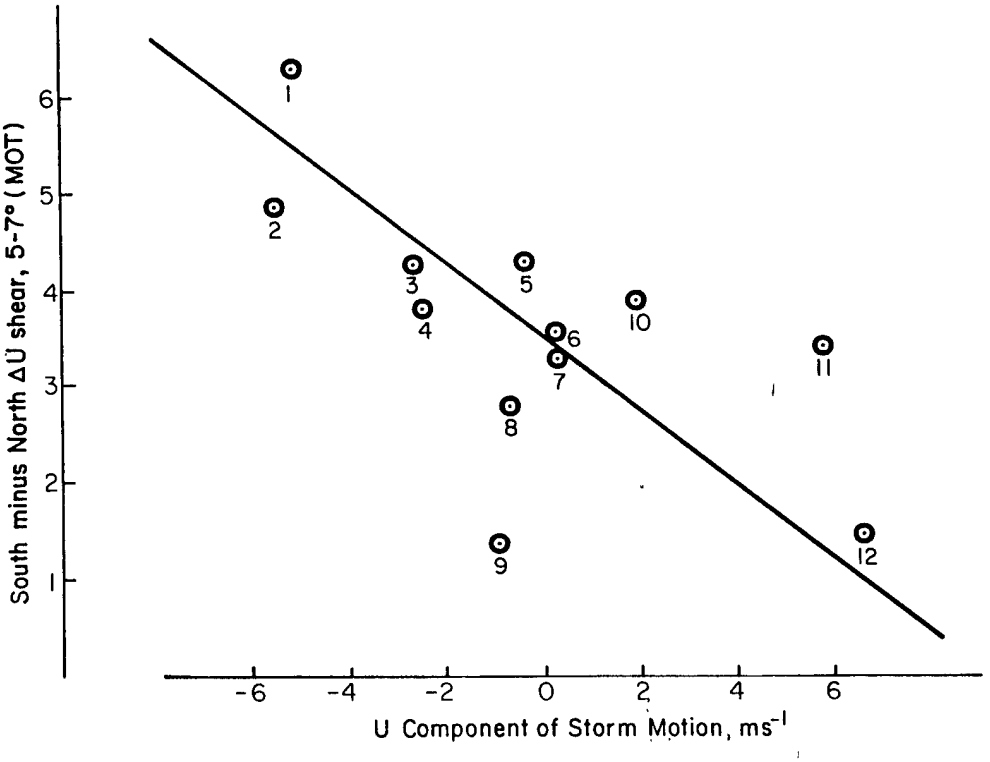

Figure 9.3: Scatterplot showing the correlation of a tropical cyclone's eastward speed with its E-W tangential wind asymmetry. The abscissa denotes the TC's eastward component of motion, while the ordinate indicates the TC's E-W tangential wind asymmetry. A positive number for the ordinate means the west winds on the south side of the TC exceed the east winds on the TC's north side. Plot points for Fig. 9.3 are detailed in Table 9.2.

9.3 Tangential Wind Asymmetries in the All North Cases

As discussed in the previous section, the north/south tangential wind asymmetry in the 850-300 mb deep layer wind flow for the 5-7° radial band exists in this TC motion category primarily due to Beta.

"Tangential wind blow through" is responsible for a pronounced east/west tangential wind asymmetry for this TC motion class by the same mechanism which operates on the All West TC cases. The only difference here is that the "tangential wind blow through" comes from a northerly direction. This rotates the tangential wind asymmetry caused by "tangential wind blow through" 90° from a north/south axis to an east/west axis.

The All Northeast TC motion cases are similar to the All North TC motion cases except that the north/south tangential wind asymmetry is weakened by "tangential wind blow through" from the east.

9.4 Propagation Influence from Tangential Wind Asymmetry

The overall pattern of tangential wind asymmetry evident in Fig. 9.1 would act to resist northwesterly TC drift. Propagation of the TC vortex to the southeast would occur according to the wind-pressure adjustment process described by Chan (1982). Interestingly, Chan also observed a linear relationship between a normalized wind-pressure imbalance and the TC speed of motion (see Fig. 9.4). When the tangential wind asymmetry in the x direction and the tangential wind asymmetry in the y direction from Fig. 9.1 are combined, the resultant tangential wind asymmetry vector always points southeast, with the 2 No Motion cases excepted as before. The average value for this vector is 4.34 ms^{-1} for the 18 cases reviewed here.

This value of 4.34 ms^{-1} is comparable to Beta drift velocities observed in model runs with no environmental flow. Flatau (1992) performed model runs for baroclinic vortices on a Beta plane and obtained a northwesterly drift speed of 2.8 ms^{-1} after 3 days. Carr and Elsberry (1992) arrived as well at a 2.8 ms^{-1} drift toward 330° in a barotropic model run. Elsberry and Abbey report Shapiro (1992) ultimately attained a propagation vector

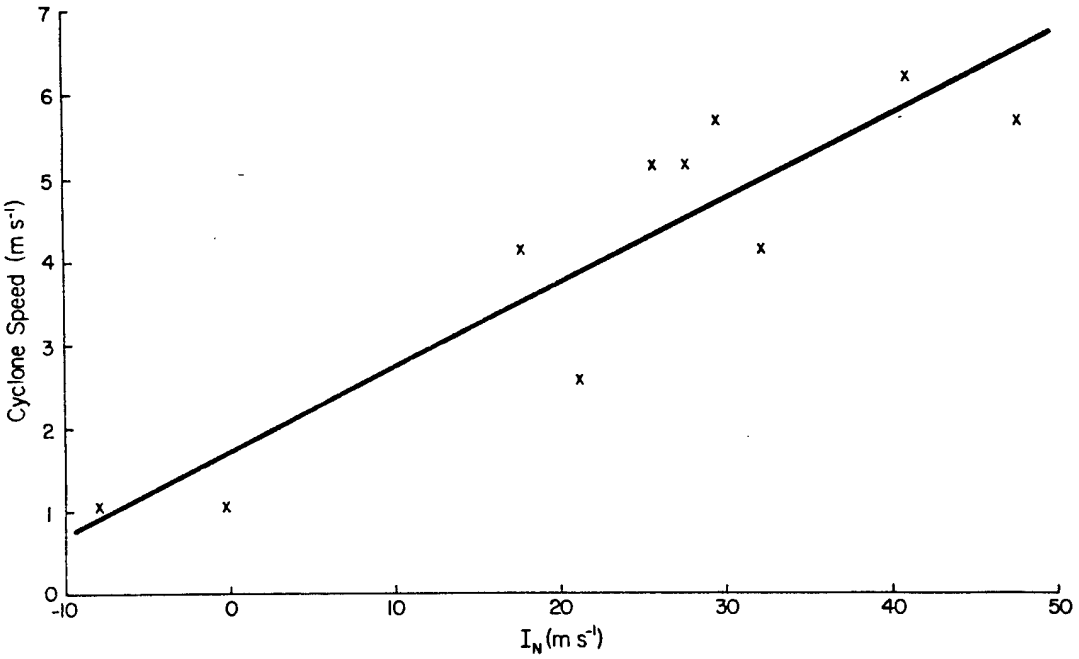

Figure 9.4: Plot of the normalized wind-pressure imbalance (I_N) against TC speed at the RMW. The straight line is the least-square fit with a correlation coefficient of 0.90. I_N is defined as $(4c\bar{v}/r)$ $(\bar{r}_m\bar{v}_m)$, where c is the environmental wind speed, $\bar{v}$ is the mean tangential wind, r is the radius (distance from the TC center), $\bar{r}_m$ is the average radius of maximum wind, and $\bar{v}_m$ is the average maximum wind between the left and right sides of the TC (from Chan, 1982).

to the NW of 2.4 ms^{-1} in a 3 layer model with a simple representation of boundary layer drag, convective heating, and momentum transports. Chan and Williams (1986) used a nondivergent, barotropic model to arrive at a Beta drift to the NW of 2.8 ms^{-1} after 60 hours of simulation. However, Fiorino and Elsberry (1989) attained Beta drift speeds as high as 5 m s^{-1} based upon an 8 m s^{-1} outer wind strength in a 300-800 km annulus. The model used was nondivergent and barotropic.

9.5 Summary

Tangential wind asymmetries 5-7° from the TC center in a 850-300 mb deep layer observed in the (MOT) system are primarily due to "tangential wind blow through". "Tangential wind blow through" happens because the TC center is embedded in a deep layer wind flow maximum. A secondary cause of tangential wind asymmetries is that a geostrophic wind must blow harder in an equatorward location than in a poleward location because f is weaker closer to the equator.

The tangential wind asymmetries exert a propagation influence toward the southeast. Almost all TC motion stratifications have positive S-N and W-E tangential wind asymmetries. As a result, wind-pressure adjustments cause the TC vortex to propagate southeast. Therefore, tangential wind asymmetries are an environmental influence which acts to resist Beta drift to the northwest.

Chapter 10

CONCLUSION

10.1 Baroclinic Influences on TCs

The most prominent feature causing TCs to propagate relative to their surrounding steering current is the TC's immersion within a baroclinic atmosphere. Because the genesis environment for TCs does not go away after they form, TC motion physics are influenced by the same type of environment which fostered TC formation.

Tropical storm tracks coincide with 850-200 mb thickness maxima. Thermal wind arguments based upon temperature gradients normal to the TC track dictate a vertical shear profile with negative parallel shear in the (MOT) system to the right of the storm track, zero shear over the center, and positive parallel shear in the (MOT) system to the left of the storm track. Because of this shear profile, the strongest deep layer winds are located over the storm center. This holds for both 1000-100 mb and 850-300 mb mass-weighted deep layer flows. Both composite rawinsonde data and 10 year climatology confirm the presence of these baroclinic features in association with TCs. The tropospheric thickness maximum and zero shear line are also over the storm center. A monsoon trough environment exhibits the above three features(thickness maximum, deep layer flow maximum, and shear profile) just discussed most clearly. In the Atlantic, the tropical storm track just west of the African coast is most similar to the monsoon trough environment of the Northwest Pacific. Thus, the three baroclinic features which characterize the TC environment can be most easily found in the Atlantic just off the African coast. In the Northwest Pacific, prevailing storm tracks from ten year climatology clearly display these three baroclinic features.

The same three baroclinic features which define the atmosphere's structure in the storm's vicinity guarantee that a TC will move faster than its outer radius deep layer steering current (5-7° radius 850-300 mb mass-weighted deep layer flow). The storm center moves faster than the surrounding deep layer flow because it resides at the location where the strongest tropospheric deep layer flow exists.

Temperature gradients can also exist along the storm track. Normally TCs move from warm to cold air. This causes a thermal wind in the cyclone's environment to move with a normal component to the right of the cyclone's direction of motion. This causes the track of the cyclone to move to the left with respect to this thermal wind flow. By contrast, west moving TCs in the Atlantic propagate to the right of their steering current. This is because they exist in a trade wind environment and move towards warmer air. The trade wind environment keeps the warmest air ahead of the Atlantic west moving storm. So, by the previous argument it propagates to the right. Temperature analyses at 850 mb as well as average height profiles for several combined pressure levels support this concept. Atlantic west moving TCs are a special class of systems whose movement is towards warmer air, while all other storm motion categories are shown to move into a cooler atmosphere.

10.2 Vortex Adjustments Made by TCs

A TC's vortex adjusts to environmental influences by developing both an asymmetric convergence and asymmetric tangential wind profile. Two major environmental influences affecting propagation are 1) pressure-wind adjustments to Beta and 2) adjustments caused by the asymmetric wind profile surrounding the TC ("blow through convergence").

The asymmetric wind profile exists primarily because the tropical storm is embedded in a deep layer flow maximum. A secondary cause of tangential wind asymmetry at a radius of 6° latitude at 850 mb is that geostrophic wind balance requires a stronger tangential wind to the south of a TC than to the north. The strongest tangential winds are almost always to the south and east, which acts to resist propagation of the storm to the northwest.

The north moving TC does not experience convergence in its northeast quadrant. This contradicts what "blow through convergence" would predict. One can infer from this that Beta dominates environmental wind asymmetry as an influence on the TC vortex. A convergence/divergence asymmetry in the northeast/southwest quadrants, respectively, of the TC exists because the 850 mb flow in the TC vortex becomes ageostrophic. The height field at 850 mb is more symmetric from north to south than is the Coriolis parameter. The Coriolis force becomes relatively weak to relatively strong from south to north, which promotes the convergence/divergence profile just discussed.

Composite GMS IR satellite imagery for a single typhoon as well as for 10 combined typhoons supports this premise. IR cloud top temperatures indicative of deep convection can be found twice as far from the composite storm center in the southwest quadrant than they are in the northeast quadrant.

For an eight case average of Atlantic and Northwest Pacific tropical storms, the strongest local absolute vorticity tendency is directed in a west-southwesterly direction. Beta drift and "blow through" convergence to the northwest of the storm combined with convergence due to ageostrophy to the south produce the strongest absolute vorticity tendency for the eight case average directed to the WSW.

There are many factors to consider regarding TC propagation. Local absolute vorticity tendencies due to advection of earth vorticity, "blow through convergence", and south side convergence caused by the relative weakness of f when compared by a symmetric N-S height gradient all influence TC propagation. Local absolute vorticity tendencies caused by asymmetric heating as a result of an uneven distribution of convection around the TC center also need to be considered. Wind-pressure adjustments by a TC vortex which has tangential wind asymmetries is yet another factor to consider for TC propagation.

All of the TC propagation influences in the previous paragraph have a tendency to largely cancel themselves out when all of them are viewed collectively. There probably is not a complete cancellation of the TC propagation tendency from these items, but enough

cancellation occurs to leave environmental baroclinicity as the primary influence affecting TC propagation.

10.3 Future Research

This work is a good continuation to investigating the physics of the tropical storm environment. Much more work remains to be done. Composite rawinsonde data as well as climatological data for other ocean basins(e.g, southern hemisphere) could be analyzed to see if the atmosphere in the vicinity of storms in other oceans exhibits the same baroclinic characteristics as are observed in the Atlantic and Northwest Pacific.

The local absolute vorticity tendencies in both large and small ROCI TCs as well as storms stratified by intensity need to be analyzed to see if propagation as a result of this influence differs between each of these stratifications. Composite satellite imagery could be compiled for each of these storm categories to see if a signature for prevalent south side convergence exists in the deep convection for these storm types as well.

The absolute vorticity advection and convergence terms in the local absolute vorticity tendency equation could be dissected to learn more about the storm's dynamics. Contributions of relative vorticity versus the Coriolis parameter to each of these terms could be investigated. Divergence caused by curvature can be compared to divergence caused by radial divergence or tangential divergence for each storm stratification to provide more clues as to what particular mechanisms are responsible for the overall convergence pattern observed in the 850-300 mb deep layer flow which comprises the tropical storm vortex between 4 and 10° radius. Obviously, radial wind "blow through" and convergence/divergence caused by ageostrophy are major players, but other factors which affect convergence within the TC vortex might be uncovered by a more thorough analysis.

REFERENCES

Carr, L. E. III and R. L. Elsberry, 1990: Observation evidence for predictions of tropical cyclone propagation relative to environmental steering. *J. Atmos. Sci.*, 4, 542-546.

Carr, L. E. III and R. L. Elsberry, 1992: Analytical tropical cyclone asymmetric circulation for barotropic model initial conditions. *Mon. Wea. Rev.*, 4, 644-652.

Chan, J. C., 1982: On the physical processes responsible for tropical cyclone motion. Dept. Atmos. Sci. Paper No. 358, Colo. State Univ., Ft. Collins, CO, 75-77, 119-143.

Chan, J-C. L. and W. M. Gray, 1982: Tropical cyclone movement and surrounding flow relationships. *Mon. Wea. Rev.*, 110, 1354-1374.

Chan, J. C. and R. T. Williams, 1987: Analytical and numerical studies of the Beta-effect in tropical cyclone motion. Part I: Zero mean flow. *J. Atmos. Sci.*, 44, 1257-1265.

Elsberry, R. L. and R. F. Abbey, Jr., 1991: Recent advances in the understanding of tropical cyclone motion. Tech. Rep. NPS-MR-91-003, Naval Postgraduate School, Monterey CA, 93943, 92 pp.

Elsberry, R. L. and R. F. Abbey, Jr., 1992: Typhoon motion and environmental scattering. Tech. Doc. WMO/TD No. 472, World Meteorological Organization, Geneva, Switzerland, pp. III.1-III.19.

Fiorino, M. and R. Elsberry, 1989: Some aspects of vortex structure related to tropical cyclone motion. *J. Atmos. Sci.*, 7, 975-90.

Fitzpatrick, M. E., 1992: Tropical cyclone motion and recurvature in TCM-90. Dept. Atmos. Sci. Paper No. 508, Colo. State Univ., Ft. Collins, CO, 19-24.

Flatau, M., 1992: The role of baroclinic processes in tropical cyclone motion. Dept. of Atmos. Sci. Paper No. 488, Colo. State Univ., Ft. Collins, CO, 140 pp.

Frank, W. M., 1976: The structure and energetics of the tropical cyclone. Dept. Atmos. Sci. Paper No. 258, Colo. State Univ., Ft. Collins, CO, 41-56.

Frank, W. M., 1977: The structure and energetics of the tropical cyclone, Part I: Storm structure. *Mon. Wea. Rev.*, 105, 9, 1119-1135.

George, J. E. and W. M. Gray, 1976: Tropical cyclone motion and surrounding parameter relationships. *J. Appl. Meteor.*, 15, 1252-1264.

Gray, W. M., 1968: Global view of the origin of tropical disturbances and storms. *Mon. Wea. Rev.*, 96, 669-700.

Gray, W. M., 1970: A Climatology of tropical cyclones and disturbances of the western Pacific with a suggested theory for their genesis/maintenance. NAVWEARSCHFAC Tech. Paper No. 19-70, 225 pp.

Gray, W. M., 1977: Tropical cyclone motion and steering flow relationships in the western Atlantic and in the western Pacific. Paper presented at the 11th AMS Technical Conference on Hurricanes and Tropical Meteorology, Miami Beach, FL, 472-477.

Gray, W. M., 1981: Recent advances in tropical cyclone research from rawinsonde composite analysis. World Meteorological Organization, Programme on Research in Tropical Meteorology, Geneva, Switzerland, 35-58.

Gray, W. M., 1992: Tropical cyclone propagation. ONR Meeting, 22-24 September, Monterey, CA, 36 pp.

Gray, W. M., S. Hodanish, C. Weatherford, and J. Martin, 1988: Tropical cyclone motion research-observation and physical implications. Prepared for the special ONR TC Motion meeting, Rainbow Beach, Australia, 29 June-1 July, 121 pp plus 87 pages of Appendices.

Hallin, S. C., 1991: Diurnal variations in tropical cyclones. Dept. of Atmos. Sci. M.S. Thesis, Colo. State Univ., Ft. Collins, CO, pp. 62-63, 65.

Holland, G. J., 1983: Tropical cyclone motion: Environmental interaction plus a beta effect. *J. Atmos. Sci.*, 40, pp 328-342.

McBride, J. L., 1979: Observational analysis of tropical cyclone formation. Dept. of Atmos. Sci. Paper No. 308, Colo. State Univ., Ft. Collins, CO, 56, 74-87.

McBride, J. L. and W. M. Gray, 1979: Observational analysis of tropical cyclone formation. Dept. of Atmos. Sci. Paper No. 308, Colo. State Univ. Ft. Collins, CO, 230 pp.

McBride, J. L. and R. Zehr, 1981: Observational analysis of tropical cyclone formation, Part II: Comparison of non-developing versus developing systems. *J. Atmos. Sci.*, 1132-1151.

Nunez, E., 1981: Tropical cyclone structure and intensity change. Dept. of Atmos. Sci., Ph.D. Thesis, Colo. State Univ., Ft. Collins, CO, 290 pp.

Shapiro, L. J. 1992: Hurricane vortex motion and evolution in a three-layer model. *J. Atmos. Sci.*, 2, 140-153.

Shoemaker, D. N., 1989: Relationships between tropical cyclone deep convection and the radial extent of damaging winds. Dept. of Atmos. Sci. Paper No. 457, Colo. State Univ., Ft. Collins, CO, 86-103.

Simpson, R. H., 1946: On the movement of tropical cyclones. *Trans. Amer. Geophys. Union*, 27, 641-655.

Tropical Cyclones of the North Atlantic Ocean, 1871-1986, 1985: Historical climatology series 6-2, NOAA, National Climatic Data Center, Asheville, NC, p. 34.

Weatherford, C., 1989: The structural evolution of typhoons. Dept. of Atmos. Sci. Paper No. 446, Colo. State Univ., Ft. Collins, CO, 87-90 pp.

Williams, K. and W. M. Gray, 1973: Statistical analysis of satellite observed cloud clusters in the western Pacific. *Tellus*, 21, 313-336.

Xu, J. and W. M. Gray, 1982: Environmental circulations associated with tropical cyclones experiencing fast, slow and looping motions. Dept. of Atmos. Sci. Paper No. 346, Colo. State Univ., Ft. Collins, CO, pp. 273.

Appendix A

APPENDIX A – OBSERVED TROPICAL CYCLONE PROPAGATION

This appendix illustrates tropical cyclone (TC) propagation which is defined as the difference in TC motion from outer radius deep layer steering flow movement. Previous analyses have shown that the 5-7° radius 850–300 mb layer mean flow give a reasonably good representation of the tropical cyclone's steering environment (Chan and Gray, 1982; Gray *et al.*, 1988).

Gray (1992) has made many new TC motion related rawinsonde composite analyses for northwest Pacific, Atlantic, and the Australia-South Pacific tropical cyclones. Composite data have been stratified by three motion direction categories (west, north, and northeast) and three speed (slow, average, and fast) categories. Stratifications have also been made for stationary or nearly stationary cyclones in each basin. Special software programs have been developed to calculate the surrounding cyclone deep layer wind components parallel and perpendicular to the fixed and moving cyclone center. A primary purpose of these analyses has been to quantitatively document the relationship between the tropical cyclone's center motion and its surrounding deep layer (850–300 mb) winds at various radii. These composited data sets show that:

1. Tropical cyclones move with a speed and direction very close to their interior, 1-3° radius tropospheric mean wind currents. There is little propagation component of the cyclone center motion relative to its deep layer interior translation or steering flow.

2. There are systematic and progressive differences between TC motion and the average 850–300 mb outer radius winds at 3-5°, 5-7°, 7-9° and 9-11° radius. Tropical cyclones move systematically and progressively with radius faster and to the left (for N. Hemisphere orientation) of their outer radius deep layer mean flow (except for westward moving Atlantic cyclones which move faster but slightly to the right of their deep layer steering current because of special Atlantic environmental conditions).

Figure A.1 illustrates how the tropical cyclone center and the mean winds at 2° and 4° radius move systematically faster and to the left of the outer 6° and 8° radii winds. This is true for nearly all of the speed and direction rawinsonde motion stratifications. Westerly, northerly and northeasterly moving tropical cyclones are all observed to have roughly the same 6° and 8° speed and direction orientations in relation to their interior 2° and 4° wind vectors. (See Figs. A.2, A.3 and A.4).

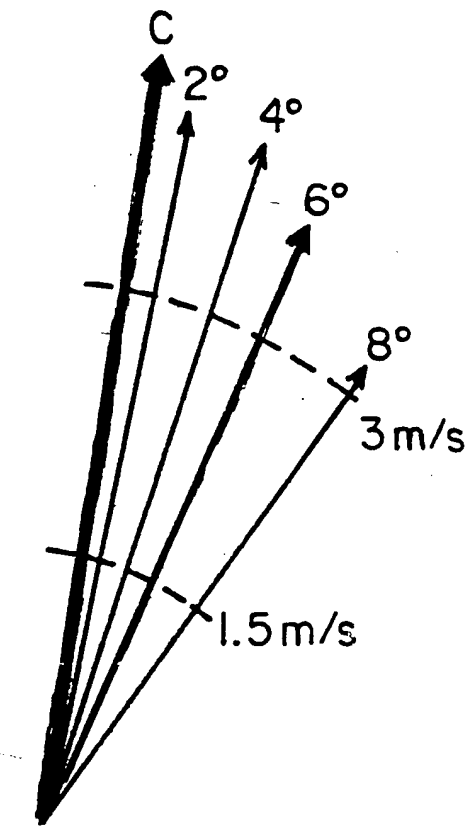

Figure A.1: Synthesis of the TC motion vector (C) relative to the 850–300 mb mean wind in the 2° (1-3°), 4° (3-5°), 6° (5-7°) and 8° radial belts.

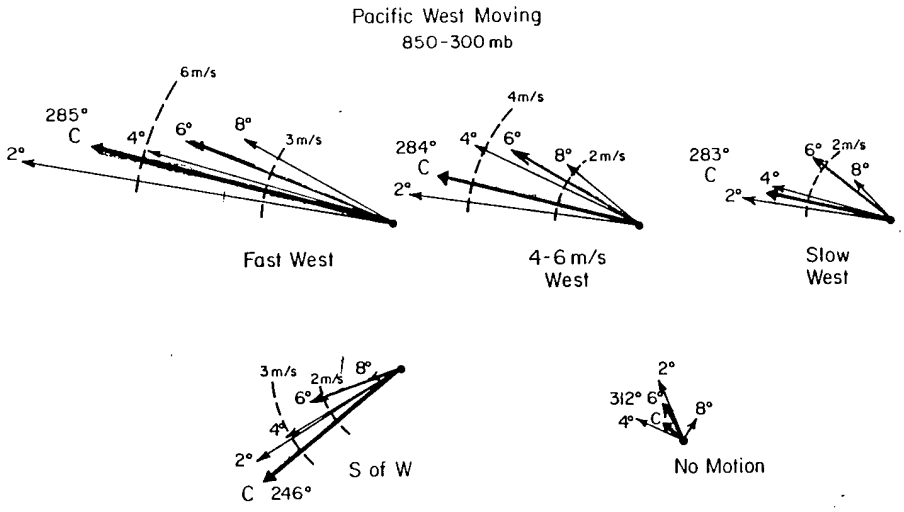

Figure A.2: Layer average (850-300 mb) symmetric wind vectors in various radial bands relative to the mean cyclone motion (c) for west moving tropical cyclones in the NW Pacific. Two degrees denotes 1-3° mean radial motion, 4° denotes 3-5° mean radial motion, etc.

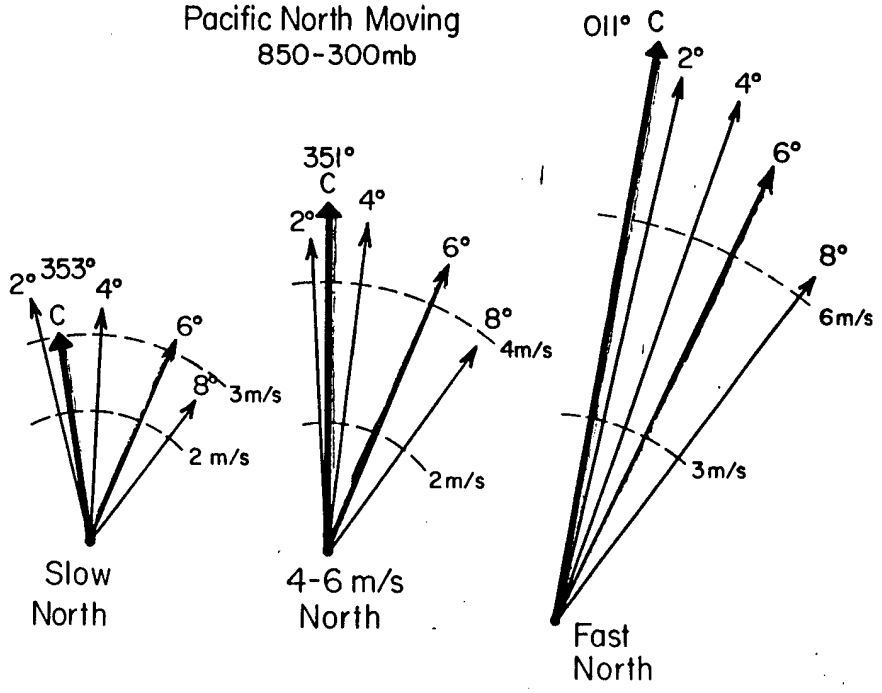

Figure A.3: Same as Fig. A.2, except for north moving tropical cyclones.

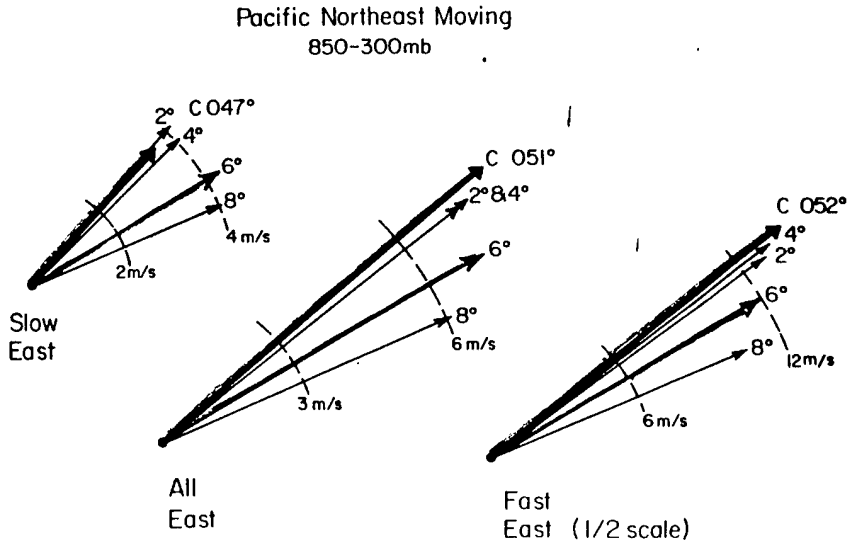

Figure A.4: Same as Fig. A.2, except for northeast moving tropical cyclones.

Appendix B

APPENDIX B – AREA AVERAGED DATA FIELDS

Area averages for four different data fields are included in this appendix. These data fields are: 1) divergence, 2) convergence times absolute vorticity, 3) absolute vorticity advection, and 4) local absolute vorticity tendency. Individual point values from the 3-5°, 5-7°, 7-9°, and 9-11° radial bands are area averaged together to obtain an individual octant average for each octant.

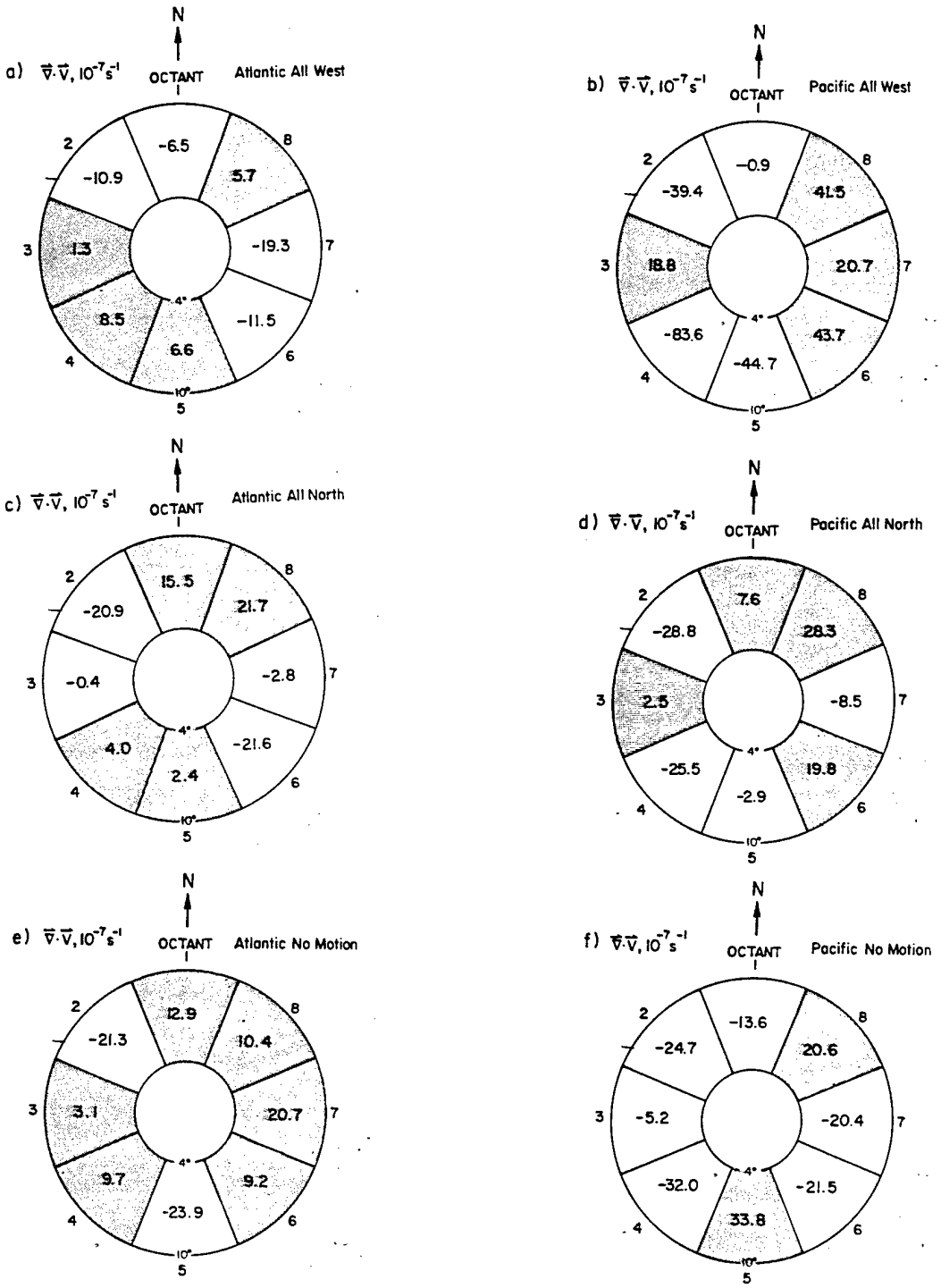

Figure B.1: Divergence in the 850-300 mb deep layer flow (MOT). Numbers in each octant are area averages of four radial segments (3-5, 5-7, 7-9, 9-11° radial bands) for Atlantic and Northwest Pacific TCs.

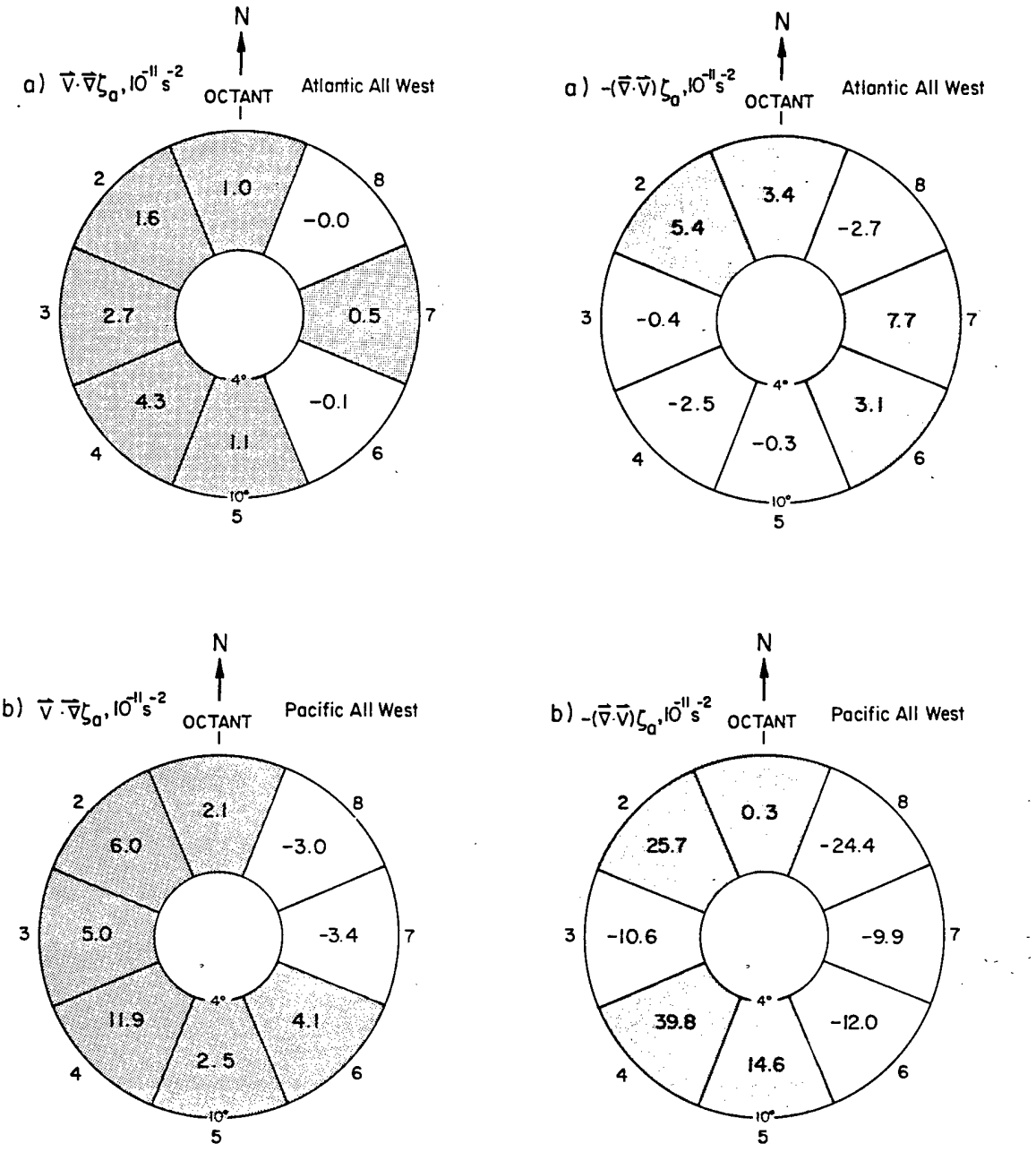

Figure B.2: (a-f) a,b. Area averaged absolute vorticity advection (AVA) and area averaged absolute vorticity times convergence (convergence term) in the 850-300 mb deep layer flow (MOT) for Atlantic and Northwest Pacific TCs. Note the larger magnitude of the convergence term in general when it is compared to the AVA term.

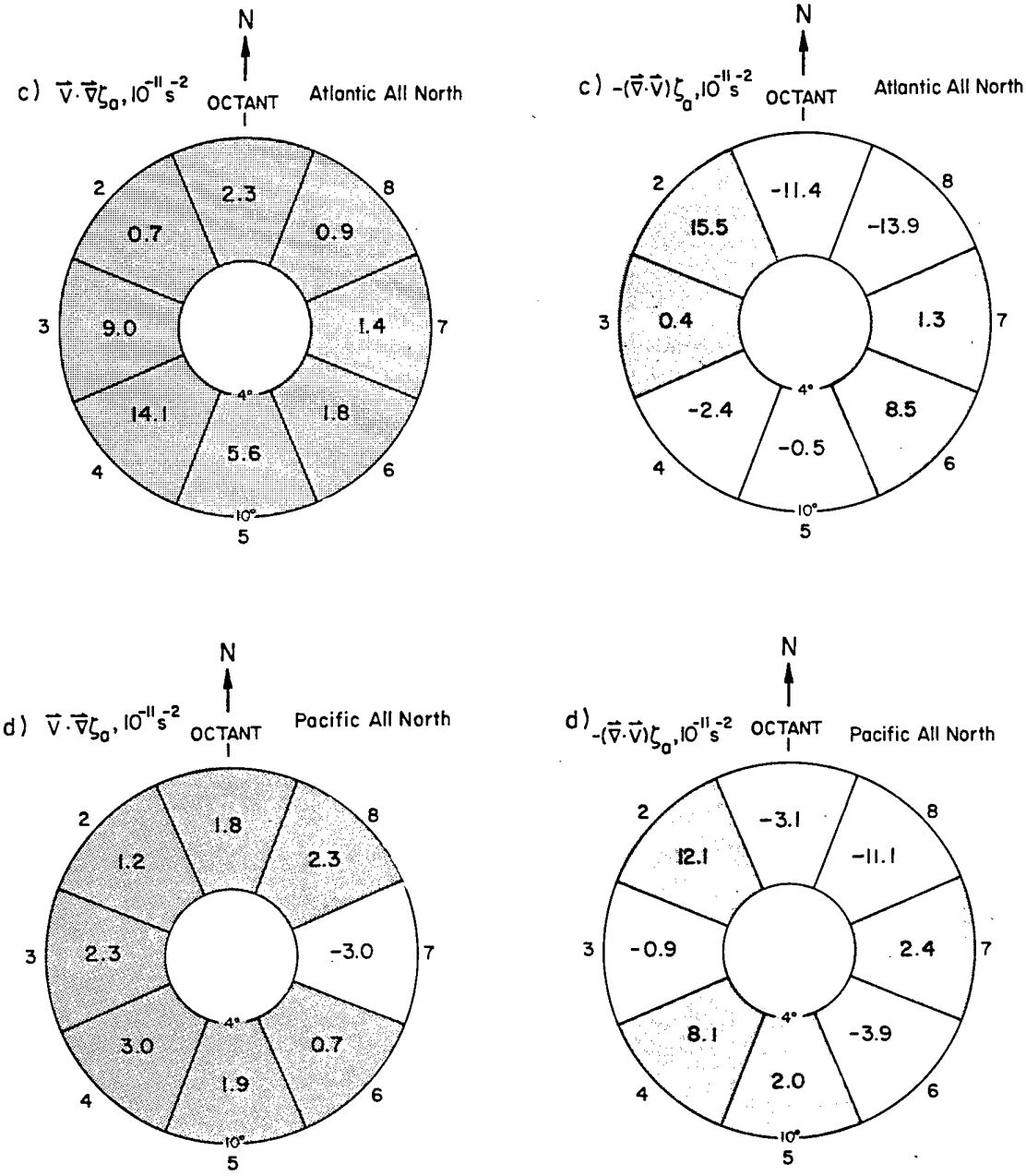
c) $\vec{V}\cdot\vec{\nabla}\zeta_a$, $10^{-11}s^{-2}$
N
OCTANT
Atlantic All North
2.3
0.9
0.7
1.4
9.0
1.8
14.1
5.6
c) $-(\vec{\nabla}\cdot\vec{V})\zeta_a$, $10^{-11}s^{-2}$
N
OCTANT
Atlantic All North
-11.4
-13.9
15.5
1.3
0.4
8.5
-2.4
-0.5
d) $\vec{V}\cdot\vec{\nabla}\zeta_a$, $10^{-11}s^{-2}$
N
OCTANT
Pacific All North
1.8
2.3
1.2
-3.0
2.3
0.7
3.0
1.9
d) $-(\vec{\nabla}\cdot\vec{V})\zeta_a$, $10^{-11}s^{-2}$
N
OCTANT
Pacific All North
-3.1
-11.1
12.1
2.4
-0.9
-3.9
8.1
2.0
2
3
4
5
6
7
8
4°
10°

Figure B.2: c,d.

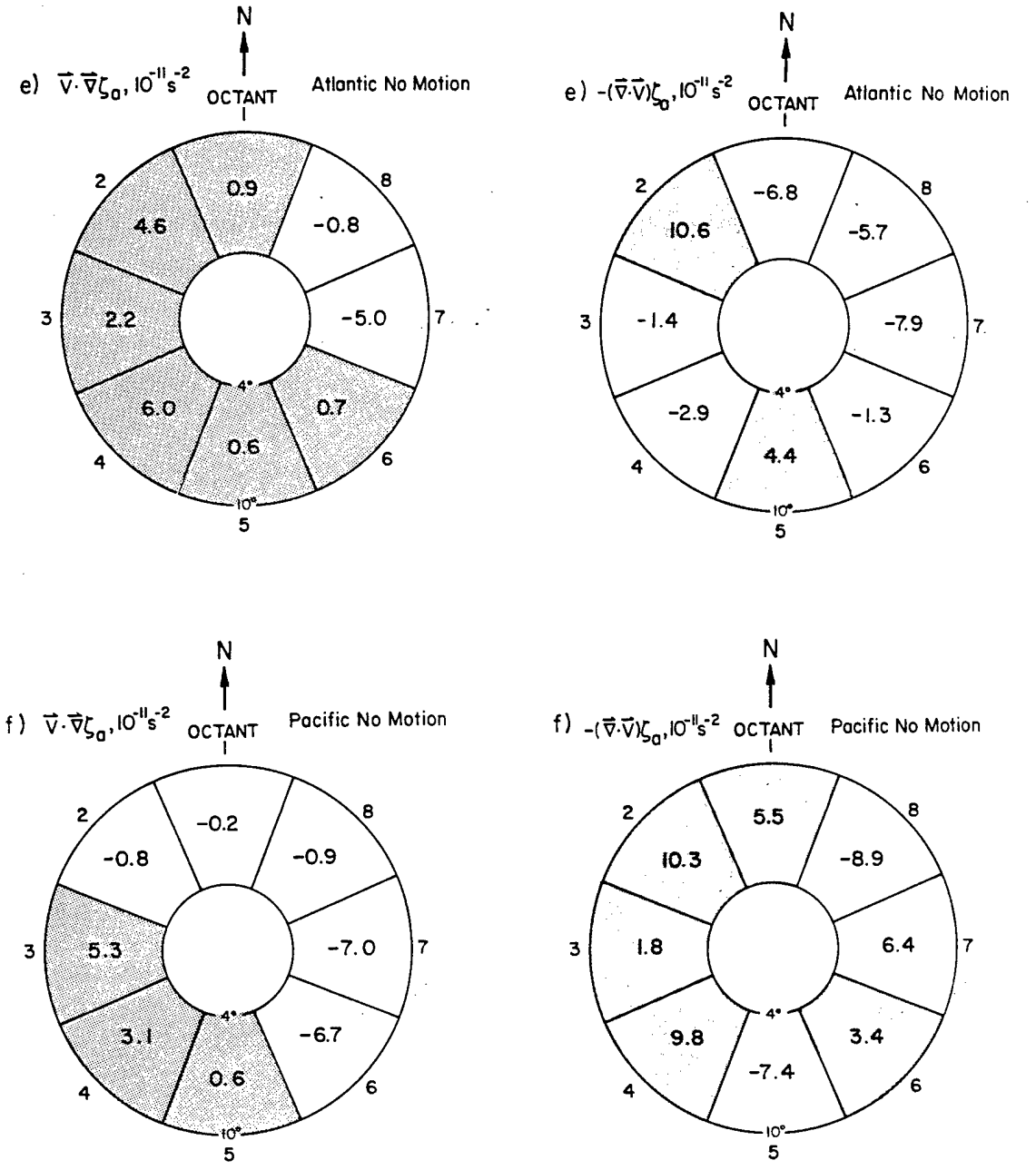
e) $\vec{V}\cdot\vec{\nabla}\zeta_a$, $10^{-11}s^{-2}$
N
OCTANT
Atlantic No Motion
0.9
-0.8
-5.0
0.7
0.6
6.0
2.2
4.6
e) $-(\vec{\nabla}\cdot\vec{V})\zeta_a$, $10^{-11}s^{-2}$
N
OCTANT
Atlantic No Motion
-6.8
-5.7
-7.9
-1.3
4.4
-2.9
-1.4
10.6
f) $\vec{V}\cdot\vec{\nabla}\zeta_a$, $10^{-11}s^{-2}$
N
OCTANT
Pacific No Motion
-0.2
-0.9
-7.0
-6.7
0.6
3.1
5.3
-0.8
f) $-(\vec{\nabla}\cdot\vec{V})\zeta_a$, $10^{-11}s^{-2}$
N
OCTANT
Pacific No Motion
5.5
-8.9
6.4
3.4
-7.4
9.8
1.8
10.3
2
3
4
5
6
7
8
4°
10°

Figure B.2: e,f.

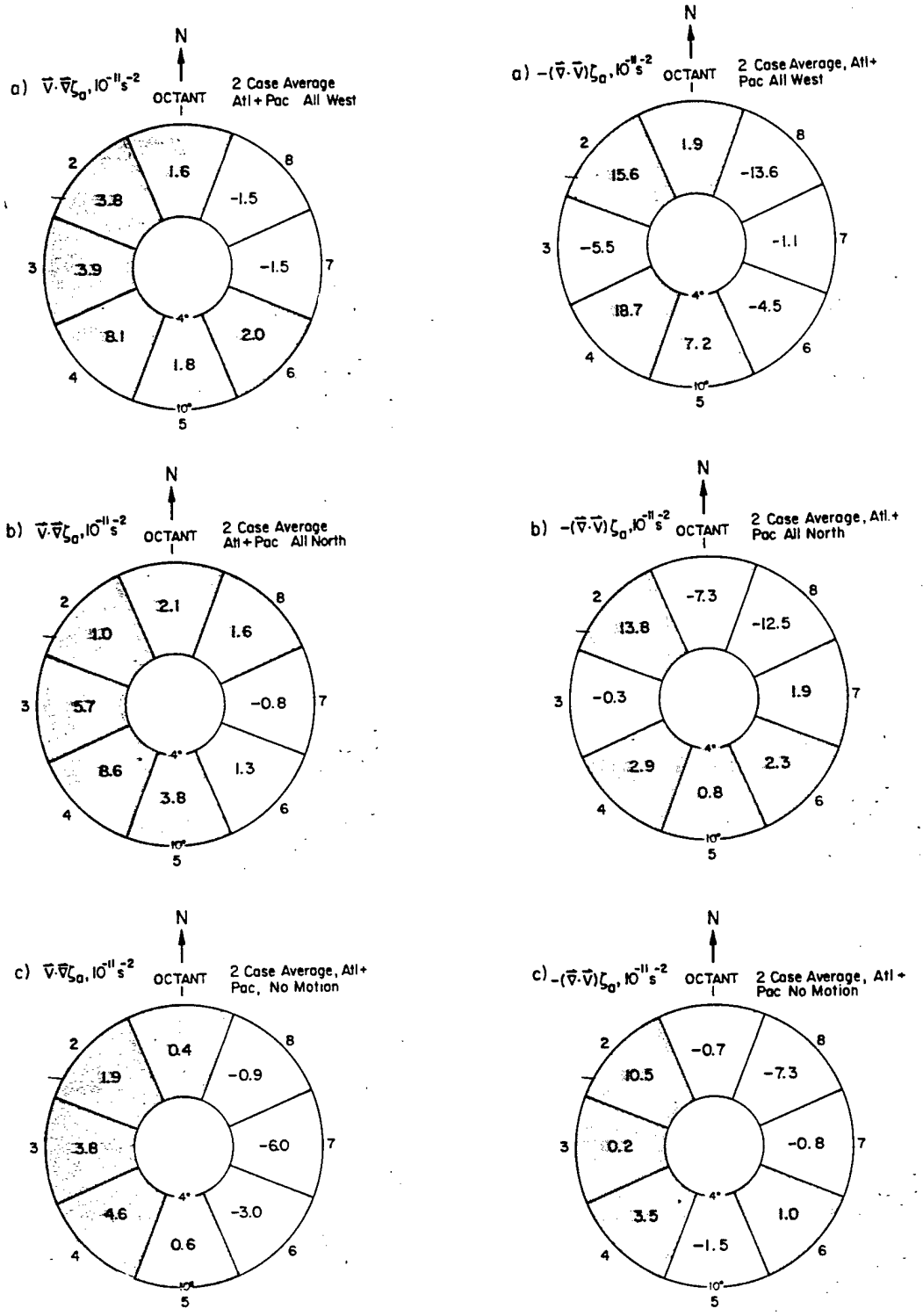

Figure B.3: Area averaged absolute vorticity advection and area averaged absolute vorticity times convergence in the 850-300 mb deep layer flow (MOT) for combined TC cases in the Atlantic and Northwest Pacific.

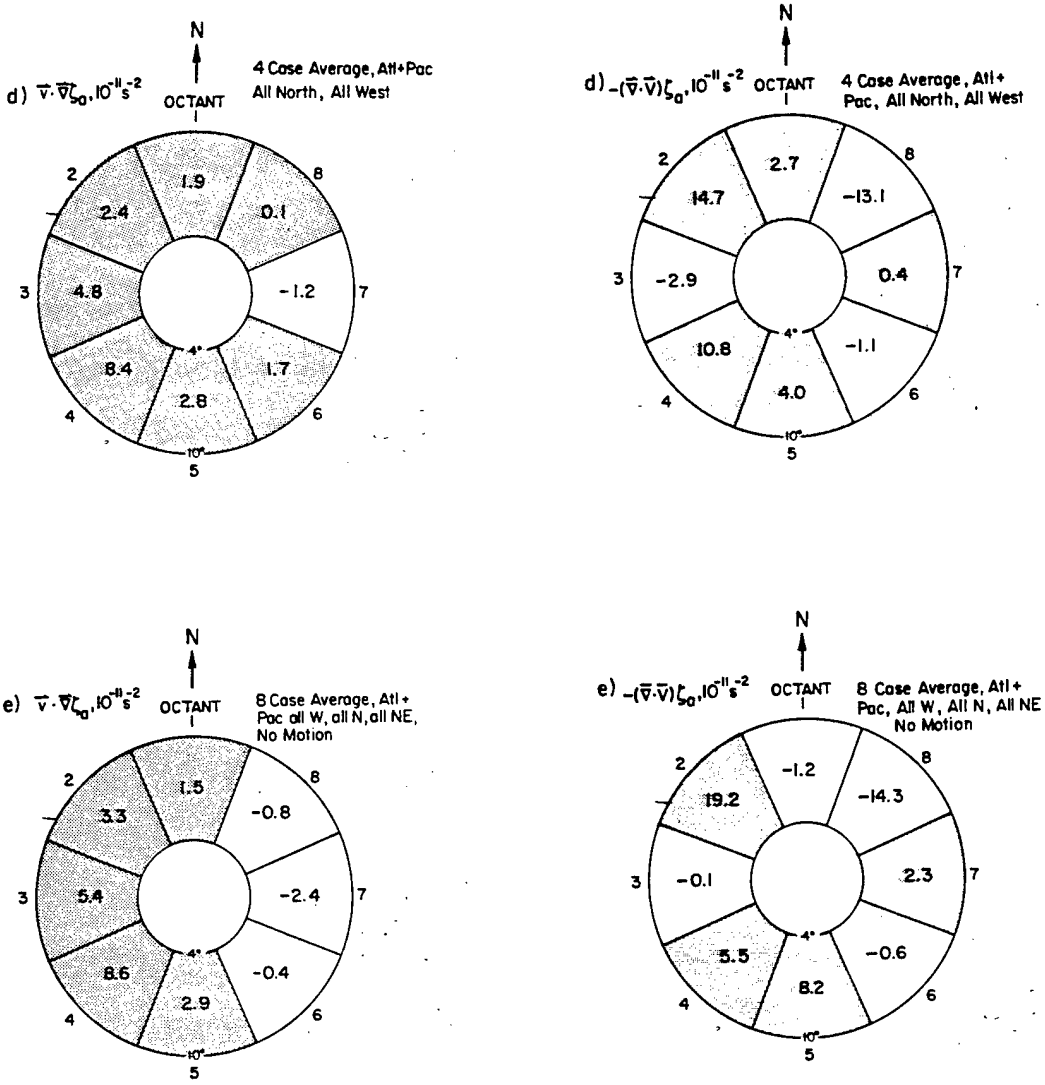

Figure B.3: Continued.

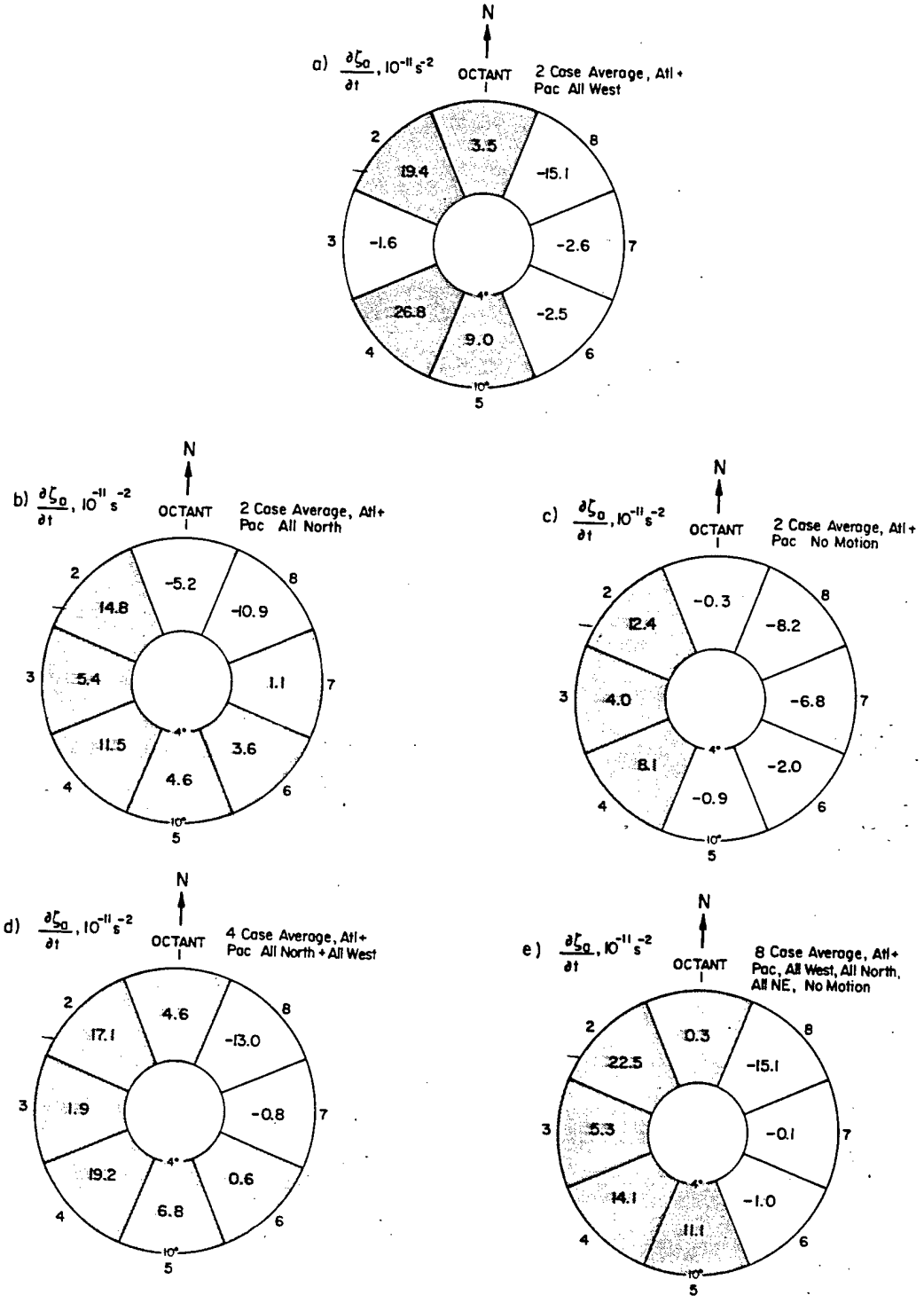

Figure B.4: a. (a-e) Area averaged local absolute vorticity tendency (vorticity advection plus absolute vorticity times convergence) in the 850-300 mb deep layer flow (MOT) for combined TC cases in the Atlantic and Northwest Pacific.